FACULDADE DE ENGENHARIA DA UNIVERSIDADE DO PORTO

Comparison of Discretization Schemes for Simulation of Transport of a Passive Scalar in an Open-Channel Confluence

João de Alcântara Sá de Sousa Coutinho

DISSERTATION CARRIED OUT TO OBTAIN THE DEGREE OF
MASTER IN ENVIRONMENTAL ENGINEERING

Mestrado Integrado em Engenharia do Ambiente

Supervisor: João Pedro Gomes Moreira Pêgo
(Assistant Professor, Department of Civil engineering - FEUP)

Receiving Institution Supervisor: Tom De Mulder
(Professor Dr. Ir., Department of Civil engineering - UGent)

June, 2021

Comparison of Discretization Schemes for Simulation of Transport of a Passive Scalar in an Open-Channel Confluence

João de Alcântara Sá de Sousa Coutinho

Mestrado Integrado em Engenharia do Ambiente

June, 2021

Resumo

Nas últimas décadas, com a crescente consciencialização sobre a poluição da água e consequentes riscos para a saúde humana e para o meio ambiente, este recurso tem sido alvo de especial atenção. Muitos estudos nesta área têm surgido, com o objetivo de uma melhor gestão e proteção dos recursos hídricos. As confluências são bastante comuns em sistemas ribeirinhos com grande importância ecológica e grande influência no transporte, distribuição e mistura de sedimentos e nutrientes, deste modo os estudos sobre a hidrodinâmica e morfodinâmica em confluências vêm ganhando atrito. Não só pela importância da proteção dos recursos hídricos, mas também porque o crescimento exponencial do poder computacional proporciona ,atualmente, melhores técnicas para estudar a elevada complexidade hidrodinâmica em confluências, que continua a ser difícil de estudar pelos meios convencionais. Desta forma, os métodos de Dinâmica de Fluídos Computacional tem vindo a ganhar popularidade, pois é possível obter resultados precisos a um preço acessível. No entanto, devido à sua natureza bastante recente, a literatura existente ainda é insuficiente, especialmente no que diz respeito à distribuição e mistura de contaminantes nas confluências.

Nesta dissertação, o objetivo inicial foi estudar a influência da camada de mistura na distribuição e mistura de um passivo escalar, numa confluência em forma de T com leitos discordantes, com o uso de LES. No entanto, devido ao confinamento provocado pela COVID-19, o objetivo foi alterado para acomodar esse contratempo. Como tal, o objetivo principal foi comparar o desempenho de métodos alternativos de discretização no OpenFOAM para prever a concentração média do tempo numa confluência em forma de T de 90º com um rácio discordante de 0,25. Como tal, três esquemas numéricos de alta resolução com limitador de fluxo foram estudados, nomeadamente: o esquema Backward Linear Limited TVD, o esquema Crank-Nicolson Linear TVD limitado e o esquema Backward Van Leer Limited TVD. Um problema de advecção pura 1D foi inicialmente planeado, a fim de mostrar o desempenho desses esquemas de segunda ordem no tempo e no espaço. Portanto, a solução esperada seria livre de oscilações esporádicas e com alguma difusividade, o que estava em grande parte de acordo com os resultados que foram obtidos do problema de advecção pura 1D.

Em relação aos resultados da simulação do Large Eddy, não houve forma de os validar, devido confinamento mencionado anteriormente e pela falta de literatura a respeito do transporte passivo escalar em confluências de formatos semelhantes. Embora não tenha sido possível concluir qual o esquema mais exato para estudar o passivo escalar na confluência, foi assumido, através da análise dos resultados, que dos três esquemas estudados, o esquema TVD limitado Backward Van Leer era o menos difusivo e o melhor a capturar nitidamente os gradientes elevados da solução. Por outro lado, foi observado que o esquema Backward Linear Limited TVD foi o mais difusivo. Além disso, todos os esquemas mostraram baixa monotonicidade nos resultados do LES, o que permitiu supor que esses esquemas podem não ser adequados para estudar o transporte do passivo escalar na confluência ou que os paramêtros da simulação não são adequados para os esquemas em questão e, devido a isto ocorreram erros de descritizaçao. Se a incorreta escolha dos parâmetros da simulação foi a causa para a falta de monotonicidade, a redução do tamanho das células e, ou, a redução dos incrementos temporais seria a solução para reduzir os erros de descritização.

Palavras-chave: Large Eddy Simulation; Esquemas de discretização; Confluência; Escoamento com superfície livre; Dinâmica de Fluidos Computacional.

Abstract

In the last decades, with the rising awareness about water pollution and its risks for human health and for the environment, a higher focus has been given to this resource. Many studies in this area have been emerging, in order to better manage and protect water resources. As such, and because confluences are common key features in riverine systems with great ecological importance and great influence on the transport, distribution and mixing of sediments and nutrients, studies on the hydrodynamics and morphodynamics in confluences have been gaining friction. Not only because of the importance of protecting water resources, but also because the exponential growth in computational power provides, nowadays, better techniques to study the complex hydrodynamics within confluences, which are still hard to study through conventional means. As such, Computational Fluid Dynamics methods have been gaining popularity, since it is possible to obtain accurate results at an affordable price. However due to their fairly recent nature there is still a lack of literature, especially in regards to the distribution and mixing of contaminants within confluences.

In this dissertation, the initial main goal was to study the influence of the mixing layer in the distribution and mixing of a passive scalar, in a T-shaped confluence with discordant beds, with the use of LES. However, due to the COVID-19 lockdown the objective was changed to accommodate those setbacks. As such the main goal was to compare the performance of alternative discretization methods in OpenFOAM to predict the time-averaged concentration in a 90^{o} degree T-shaped confluence with a discordant ratio of 0.25. As such, three high resolution numerical schemes with flux limiter were studied, namely: the Backward Linear Limited TVD scheme, the Crank-Nicolson Linear limited TVD scheme and the Backward Van Leer Limited TVD scheme. A 1D pure advection problem was initially devised, in order to show the performance of these second-order accurate in time and space schemes. Therefore, the expected solution would be free from sporadic oscillations and with some diffusivity, which was mostly in accordance with the results that were obtained from the 1D pure advection problem.

In regards to the Large Eddy simulation results, there was no way to validate them, due to the previously mentioned lockdown and due to the lack of literature in regards to the passive scalar transport in similar shaped confluences. Although it was not possible to conclude which scheme was more accurate to study the passive scalar concentration in the confluence, it was assumed, through analysis of the results, that from the three schemes the Backward Van Leer limited TVD scheme was the least diffusive and the one to more neatly capture the high gradients of the solution, while the Backward Linear Limited TVD scheme was the most diffusive. Moreover all the schemes showed bad monotonicity in the LES results, which permitted the assumption that this schemes might not be suitable to study the transport of the passive scalar in the confluence, or that the simulation parameters for the studied schemes are not ideal and, due to this discretization errors occured. If the incorrect choice of the simulation parameters was the cause for the lack of monotonicity, the reduction of the size of the cells and, or, the reduction of the time step would be the solution to reduce the discretization errors.

Keywords: Large Eddy Simulation, Discretization schemes, Confluence, Open-channel flow, Computational Fluid Dynamics.

Acknowledgments

I would like to thank both my supervisors Professor Tom De Mulder and Professor João Pedro Pêgo for the opportunity to work abroad in this thesis, for the continuous guidance provided and for the experience and knowledge shared with me.

I would like to thank Pedro Xavier Ramos for providing me with all the simulations, which without would not be possible to produce the results and thus write this thesis, and for all his time, guidance and knowledge provided.

I would like to thank Tian Jin for providing and helping with the scripts used in this thesis, which was super valuable.

An overall thank you to all the Staff from the Hydraulics Laboratory in Ghent University, for receiving me with open arms and for always being there when i required.

I would like to thank all my friends for supporting me through this hard time, specially the "J guys" and the three "praxeteiros" which maintained me sane during all the COVID-19 quarantine.

I want to thank all my family, for always worrying about me and for always being present when i most needed them.

Finally, a special thanks to my parents, for always being present and for giving me strength to complete this stage of my life. Without them this would not be possible. I am very grateful for all the opportunities and unconditional love they provided me and for all the values they transmitted and teached me.

Contents

List of Figures

List of Tables

Nomenclature

Symbols

A_{cs}	Total cross-section area
A_i	Area of a mesh cell
c	Concentration
CFL	Courant Number
cof	Linear Limited OpenFOAM coefficient
C_s	Smagorinsky constant
E	Mixing Coefficient
L	Maximum spatial domain
F	Flux function scheme
f^{low}	Low resolution term
f^{high}	High resolution term
Fr	Froude number
g	Gravitational acceleration
h_{CRL}	Curved rigid lid height
h_d	Downstream water depth
h_{FRL}	Flat rigid lid height
H_m	Main channel surface water height
h_s	Step height
H_t	Tributary channel surface water height
j	Index
K	Diffusivity
n	Index
N	Number of time domain intervals
M	Number of spatial domain intervals

ocCof	Crank-Nicolson OpenFOAM coefficient
P	Pressure
pMean	Time-averaged pressure
q	Discharge ratio
Q_{main}	Main channel discharge
Q_{tot}	Total discharge (i.e. downstream discharge)
Q_{trib}	Tributary channel discharge
Re	Reynolds number
s	Concentration
s_{avg}	Total averaged concentration at the cross section
sMean	Time-averaged concentration
s_{us}	Imposed upstream concentration
t	Time
T	Maximum time domain
u	Velocity
U_d	Averaged downstream velocity
v_e	Exact propagation speed
v_n	Numerical propagation speed
W_d	Channel width
x	Position Vector
x/W_d	Dimensionless position vector
y	Position Vector
y/W_d	Dimensionless position vector
z	Position Vector
z/W_d	Dimensionless position vector

Greek Letters

Δ	Computational step
∇	Gradient operator
ϕ	Flux limiter function
ρ	Fluid density
σ	Bed discordance ratio

Abbreviations and Acronyms

CHZ	Confluence Hydrodynamic Zone
CFD	Computational Fluid Dynamics
DES	Detached Eddy Simulation
DNS	Direct Numerical Simulations
EU	European Union
FTCS	Forward time centered space
LES	Large Eddy Simulation
NASA	National Aeronautics and Space Administration
RANS	Reynolds-Averaged Navier-Stokes
SGS	Subgrid-scale
TVD	Total Variation Diminishing
UGent	Universiteit Gent (Ghent University)
WHO	World Health Organization
1D	One-Dimensional
3D	Three-Dimensional

Chapter 1

Introduction

1.1 Background

Throughout human history access to clean water has always been a defining problem. Civilizations that managed water correctly thrived and grew, while others perished. Out of all the water present on Earth, according to NASA (2020) (National Aeronautics and Space Administration), 96.5% is salt water and, from the remaining 3.5%, around 2% is fresh water frozen as ice, around 1% is fresh water in rivers, lakes, streams and in the ground and a very small percentage is in the atmosphere as water vapour.

Regardless of the physical state of water or where it is found, water is one of the most valuable natural resources and it has no substitute. Water has a broad usage and every living organism requires it to survive. Besides incorporating every living being, being used by plants for photosynthesis and the need for animals and humans to consume it, water is used for a series of healthy practices, like hygiene. It is an important resource in agriculture, to irrigate crops, in industries, to produce consumer products, as well as in industrial activities, like mining or for spinning the turbines at hydroelectric power plants to produce energy.

Water has the property of dissolving a wide range of solutes. This is why water is so important at the biological level and for most human activities. While this property is an advantage, it can also be a disadvantage, since this ability makes water susceptible to dissolve substances that can be harmful to the environment and the ecosystem with which it comes into contact. As such, when the normal properties of water are changed due to the presence of foreign materials the water is considered polluted.

In the past decades water pollution has increased due to a growth in population. The necessity to supply bigger populations led to huge forest losses for agriculture intensification and livestock, which increased runoff and animal source pollution. The growth in the industrial sector also contributed for an increase in water pollution, due to untreated waste discharges on rivers. Along with these causes, human activities, domestic waste and sewage discharges without previous treatment, volcano eruptions, storms and floods all contributed for an increase in water pollution. Nowadays many rivers are polluted and many populations around the world suffer with lack of clean water, which is further aggravated by climate change which has negative effects. It causes an expansion of dry areas worldwide (i.e. reducing the amount of fresh water available) and melting glaciers, which increases the possibility of natural disasters. According to World Resources Institute (2015) by the year 2040 most of the world will not have enough water to meet demand for the year round, if water is incorrectly managed.

Over the last few decades, with the rising awareness about water pollution and its consequences many governments passed and tweaked key pieces of legislation in order to better manage and protect this resources. For instance, the main directive related to water resources implemented by the European Union is the Water Framework Directive (directive 2000/60/EC of the European Parliament and of the Council, of 23 October 2000) and aims to protect and improve water quality of all water bodies and all their dependent habitats (European Parliament and Council directive 2000/60/EC (2000); European Commission (-)).

The first step, in order to preserve water resources, aquatic ecosystems and all other organisms that depend on this resource, is to understand how it travels and behaves in nature. It is common knowledge that many rivers are supplied by rainfall and runoff. During the time that rainwater stays in the air, it might dissolve airborne contaminants, resulting in a decrease in its quality and afterwards negatively impacting the environment. Rain that falls directly into bodies of water might, for example, provoke quick changes in water acidity, which then can lead to the death of many water species. On the other hand, rain that falls on the ground might infiltrate and increase soil acidity and consequently be prejudicial to plants and/or affect aquifers, which might be used for human consumption or end up supplying another water body. When water is not able to infiltrate in the soil, runoff happens instead. The path where that runoff travels until it reaches a river affects the water quality. If it moves through an agricultural area it is able to carry different pollutants, like pesticides, fertilizers, herbicides and heavy metals. Likewise, runoffs in urban areas, which are very common due to the high impermeability of the streets, might also feed nearby rivers and transport waste, like plastic and cigarette butts, and many other pollutants, like oils and animal excreta.

Fertilizers and animal, or human, excreta stimulate algae growth due to the release of nitrogen and phosphorus in the water. If these nutrients are in excess in the water, it might provoke a phenomenon called eutrophication, when algae start reproducing extremely quick and end up covering the surface of the river. The huge amount of algae at surface water prevents external oxygen from dissolving in water and blocks light from reaching the deep waters of the river, preventing photosynthetic organisms within the river from producing oxygen. Pollutants such as oils might also have a similar effect, preventing oxygen exchanges between air and water and blocking light from reaching the depth of the river, since oils are generally less dense and immiscible in water. The increase in biomass and nutrients in the river also stimulate microorganism growth in the water. These microorganisms will then consume the existing dissolved oxygen for their metabolic functions and contribute to a depletion of oxygen on the water. If the demand is higher than the amount that is being replenished, a hypoxic zone (i.e. oxygen-less zone or "dead zone") is formed, where most marine life is not able to survive. The areas of the river where there is little mixing, or the water is stagnant, are more likely to be affected by this type of scenario, such as the water on the upstream side of a dam. Water retained on dams most of the times is stagnant and might be used to irrigate the surrounding agricultural fields. If the aforementioned scenario occurs in such location, in addition to destroying the ecosystem within the river, can also have impacts on the surrounding agricultural fields, if they depend on this water, as oxygen-free water limits the growth of plants.

Pollutants like pesticides, herbicides or other chemicals, plastic and heavy metals might cause adverse effects on the health of living organisms that get into contact with them. The presence of these pollutants in water makes it easier for organisms to absorb them, over time, accumulate them (i.e. bioaccumulation) and, ultimately, contribute to their death. Since rivers are sources of food, organisms that survive the pollutants might later be consumed by other species, or humans, and the bioaccumulated contaminants might be transferred through food chains, having long term repercussions on the ecosystem health.

In most cases, rivers are used as drinking water sources. When the water is polluted there is a need to remove the source of the contamination and the contaminants from the water before being used or consumed. According to WHO (2019) (World Health Organization), contaminated water might transmit diseases such as dysentery, typhoid and polio and is estimated to cause 485 thousand diarrhoeal deaths each year, being that at least 2 billion people worldwide consume water from sources contaminated with excreta.

Rivers are known to have a natural capacity for self-purification. Over time, if the total amount of pollutants does not exceed the river self purification capacity, they might be removed by chemical processes such as oxidation, physical processes such as dilution and filtering, and biological processes such as decomposition by microorganism or the consumption of the contaminant by animals. When the amount of contaminants is excessive an intervention is required. However the solutions available to do so vary depending on the contaminants present in the water and might be very time consuming and expensive.

In recent years, a lot of focus has been given to confluences. Confluences are common key features in fluvial and artificial open-channel networks, with great ecological importance and with great influence in the transport of sediments, nutrients and with a relevant role in erosion phenomena and mixing processes. These are structures with extremely complex hydrodynamics and are usually difficult to study by conventional means. Confluences found in nature have distinct parameters, shapes and sizes, which complicates comparisons between each other, and consequently causes a need for more research in order to fully understand them. On the other hand, since humans have control over the design and construction of artificial confluences, these can be used to study parameters and shapes without many of the problems that turn up while studying natural confluences. However this last solution might be costly and requires specific equipment and space.

Acquiring knowledge about confluences is important for a multitude of reasons. It is important for many engineering problems, such as the effects of erosion caused by the confluence hydrodynamics on columns of a bridge that is situated in a confluence, and is also important to understand how sediments are transported and where they deposit within the confluence. Its study might enable an assessment of how much sediments are reaching the coast and if the main river is feeding or not, for example, a beach (i.e. if the river's sediment load helps or not to maintain a beach), or even help with navigation on the river. Moreover sediments might carry pollutants which makes their transport and sedimentation patterns within confluences very important, in order to better manage them. Not only are pollutants found in sediments, but also in the flow. By studying the hydrodynamics in confluences it is possible to better assess pollutant dispersal on rivers, which is important, especially when there is a nearby population using it as a drinking water source. As such, mixing processes within confluences are extremely common and very important since they highly contribute for a faster dispersion and dilution of the contaminant, highly contributes for aeration on the river, which might be important for its auto-purification and contributes for heat transfer (i.e. cools the water), which is important for the maintenance of marine life that can not withstand drastic changes in water temperature.

Over the years, advances in technology have provided greater leverage for improvement of old techniques and allowed the emergence of newer ones. The exponential evolution of computers in recent years, in terms of speed and computational power, enabled the appearance of computational methods, which made tasks, that once seemed extremely hard or even impossible, viable. However, even though these methods can be applied in many scientific areas to solve such situations, their relatively recent nature compels the need for more research and development.

Computational methods remove many of the limits imposed by conventional means and make it possible to study specific parameters with a high level of detail. In general, they are less expensive, the necessary equipment requires less space to be assembled and its use is more flexible, as there is no need to physically change the equipment in order to study different variables. The disadvantage of these modern techniques is the need for qualified operators and, due to the little amount of literature in some cases, it is sometimes required to validate the results through practical experiences. However, with continuous research and development of these methods, they are becoming more accurate over time. As such, computational methods have been shown to be great alternatives for conventional means and a great method to study confluences and different parameters with great detail.

1.2 Objective

The initial main goal of this thesis was to study the influence of the mixing layer in a passive scalar concentration, in a T-shaped (i.e. 90 degree) confluence with discordant beds. The mixing layer is important since it has a direct influence on how pollutants and nutrients are mixed in the flow. However due to the recent pandemic situation part of the work that was initially foreseen to be done, turned impossible to accomplish, which limited the scope of the present dissertation.

As such, to accommodate the setbacks, the new main goal is to critically compare the performance of alternative discretization methods in OpenFOAM for predicting the mean (i.e. time-averaged) concentration field in the same T-shaped confluence with discordant beds.

Therefore, three different schemes (Backward Van Leer limited TVD, Backward LinearLimited TVD and Crank-Nicolson LinearLimited TVD) were studied and compared, performance wise. The schemes were introduced through the implementation of a simple 1D transport problem and afterwards the results from the passive scalar transport LES simulations, using the mentioned schemes, were compared and discussed.

Despite the fact that Reynolds Averaged Navier-Stokes (RANS) is commonly the chosen model in a big portion of the literature, access to High Performance Computing (HPC), in Ghent University, made the use of the Large Eddy Simulation (LES) method possible, since this technique requires a higher computational effort, but simulates the large scales of the flow (produces high fidelity results). RANS model is normally used because of its success, proven efficiency and because it is often the most cost-effective way to run a CFD simulation. Although RANS has the advantage of requiring lesser computational effort, compared to LES, it has the downside of providing less accurate results, which cannot always be used to solve certain fluid mechanics problems.

1.3 Dissertation Structure

This dissertation is split into six main chapters, Introduction, State of the Art, 1D Advection Problem, Description of LES Simulations, Comparison of LES Results, Conclusions and Recommendations.

In the current chapter, chapter 1, it is displayed a brief background to the importance of the theme of this dissertation, its main objective, and its structure.

In chapter 2, a brief literature review is presented, in which the study, throughout the years, on the hydrodynamics and morphodynamics within confluences is discussed, as well as the main existing CFD methods capable of taking into account the effects of turbulence in the flow, since turbulence is a characteristic of the flow in confluences. Subsequently, the discretization methods considered in this dissertation are compared through the study of a simple 1D transport problem, governed by a pure advection equation.

In chapter 3, The results for the simple 1D transport problem are presented and discussed, for each studied discretization scheme, since it is possible to demonstrate their performance by comparing the respective approximate finite-difference solutions to the exact solution.

In chapter 4, a brief description of the LES model characteristics, and the specific flow and transport configuration studied in this dissertation are presented.

In chapter 5, the OpenFoam results of the passive scalar transport simulations, for the different discretization methods are presented and discussed.

At last, in chapter 6 the main conclusions of this dissertation and suggestions for future works are stated.

Chapter 2

State of the Art

2.1 Literature review

Over the last four decades studies on confluences yielded significant advances, mainly in regards to their flow features (Bilal et al. (2020)). As two flows merge, complex changes on the flow hydrodynamics occur and, due to complex erosion and deposition processes, the bed morphology changes at the confluence and downstream of it (Mosley (1976); Ashmore and Parker (1983); Bombar and Cardoso (2020)). The place within the confluence where these processes occur is called the confluence hydrodynamic zone (CHZ) and its size extends accordingly with the mixing layer or accordingly to the size where the pressure gradients, related to the convergence of flows, exert influence in the flow field (Kenworthy and Rhoads (1995)).

In order to characterize the CHZ, Best (1987) conducted experimental work with different asymmetrical confluences and proposed a hydrodynamic model with a layout of the main flow patterns that develop within this type of confluences. According to Best (1987) and illustrated in Figure 2.1, the highly complex three-dimensional flow CHZ has a stagnation zone near the upstream junction corner, a flow deflection zone where each stream enters the confluence zone, a shear or mixing layer between both flows, a separation/recirculation zone at the downstream junction corner, a contraction zone opposite to the recirculation zone where the flow is constricted, an acceleration zone between the separation zone and the shear layer and a flow recovery zone at the downstream end of the CHZ.

Much of the initial work emphasized the study of these zones in regards to their location and shape, specially the mixing layer and the recirculation zone, which were researched through field observations and experimental work (Mosley (1976); Ashmore and Parker (1983); Best and Reid (1984)). Those studies showed that the main parameters that affected the morphology and hydrodynamics within confluences were the confluence junction angle, discharge ratio, froude number and width ratio. However experimental work only accounted confluences with junctions of concordant beds. At the time, most of the natural confluences were assumed to have junctions with concordant channels and, as such, most of the studies focused on these confluences (Best and Roy (1991)). However, Kennedy (1984), through bathymetric surveys, observed that discordant

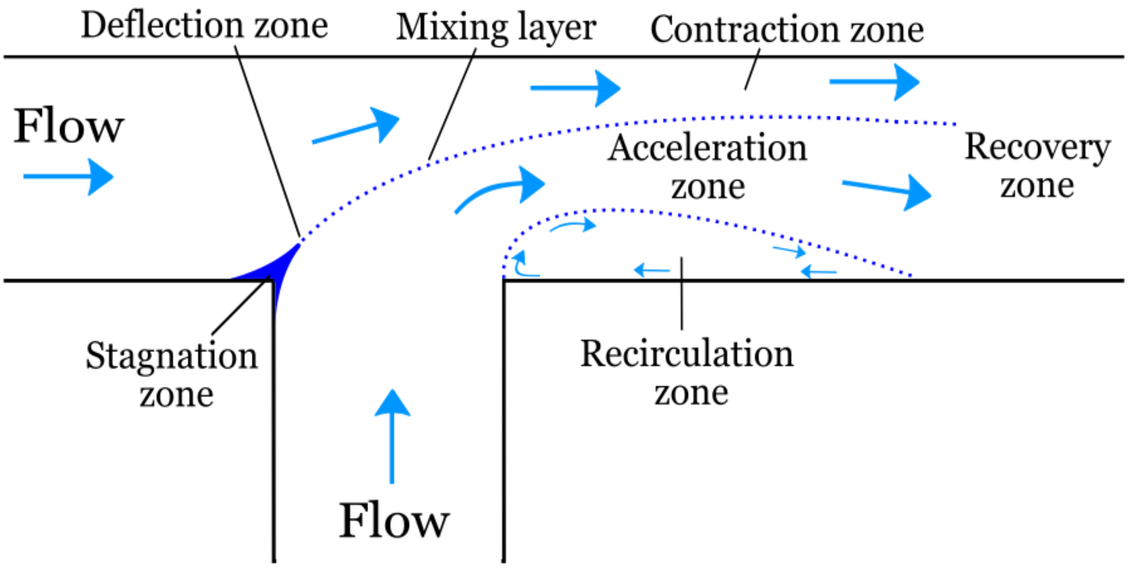

Figure 2.1: Conceptual model of an asymmetrical open-channel confluence (adapted from Best (1987)).

confluences were more common than what it was thought before and provided enough evidence to invalidate the aforementioned assumption about the predominance of natural confluences with concordant junction beds. As a result, it drew the attention of researchers to study the influence of bed discordance in both the hydrodynamics and morphodynamics within confluences (Sukhodolov et al. (2017)).

The work of Best and Roy (1991) was one of the first studies that gave insight about the influence of bed discordance on the flow dynamics within a confluence. Best and Roy (1991) studied an experimental flume with two parallel channels, where one of the channels was shallower, and observed fluid upwelling on the tributary side and distortion of the mixing layer. Although the authors only studied zero degree junction angles, they pointed out that for confluences with discordant channels, a distortion on the mixing layer would be expected for any junction angle and the location of the fluid upwelling would change with junction angle and discharge ratio. These observations were confirmed in subsequent works, in which was also observed that the vertical motion secondary flows, that may develop in the lee of the step, enhanced mixing rate and had significant implications on sediment transport and bed morphology (Gaudet and Roy (1995); Biron et al. (1996b,a); Serres et al. (1999); Boyer et al. (2006); Lane et al. (2008)).

Mixing rate and mixing distance in a confluence may vary due to bed discordance and, according to Lewis and Rhoads (2015), due to momentum flux ratio, cross-sectional area and density difference. Furthermore Bryan and Kuhn (2002) studied both asymmetrical and symmetrical confluences, and observed effective mixing in all studied asymmetrical confluences, due to flow separation, and little to none in symmetrical confluences, which suggested that in most cases symmetry may also influence mixing rate. When mixing is slow, complete mixing and recovery may be prolonged, requiring a longer distance to occur after the confluence (Lane et al. (2008); Bouchez et al. (2010)) and when mixing is fast, complete mixing and recovery occur faster and in a much shorter distance, closer to the confluence (Gaudet and Roy (1995); Kenworthy and Rhoads (1995); Rhoads and Sukhodolov (2001)). Mixing processes facilitate spreading and dissolution of pollutants, present in a tributary, into the post-confluence channel. When mixing is slow and, as such, not efficient, the contaminated flow remains throughout long distances along one of the two banks, otherwise, if it is fast, the downstream flow quickly becomes contaminated, but since there is a higher dissolution and distribution of the pollutant in the total volume of water, its concentration decreases faster (Launay et al. (2015)).

In the literature there is still a small amount of knowledge about the distribution and mixing of contaminants within confluences, specially in rivers, due to the different behaviors that each contaminant may have in the hydrodynamics and morphodynamics of the confluence, which may affect mixing and the spatiotemporal distribution of the contaminant in the confluence and in the downstream branch (Schemel et al. (2007); Horák and Hejcman (2016); Yuan et al. (2018); Pouchoulin et al. (2018); Zhang et al. (2020)). One of the most recent studies on this subject was the work of Zhang et al. (2020), in which a natural asymmetric confluence with a highly polluted tributary with typical contaminants (i.e. organic contaminants, ammonia nitrogen, $NH_3 - N$, and phosphorus, P), of discordant bed and with a different discharge from the main river was studied. The authors observed that the spatial distribution and mixing patterns were similar between the pollutants, and when the tributary flow discharge was high, the concentration of pollutants quickly occupied most of the downstream channel, and, when the flow discharge was extremely small, the high concentration of contaminants in the flow remained along the bank side of the tributary, but due to rapid mixing complete mixing was still achieved very close to the confluence.

Until the last two decades, studies on the hydrodynamics in open-channel confluences were mainly studied through field and experimental work. However, these methods depend on observations, estimates and a large amount of simultaneous measurements, such as velocity measurements, which are impractical, subject to errors and may not accurately represent all complex processes within the confluence (Bradbrook et al. (2000b)). Also some unstable phenomena in the flow may be hard to capture through these methods (Bradbrook et al. (2001)) and the use of tracers in many studies, that are used to represent mixing processes, may not represent reality, due to their density, which, as mentioned before, has been shown to be a parameter that may influence mixing in open-channel confluences (Lewis and Rhoads (2015); Zhang et al. (2020)). Recent development of better and faster computers have propelled the use of 3D numerical modeling as a good alternative to conventional methods (Biron et al. (2004); Sharifipour et al. (2015); Luo et al. (2018); Ramos et al. (2019b)), due to its capability to provide better and accurate results to study the complex flow fields and processes in confluences (Bradbrook et al. (1998); Lane et al. (1999); Biron et al. (2004); Shakibainia et al. (2010); Schindfessel et al. (2015); Jin et al. (2020)). Numerical tools allow a more in depth study of each variable, since it is possible to modify them individually, which provides the possibility for a better assessment of their importance and influence over different flow characteristics (Bradbrook et al. (2000a, 2001); Constantinescu et al. (2011)).

Therefore, computational fluid dynamics (CFD) has been widely implemented, due to its capability to handle a wide range of engineering problems and to produce detailed and easy-to-view results, as well as its ability to make it possible to obtain results in a more economical way, time and cost wise, compared to conventional methods (Sharifipour et al. (2015)). In order to produce CFD simulations a numerical modeling strategy has to be chosen, according to the problem that is being studied, the desired outcome and available resources. As such, and taking into account that the complex flow in confluences is turbulent, the main methods that currently exist capable of taking into account the effects of turbulence are RANS-based, LES, and DNS (Rodi et al. (2013)).

First of all, the Reynolds-Averaged Navier-Stokes based methods solve both RANS and continuity equations, which express the conservation and momentum of mass, respectively. However, due to the Reynolds-averaging, new unknowns appear in the momentum equations, called Reynolds stresses, and express the turbulent exchange of momentum due to the motion of turbulent eddies (Rodi et al. (2013)). As such, to close the equations, the Reynolds stresses have to be modeled as a function of the mean (i.e. time-averaged) velocity components and pressure, which is possible by providing a turbulence model (Rodi et al. (2013)). The turbulence model has to model the influence of both large and small scales of turbulence onto the mean flow. Since this method solves RANS equations yielding mean quantities, the computing effort is small and, therefore, this is the most economical method. However, this method has difficulties to accurately capture complex flow phenomena, such as large-scale turbulence, and mass exchange processes, due to its dissipative nature, and since the required turbulence model accounts for all turbulence scales, in which some strongly depend on the boundary conditions of the case being studied, it makes this method suffer from limited generality, i.e. RANS is not suitable for solving all problems (Constantinescu (2013); Rodi et al. (2013)).

Second, the Direct Numerical Simulation (DNS) method is capable of resolving all the scales of turbulent motion, up to the dissipative range, without the introduction of a turbulence model. However, in order to resolve all turbulence scales, the size of the computational grid has to be smaller than the size of the smallest and most dissipative turbulence scales, thus requiring a huge amount of computational power (Rodi et al. (2013)). For complex flows, with high Reynolds numbers, the required computational effort increases, exceeding the capabilities of the currently available computers, but for simple flows, with low Reynolds numbers, this method is nowadays possible (Rodi et al. (2013); Constantinescu (2013)).

Finally, the LES method directly resolves the larger scales of turbulence in space and time on the computational grid, with the use of discretization methods to discretize the differential terms in the Navier-Stokes and continuity equations. The unresolved scales (i.e. small scales of turbulence), which cannot be solved due to their smaller size than the computational grid, are instead modeled with the use of a subgrid-scale (SGS) model (Rodi et al. (2013)). Since this method does not directly resolve the small scales, but instead models them, a more affordable mesh size can be used, thus requiring less computational effort than the DNS method, but still more than RANS-based methods. Compared to the RANS-based method, the advantage of the LES method is the ability to provide a more in-depth study of the coherence structures and turbulence characteristics. In addition, in recent years, due to the availability of high-performance computers, the LES method became suitable for research and practical applications (Rodi (2017)).

Not only is it possible to study the complex hydrodynamics of a turbulent flow with 3D numerical modeling, but is also possible to study the transport and mixing of dissolved and suspended passive scalars (i.e. substance/contaminant that has no dynamical effects on the flow). When using Reynolds-Averaging, the advection terms in the transport equation, for a passive scalar, will produce new unknowns called Reynolds fluxes (Rodi et al. (2013)). To close the equation the Reynolds fluxes are expressed as a function of the mean (i.e. time-averaged) concentration and velocity components, by means of the eddy diffusivity for mass transport (Simoes and Wang (1997); Gualtieri et al. (2017)). The eddy diffusivity is expressed as the ratio of the eddy viscosity and the turbulent Schmidt number (Simoes and Wang (1997)). Notice that for the schmidt number different values are adopted in the literature (Gualtieri et al. (2017)). When using LES, the large turbulent scales in the concentration field are resolved in space and time on the computational mesh, and the small scales modeled by a SGS model. For this case, a standard smagorinsky model and a value of the turbulent schmidt number can be used, or, to avoid the uncertainty of the schmidt number a Dynamic Smagorinsky model can be used instead (Rodi et al. (2013)).

2.2 Discretization

Most of the times for a problem described by differential equations and initial/boundary conditions the analytical solution is unknown. Therefore, one may use a discretization method in order to solve it, obtaining an approximated solution. In the literature different methods are available, however focus will be given to the finite difference method, because of its simplicity. With the use of this method and when the exact solution of the problem is known, it is possible to demonstrate the performance of a numerical discretization scheme. As such, in this subchapter the finite difference method will be presented, as well as basic different numerical discretization schemes and the schemes that were considered in the LES simulations for the transport of a passive scalar.

2.2.1 Finite difference method

The finite difference method is easy to implement, suitable to parallelization (i.e. to break a problem into pieces and independently solve them simultaneously, which means faster computation of the solution) and possible high-order accuracy (Coleman and Sandberg (2010); Olaiju et al. (2018)). When using this method a finite system of equations is obtained from the differential equation governing the problem, through discretization of the domain and operators (Ames (1992)). As such the derivatives are replaced by finite difference quotients, which can be illustrated using a pure advection equation (Equation 3.2), in which the mathematical definition of the (partial) derivative of c to x is (Riddaway (2002)):

$$\frac{\partial c}{\partial x} = \lim_{\Delta x \to 0} \frac{c(x+\Delta x,t) - c(x,t)}{\Delta x} \tag{2.1}$$

If the limit is omitted, the forward difference scheme is obtained:

$$\frac{\partial c}{\partial x} = \frac{c(x+\Delta x,t) - c(x,t)}{\Delta x} + \mathcal{O}(\Delta x) \tag{2.2}$$

Where $\mathcal{O}(\Delta x)$ is the truncation error. The truncation error for difference schemes can be determined by the Taylor series and it will represent the difference scheme's order of accuracy. For the forward difference scheme, since Δx is raised to the power 1, is said to be of first order accuracy. This shows how fast the truncation error diminishes if the step Δx is reduced. As such, for a higher order accuracy scheme, when the step is reduced, the approximated solution will theoretically be more accurate than for a lower order accuracy scheme.

Similarly to the forward difference scheme, the backward difference scheme can be written as:

$$\frac{\partial c}{\partial x} = \frac{c(x,t) - c(x-\Delta x,t)}{\Delta x} + \mathcal{O}(\Delta x) \tag{2.3}$$

And the central difference scheme can be written as:

$$\frac{\partial c}{\partial x} = \frac{c(x+\Delta x,t) - c(x-\Delta x,t)}{2\Delta x} + \mathcal{O}(\Delta x^2) \tag{2.4}$$

Notice that the central difference scheme is second order accurate.

Additionally the finite difference can also be used for time derivatives. Therefore, similarly to Equation 2.1, the mathematical definition of the (partial) derivative of c to t is (Riddaway (2002)):

$$\frac{\partial c}{\partial t} = \lim_{\Delta t \to 0} \frac{c(x,t+\Delta t) - c(x,t)}{\Delta t} \tag{2.5}$$

If the limit is omitted, the forward time difference scheme is obtained:

$$\frac{\partial c}{\partial t} = \frac{c(x,t+\Delta t) - c(x,t)}{\Delta t} + \mathcal{O}(\Delta t) \tag{2.6}$$

Where $\mathcal{O}(\Delta t)$ is the truncation error. Similarly, the backward time difference scheme can be written as:

$$\frac{\partial c}{\partial t} = \frac{c(x,t) - c(x,t-\Delta t)}{\Delta t} + \mathcal{O}(\Delta t) \tag{2.7}$$

And the centred time difference scheme can be written as:

$$\frac{\partial c}{\partial t} = \frac{c(x,t+\Delta t) - c(x,t-\Delta t)}{2\Delta t} + \mathcal{O}(\Delta t^2) \tag{2.8}$$

In regards to the domain, this is discretized in time and space, meaning that the approximate solution is calculated in a finite number of points (Causon and Mingham (2010)). Therefore a computational grid is considered. There are two types of grids, irregular and regular ones. Irregular grids create bothersome programming details, since the approximation of the difference equations change from location to location, and are more complex thus requiring stronger computational power, whereas regular grids (i.e. rectangle, triangle or hexagon shaped) are simpler, being the preferable choice (Ames (1992)).

For these reasons a regular computational grid, with columns and rows normal to each other, as depicted in Figure 2.2 is preferred. The columns are given by the subdivision of the spatial domain in a number of equal finite intervals, M, with step Δx (i.e. spatial step) and the rows are given by the subdivision of the time domain in a number of finite intervals, N, with step Δt (i.e. time step). The unknowns are located at the intersection of the grid lines and, in this document, are denoted as c_j^n, with $j = 0$ to M and $n = 0$ to N.

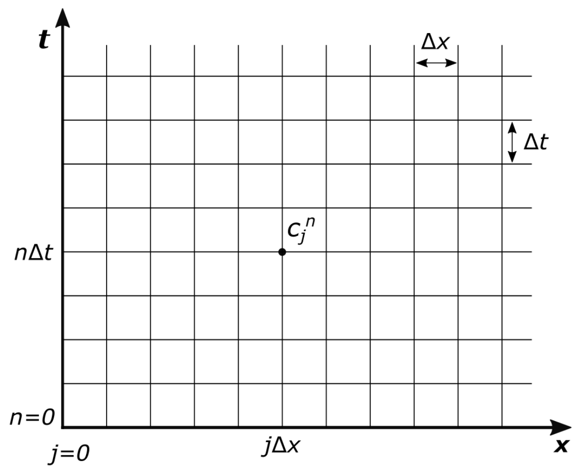

Figure 2.2: Grid for a finite-difference method (adapted from Vreugdenhil (1989))

The best scenario would be to produce exact solutions, but, as a result of discretization, the numerical method is inherent to discretization errors, thus the solutions are never completely exact (Kundu (2012)). However, the user can try to minimize these errors with the hope that the approximate solution will be close to the exact one. The magnitude of these errors might change depending on the chosen numerical discretization scheme and will be different depending on the chosen distribution of grid points. In order to choose the appropriate numerical discretization scheme, the scheme has to fulfill certain general requirements in terms of consistency, stability and convergence. In regards to the distribution of grid points, to reduce the magnitude of the discretization errors and, in turn, produce more accurate solutions, smaller Δx should be applied, which requires the user to choose a larger M. However, by increasing M the computer effort is higher, thus the computation time required to solve the problem increases (Causon and Mingham

(2010)). Therefore, is important to be aware of the available resources and, according to them, choose the smallest Δx possible, thus achieving the best accuracy possible.

Likewise, choosing an appropriate Δt is equally important. Small Δt will reduce the magnitude of the discretization errors, but one must take care when choosing Δt, since its size is limited depending on both the chosen grid size and numerical scheme. Furthermore, smaller Δt means that a higher number of iterations is required in order to reach a solution, which will increase the computation time and, since each iteration gives an approximate result to the required solution, a higher number of iterations might increase the error in the approximate solution (Causon and Mingham (2010)).

In order to better understand and analyse the numerical solution, a user must be familiar with the types of errors associated with discretization. As such, the type of errors, that make the approximate solution differ from the exact solution, are the phase errors (numerical dispersion) and amplitude errors (numerical diffusion or numerical damping) (Mulder (2020)). In order to visually/show the effects that these errors have in a solution, a pure advection of a wavy like initial condition is represented in Figure 2.3.

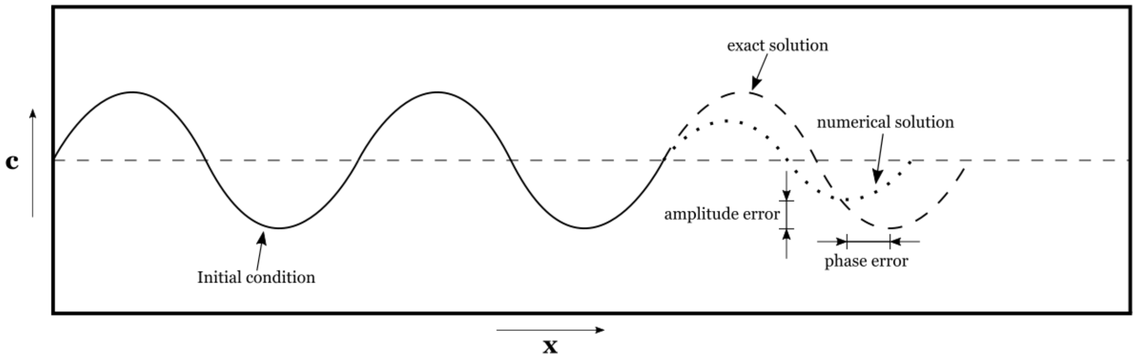

Figure 2.3: Amplitude error and phase error due to numerical discretization of a pure advection equation, with an initial given condition (adapted from Mulder (2020)).

The phase error is a type of error associated with a difference between the phase speed of the exact solution and the numerical solution. By defining v_n as the numerical propagation speed and v_e as the exact propagation speed and relating both, three different situations are presented, according to Xue (2001):

If $v_n/v_e < 1$, the numerical solution has lag compared to the exact one (moves slower);

If $v_n/v_e > 1$, the numerical solution leads compared to the exact one (moves faster);

If $v_n/v_e = 1$, there is no phase error, both exact and numerical solutions have the same propagation speed.

In relation to amplitude errors, the amplification factor (or damping factor), which is the ratio of the numerical to the exact amplitude, should be equal to 1, otherwise the wave will grow or decay in time (Xue (2001)). This numerical damping can affect the accuracy of the numerical solution, leading to poor results (Rafei et al. (2017)). However in some cases it can be used to increase numerical stability (see Bathe and Baig (2005) and Bathe and Noh (2012)).

A numerical discretization scheme is said stable when the approximate numerical solution of the discretized equation is a sufficiently close approximation of the exact solution. This means that spontaneous disturbance (i.e. round-off errors) decay during the calculations and do not cause overflow or underflow (Kundu (2012); Mulder (2020)). If instead these spontaneous disturbances grow exponentially during the calculations, the numerical solution will be far from the exact solution, thus the numerical discretization scheme will be unstable and the computation might "crash". The stability of a numerical scheme for a pure advection equation can be studied through the Courant number, firstly introduced by Courant et al. (1967):

$$CFL = \frac{u\Delta t}{\Delta x} \tag{2.9}$$

where CFL (Courant-Friedrichs-Lewy) is the Courant number, and u the advection velocity. For an advection equation with a constant velocity u and a selected Δt and Δx, the CFL is known. As such, most of the explicit numerical schemes are associated to a CFL condition, which if respected it is said that the numerical scheme is conditionally stable. If this condition is not respected, then the numerical scheme will produce unstable solutions. As such, the choice of Δt depends on the choice of Δx, and vice-versa. In the case of implicit numerical schemes these are considered unconditionally stable, since the unknown values are solved from a set of equations (Mulder (2020)). This means that Δx can be chosen freely for these cases, but one can not forget the limitations mentioned before about very small Δx.

Other than stability, a numerical discretization scheme should fulfill the requirements in terms of consistency and convergence. As such, according to Mulder (2020) a numerical scheme is said consistent when in the limit that $\Delta t \to 0$, $\Delta x \to 0$, the discretized equation should tend to the exact differential equation and it is said convergent when in the limit that $\Delta t \to 0$, $\Delta x \to 0$, the approximate numerical solution of the discretized equation should tend to the exact solution of the differential equation. Notice that, according to the Lax Equivalence Theorem (Richtmyer (1967)), if a numerical discretization scheme meets the consistency and stability requirements, then it also fulfills the convergence requirement.

2.2.2 Time stepping

When using discretization methods one must be aware of explicit and implicit approaches. As such, a finite difference scheme is said to be explicit when the differential equation is discretized in such a way that all unknown values can be calculated from known values from previous time levels (n), which means that considering values c, all values of c_j^2 (for all indices j) can be calculated from the values of c_j^1 (for all indices j), and likewise values of c_j^1 can be calculated from the values of c_j^0 (for all indices j) that are known because of the given condition (Brio (2010)).

A finite difference scheme is said implicit when the differential equation is discretized in a way that the calculation of unknown values depends both on known values from the previous time level (n) and also on values that are not yet known at the new time level (n+1) (Brio (2010)). As such this method requires a set of algebraic equations to be solved in every time step, in order to find the values at the new time level.

Notice that the previously mentioned equations, for the different schemes, are in their explicit format and will slightly change for an implicit approach.

2.2.3 Advection schemes

Considering the pure advection equation and the previously mentioned schemes, for time and space, it is possible to obtain schemes discretized both in time and space, by coupling two schemes (one to discretize space and another to discretize time). The common schemes discretized in time and space, in the literature, use the forward or centered time differences (Riddaway (2002)). As such, in this subchapter only schemes based on the forward time difference scheme (Equation 2.6) will be presented.

2.2.3.1 First order upwind scheme

The first order upwind scheme is discretized in time with the forward time difference scheme (Equation 2.6) and, assuming that $u > 0$, discretized in space with the backward difference scheme (Equation 2.3), otherwise, if $u < 0$, the scheme is discretized in space with the forward difference scheme (Equation 2.2). In this case it will only be considered the $u > 0$ situation. As such, the difference equations associated are Equation 2.10 and Equation 2.13.

For the upwind scheme, with explicit time stepping (Zijlema (2015)):

$$\frac{c_j^{n+1} - c_j^n}{\Delta t} + u\frac{c_j^n - c_{j-1}^n}{\Delta x} = 0 \tag{2.10}$$

Which, considering the Courant number:

$$CFL = \frac{u\Delta t}{\Delta x}, \tag{2.11}$$

Equation 2.10 can be rewritten as:

$$c_j^{n+1} = c_j^n - CFL * (c_j^n - c_{j-1}^n) \tag{2.12}$$

If instead, implicit time stepping is considered (Mulder (2020)):

$$\frac{c_j^{n+1} - c_j^n}{\Delta t} + u\frac{c_j^{n+1} - c_{j-1}^{n+1}}{\Delta x} = 0 \tag{2.13}$$

Considering the Courant number (Equation 2.11), the implicit version (Equation 2.13) can then be rewritten as follows:

$$c_j^{n+1} = c_j^n - CFL * (c_j^{n+1} - c_{j-1}^{n+1}) \tag{2.14}$$

The first order upwind scheme is first order accurate in time and first order accurate in space. To prove this method's accuracy a Taylor series can be used to obtain the truncation error and, if $u > 0$ and the explicit time scheme is used, the following equation can be written (Ullrich (2010)):

$$\left[\frac{c_j^{n+1} - c_j^n}{\Delta t} + u\frac{c_j^n - c_{j-1}^n}{\Delta x}\right] - \left[\frac{\partial c}{\partial t} + u\frac{\partial c}{\partial x}\right] = \frac{\Delta t}{2}\frac{\partial^2 c}{\partial t^2} - u\frac{\Delta x}{2}\frac{\partial^2 c}{\partial x^2} + \ldots \tag{2.15}$$

The truncation error is then:

$$\frac{\Delta t}{2}\frac{\partial^2 c}{\partial t^2} - u\frac{\Delta x}{2}\frac{\partial^2 c}{\partial x^2} + \ldots \tag{2.16}$$

which is $\mathscr{O}(\Delta t)$ and $\mathscr{O}(\Delta x)$, which are both to the power of 1. This shows the first order accuracy mentioned before in time and space. Also, since the truncation error is $\mathscr{O}(\Delta t, \Delta x)$ it approaches zero as $\Delta t \rightarrow 0$ and $\Delta x \rightarrow 0$, meaning that it is a consistent scheme (Ullrich (2010)).

In terms of stability, the explicit upwind scheme is said stable when $CFL \leq 1$. If the condition for stability is met, and since this method its proven consistent, the explicit upwind scheme meets the convergence requirement (Mulder (2020)). In regards to the implicit upwind scheme, this scheme is unconditionally stable, for the same reasons that were explained in the previous subchapters.

2.2.3.2 Second order Central scheme

In relation to the central scheme, which is also known in the literature as the Forward Time Centered Space (FTCS) scheme, is discretized in time with the forward time difference scheme (Equation 2.6) and discretized in space with the central difference scheme (Equation 2.4). As such, the discretized equations associated with it are Equation 2.17 and Equation 2.19.

For the central scheme, with explicit time stepping (Zijlema (2015)):

$$\frac{c_j^{n+1} - c_j^n}{\Delta t} + u\frac{c_{j+1}^n - c_{j-1}^n}{2\Delta x} = 0 \tag{2.17}$$

Which, considering the Courant number (Equation 2.11), can then be rewritten as the following equation:

$$c_j^{n+1} = c_j^n - \frac{CFL}{2}(c_{j+1}^n - c_{j-1}^n) \tag{2.18}$$

If instead, implicit time stepping is considered (Chandrashekar (2013)):

$$\frac{c_j^{n+1} - c_j^n}{\Delta t} + u\frac{c_{j+1}^{n+1} - c_{j-1}^{n+1}}{2\Delta x} = 0 \tag{2.19}$$

Also, considering the Courant number (Equation 2.11), the implicit version can then be rewritten as follows:

$$c_j^{n+1} = c_j^n - \frac{CFL}{2}(c_{j+1}^{n+1} - c_{j-1}^{n+1}) \tag{2.20}$$

As shown before, with the use of the Taylor series the truncation error can be obtained and so the following equation can be written for the explicit central scheme:

$$\left[\frac{c_j^{n+1} - c_j^n}{\Delta t} + u\frac{c_{j+1}^n - c_{j-1}^n}{2\Delta x}\right] - \left[\frac{\partial c}{\partial t} + u\frac{\partial c}{\partial x}\right] = \frac{\Delta t}{2}\frac{\partial^2 c}{\partial t^2} - u\frac{\Delta x^2}{6}\frac{\partial^3 c}{\partial x^3} + \ldots \tag{2.21}$$

The truncation error is then:

$$\frac{\Delta t}{2}\frac{\partial^2 c}{\partial t^2} - u\frac{\Delta x^2}{6}\frac{\partial^3 c}{\partial x^3} + \ldots \tag{2.22}$$

which shows $\mathcal{O}(\Delta t)$ and $\mathcal{O}(\Delta x^2)$. This shows that this scheme is first order accurate in time and second order accurate in space. This method is considered consistent since the truncation error is $\mathcal{O}(\Delta t, \Delta x^2)$ and for this reason it nullifies if $\Delta t \to 0$, $\Delta x \to 0$. Besides this, the implicit central scheme has also the same truncation error, being also considered first order accurate in time and second order accurate in space and consistent (Mulder (2020)).

In terms of stability the explicit central scheme shows to be unstable for any value of Courant number, which makes it useless in practice (Chandrashekar (2013)). However the implicit central scheme is considered unconditionally stable.

2.2.3.3 TVD scheme with flux limiter

Conventional finite difference schemes like the ones mentioned before, frequently give poor results for problems with discontinuities in their solutions (Shu (1988); Ascher (2008)). Therefore TVD schemes with flux limiter can be used as an alternative to resolve such problems, since these have high-order accuracy in smooth regions and are capable of resolving the discontinuities without invalid oscillations, usually giving very good results (Shu (1988); Zhang et al. (2015)).

This is because in a TVD the amount of oscillations decreases in time, thus the name "Total Variation Diminishing", as mentioned by Bertoluzza et al. (2009). Also, accordingly to Laney (1998), TVD implies monotonicity preservation, being an optimal scheme in cases where is hard to achieve monotonicity, but it is to be avoided in cases where monotonicity preservation is easy to be achieved, with the consequence of intensifying that effect.

In this case, a TVD scheme with a flux limiter is discretized in time with the forward time difference scheme (Equation 2.6) and discretized in space with a combination of a first order scheme and a second order scheme. The main idea of using a first order scheme and a second order scheme, to discretize space, is to combine the advantages of both. As mentioned before, higher order schemes are capable of producing solutions with a better accuracy than low order schemes. However, the downside of high order schemes is their dispersive nature, which can lead them to fail when they encounter regions containing sharp gradients or discontinuities, introducing nonphysical oscillations. On the other hand, low order schemes are known to be very diffusive. This diffusive nature make low order schemes capable of producing results in regions with discontinuities or sharp gradients, without producing nonphysical oscillations. Therefore, TVD schemes with flux limiter are capable of changing between a first order scheme and a second order scheme, depending on the situation. For smooth regions the second order scheme gives high accuracy solutions and in regions with sharp gradients or with discontinuities the low order scheme is capable of giving solutions without spurious oscillations. (Hellevik (2020))

For a TVD scheme with flux limiter the discretized equations associated with it are Equation 2.23, for an explicit time stepping and Equation 2.32 an implicit time stepping (Hellevik (2020)). As such, if an explicit time stepping is considered the schemes necessary for the TVD method can be written in terms of the numerical flux limiter function, ϕ:

$$\frac{c_j^{n+1} - c_j^n}{\Delta t} + \frac{F^n_{j+\frac{1}{2}} - F^n_{j-\frac{1}{2}}}{\Delta x} = 0 \tag{2.23}$$

Where $F^n_{j+\frac{1}{2}}$ can be calculated by:

$$F^n_{j+\frac{1}{2}} = f^{low}_{j+\frac{1}{2}} - \phi(r_j).(f^{low}_{j+\frac{1}{2}} - f^{high}_{j+\frac{1}{2}}) \tag{2.24}$$

And where $F^n_{j-\frac{1}{2}}$ can be calculated by:

$$F^n_{j-\frac{1}{2}} = f^{low}_{j-\frac{1}{2}} - \phi(r_{j-1}).(f^{low}_{j-\frac{1}{2}} - f^{high}_{j-\frac{1}{2}}) \tag{2.25}$$

The low resolution fluxes, $f^{low}_{j+\frac{1}{2}}$ and $f^{low}_{j-\frac{1}{2}}$, are obtained from an upwind scheme (Equation 2.26 and Equation 2.27), the high resolution ones, $f^{high}_{j+\frac{1}{2}}$ and $f^{high}_{j-\frac{1}{2}}$, are obtained from a Lax-Wendroff scheme (Equation 2.28 and Equation 2.29) and the gradients, r_j and r_{j-1} obtained from Equation 2.30 and Equation 2.31, respectively:

$$f^{low}_{j+\frac{1}{2}} = uc^n_j \tag{2.26}$$

$$f^{low}_{j-\frac{1}{2}} = uc^n_{j-1} \tag{2.27}$$

$$f^{high}_{j+\frac{1}{2}} = u(\frac{c^n_{j+1}+c^n_j}{2}) - u\frac{CFL}{2}(c^n_{j+1}-c^n_j) \tag{2.28}$$

$$f^{high}_{j-\frac{1}{2}} = u(\frac{c^n_j+c^n_{j-1}}{2}) - u\frac{CFL}{2}(c^n_j-c^n_{j-1}) \tag{2.29}$$

$$r_j = \frac{c^n_j - c^n_{j-1}}{c^n_{j+1}-c^n_j} \tag{2.30}$$

$$r_{j-1} = \frac{c^n_{j-1} - c^n_{j-2}}{c^n_j-c^n_{j-1}} \tag{2.31}$$

If instead implicit time stepping is considered, all implicit schemes necessary for the TVD method can be written in terms of the numerical flux limiter function, ϕ:

$$\frac{c^{n+1}_j - c^n_j}{\Delta t} + \frac{F^{n+1}_{j+\frac{1}{2}} - F^{n+1}_{j-\frac{1}{2}}}{\Delta x} = 0 \tag{2.32}$$

Where $F^{n+1}_{j+\frac{1}{2}}$ can be calculated by:

$$F^{n+1}_{j+\frac{1}{2}} = f^{low}_{j+\frac{1}{2}} - \phi(r_j).(f^{low}_{j+\frac{1}{2}} - f^{high}_{j+\frac{1}{2}}) \tag{2.33}$$

And where $F^{n+1}_{j-\frac{1}{2}}$ can be calculated by:

$$F^{n+1}_{j-\frac{1}{2}} = f^{low}_{j-\frac{1}{2}} - \phi(r_{j-1}).(f^{low}_{j-\frac{1}{2}} - f^{high}_{j-\frac{1}{2}}) \tag{2.34}$$

the low resolution fluxes, $f^{low}_{j+\frac{1}{2}}$ and $f^{low}_{j-\frac{1}{2}}$, are obtained from the upwind scheme (Equation 2.35 and Equation 2.36), the high resolution ones, $f^{high}_{j+\frac{1}{2}}$ and $f^{high}_{j-\frac{1}{2}}$, are obtained from the central scheme (Equation 2.37 and Equation 2.38) and the gradients, r_j and r_{j-1} obtained from Equation 2.30 and Equation 2.31, respectively:

$$f^{low}_{j+\frac{1}{2}} = uc^{n+1}_j \tag{2.35}$$

$$f^{low}_{j-\frac{1}{2}} = uc^{n+1}_{j-1} \tag{2.36}$$

$$f^{high}_{j+\frac{1}{2}} = u(\frac{c^{n+1}_{j+1} + c^{n+1}_{j}}{2}) \tag{2.37}$$

$$f^{high}_{j-\frac{1}{2}} = u(\frac{c^{n+1}_{j} + c^{n+1}_{j-1}}{2}) \tag{2.38}$$

The main reason why TVD schemes are able to change between a first order scheme and a second order scheme, producing high resolution solutions without spurious oscillations, is because of the flux limiters associated with them (Sweby (1984)). As mentioned by Kärrholm and Tao (2008), there are many possible limiter functions and each one has its own pros and cons. As such, they do not work well for every existing problem. As such, there is a necessity to find the optimal flux limiter for each case and since there is a big array of limiter functions, only the ones studied will be mentioned in the next subchapter.

2.2.4 Discretization methods studied

The three discretization schemes studied in this dissertation were the Backward Linear Limited TVD scheme, the Backward Van Leer limited TVD scheme and the Crank-Nicolson Linear Limited TVD scheme. Also, an implicit time stepping was considered and, as such, the schemes will be presented in their implicit format.

In the first place, the simulations of the transport of a passive scalar in this dissertation were produced with the use of the OpenFOAM tool. In the OpenFOAM tool the backward time scheme is second order accurate in time, instead of the previously mentioned backward time scheme (Equation 2.7), that was first order accurate in time. According with (OpenCFD Ltd (-a)), this scheme is implicit and conditionally stable, and the expression associated with it will be:

$$\frac{\partial c}{\partial t} = \frac{3c(x,t+\Delta t) - 4c(x,t) + c(x,t-\Delta t)}{2\Delta t} + \mathscr{O}(\Delta t^2) \tag{2.39}$$

2.2.4.1 Backward linear limited TVD scheme

The backward linear limited TVD scheme is discretized in time with the second order backward time scheme (Equation 2.39) and discretized in space with the combination of the upwind scheme and the central scheme, mentioned before for the implicit TVD scheme approach. Therefore the discretized equation associated with this scheme is:

$$\frac{\frac{3}{2}c^{n+1}_{j} - 2c^{n}_{j} + \frac{1}{2}c^{n-1}_{j}}{\Delta t} + \frac{F^{n+1}_{j+\frac{1}{2}} - F^{n+1}_{j-\frac{1}{2}}}{\Delta x} = 0 \tag{2.40}$$

Where $F^{n+1}_{j+\frac{1}{2}}$ is Equation 2.24 and $F^{n+1}_{j-\frac{1}{2}}$ is Equation 2.25.

When using a TVD scheme, a flux limiter has to be chosen. As mentioned before, in the literature there are a lot to choose from, and is important to be aware that some are better for certain cases compared to others. According to Kärrholm and Tao (2008) there is no reference for the Linear Limited flux limiter (known as Limited Linear in the OpenFOAM toolbox), since it is an OpenFOAM "invention". Equation 2.41 defines the Linear Limited flux function.

$$\phi(r) = max\left[0, min\left(\frac{2}{cof}r, 1\right)\right] \tag{2.41}$$

Where r is the gradient (Equation 2.30 and Equation 2.31) and where *cof*, which is the Linear Limited OpenFOAM coefficient, can be set by the user at a value between 0 and 1 (by default 1).

2.2.4.2 Backward Van Leer limited TVD scheme

As well as the scheme mentioned above, the Backward VanLeer limited TVD scheme also uses the backward time scheme for the discretization in time and for the discretization in space, the implicit TVD approach mentioned before. As such the equation used for the Backward Linear Limited scheme (Equation 2.40) will also be used for this TVD scheme. The main difference will be the flux limiter, which for this one will be the Van Leer flux limiter (Leer (1974)), as defined in Equation 2.42.

$$\phi(r) = \frac{r + |r|}{1 + |r|} \tag{2.42}$$

Where r is the gradient (Equation 2.30 and Equation 2.31).

2.2.4.3 Crank-Nicolson Linear Limited TVD scheme

In regards to the Crank-Nicolson Linear Limited TVD scheme, this is discretized in time with the Crank-Nicolson time scheme and discretized in space with the implicit TVD approach as well. This time scheme is second order accurate, implicit and unconditionally stable (Adak (2020); Mulder (2020)).

The Crank-Nicolson scheme in its pure form can be interpreted as a two-step scheme. Therefore, the time step, Δt, is split in two consecutive sub steps, $\Delta t/2$ (Mulder (2020)). For the first sub step the implicit Euler time stepping method is applied:

$$\frac{c_j^{n+\frac{1}{2}} - c_j^n}{\Delta t/2} + \frac{F^{n+\frac{1}{2}}_{j+\frac{1}{2}} - F^{n+\frac{1}{2}}_{j-\frac{1}{2}}}{\Delta x} = 0 \tag{2.43}$$

For the second sub step the implicit Euler time stepping method is also applied:

$$\frac{c_j^{n+1} - c_j^{n+\frac{1}{2}}}{\Delta t/2} + \frac{F_{j+\frac{1}{2}}^{n+\frac{1}{2}} - F_{j-\frac{1}{2}}^{n+\frac{1}{2}}}{\Delta x} = 0 \tag{2.44}$$

Taking the sum of these two sub steps (Equation 2.43 and Equation 2.44) and dividing both terms by 2, yields the pure Crank-Nicolson, in which its expression is:

$$\frac{c_j^{n+1} - c_j^{n}}{\Delta t} + \frac{F_{j+\frac{1}{2}}^{n+\frac{1}{2}} - F_{j-\frac{1}{2}}^{n+\frac{1}{2}}}{\Delta x} = 0 \tag{2.45}$$

According to the OpenFOAM user guide (OpenCFD Ltd (-b)), the Crank-Nicolson scheme, in OpenFOAM, blends the pure Crank-Nicolson scheme with the implicit Euler scheme:

$$\frac{c_j^{n+1} - c_j^{n}}{\Delta t} + ocCof * \left(\frac{F_{j+\frac{1}{2}}^{n+\frac{1}{2}} - F_{j-\frac{1}{2}}^{n+\frac{1}{2}}}{\Delta x} \right) + (1 - ocCof) * \left(\frac{F_{j+\frac{1}{2}}^{n+1} - F_{j-\frac{1}{2}}^{n+1}}{\Delta x} \right) = 0 \tag{2.46}$$

Where *ocCof* can be between 0 and 1. In case of *ocCof*=1 the pure Crank-Nicolson scheme is adopted, for *ocCof*=0 the implicit Euler method is adopted. For robustness, a value of 0.9 is used. The Linear Limited flux is introduced in the equation, by replacing the F variable with the Linear Limited scheme, as shown before.

Chapter 3

1D advection problem

A simple 1D advection problem was formulated in order to demonstrate the performance of the different discretization schemes introduced in Chapter 2 by comparing their approximated finite-difference solutions with the known exact solution. Note that most of the times the exact solution for a problem is unknown. However since this problem was devised for demonstration purposes the exact solution is known.

3.1 Mathematical formulation

In this dissertation a general one-dimensional transport equation of the advection-diffusion type in a finite spatial domain was considered for a made up 1D advection problem as defined in Equation 3.1.

$$\frac{\partial c}{\partial t} + u\frac{\partial c}{\partial x} = K\frac{\partial^2 c}{\partial x^2} \tag{3.1}$$

Here c is a quantity (e.g the concentration of a pollutant dissolved in the water) transported along a flow with velocity u $[m/s]$ and K $[m^2/s]$ is the diffusivity of the substance in the flow. Furthermore t and x represent time and space co-ordinate, respectively. In order to make the problem simpler to be solved, the diffusivity was neglected (i.e. $K = 0$). The equation 3.1 was then reduced to a pure advection equation (Equation 3.2).

$$\frac{\partial c}{\partial t} + u\frac{\partial c}{\partial x} = 0 \tag{3.2}$$

With an initial condition,

$$c(x, t = 0) = f(x), \tag{3.3}$$

With spatial domain $0 \leq x \leq L$, and with a boundary condition,

$$c(x = 0, t) = g(t), \tag{3.4}$$

With time domain $0 \leq x \leq T$.

3.2 Parameters and results

The parameters and values used for this problem are shown in Table 3.1.

Table 3.1: Parameters considered for the 1D advection problem.

L [m]	T [s]	u [m/s]	f(x) [%]	g(t) [%]	M	N	Δ x [m]	Δ t [s]	CFL
100	60	0.9	0	1	100	60	1	1	0.9

Here, L is the maximum spatial domain and T is the maximum time domain, u is the velocity of the flow and f(x) and g(x) the initial condition and the boundary condition, respectively. M is the number of intervals in the spatial domain with spatial step Δx and N the number of intervals in the time domain with time step Δt and CFL the courant number.

Knowing the velocity of the flow, the time step and the two conditions $f(x)$ and $g(t)$ (Equation 3.3 and Equation 3.4), it is known that the exact solution for this problem is a step function at $x = 0.9$ m/s $*$ 60 s $=$ 54 m, where the concentration suddenly drops from 1 % to 0 %.

As such a pure advection equation was considered (Equation 3.2), which was then solved, by means of three different numerical schemes (Backward Linear Limited TVD scheme, Backward Van Leer limited TVD scheme and Crank-Nicolson Linear Limited TVD scheme). To produce the results for the different schemes, Matlab scripts were used. The solutions for each scheme and comparison with the exact solution are shown in Figure 3.1, Figure 3.2 and Figure 3.3.

At first sight, it can be said that all three schemes suffered from numerical diffusion (i.e. amplitude errors, mentioned in Subchapter 2.2.1), since their solutions differ in amplitude from the exact solution. This was expected, since as mentioned before, the flux limiters in the TVD schemes exist to circumvent critical conditions, such as steep gradients or discontinuities, by changing from a high-order scheme to a low-order diffusive scheme, at these locations in the solution, and changing back to a high-order scheme where the solution is smooth (Zhang et al. (2015)). This way it prevents spurious oscillations from happening, thus these schemes are normally monotone, which can also be observed in the results for this 1D problem, since the concentration stayed between 1 and 0, for the exception of the Backward Van Leer scheme. In regards to their performance, the Backward LinearLimited TVD and the Crank-Nicolson LinearLimited TVD schemes showed to be very similar in terms of accuracy. However, between the two, the first one seemed to have an easier time to capture the jump, although the difference was very small.

The Backward Van Leer Limited TVD scheme, revealed to be the best to more sharply capture the jump. However showed higher difficulty to maintain boundedness, going above 1 % concentration around $x = 10$ m. Although instability is related to spurious oscillations, the spurious oscillations in this case don't mean that this scheme is unstable. If this scheme was unstable the spurious oscillations would cover the complete computational domain, which is not what is observed in Figure 3.3.

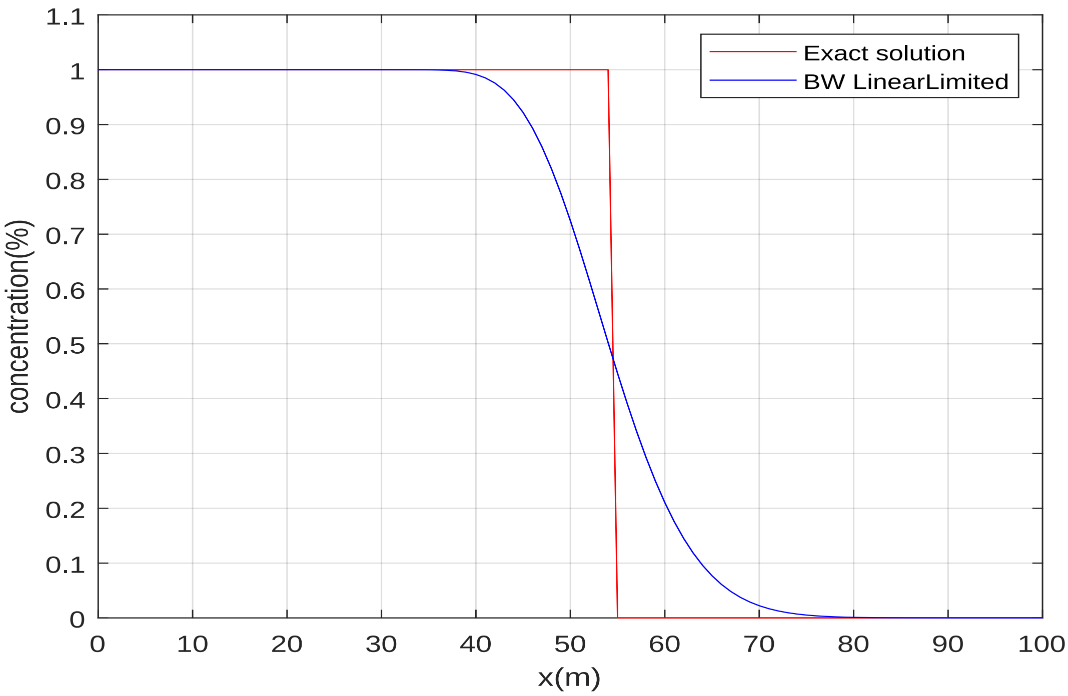

Figure 3.1: Backward Linear Limited 1D advection problem solution versus exact solution.

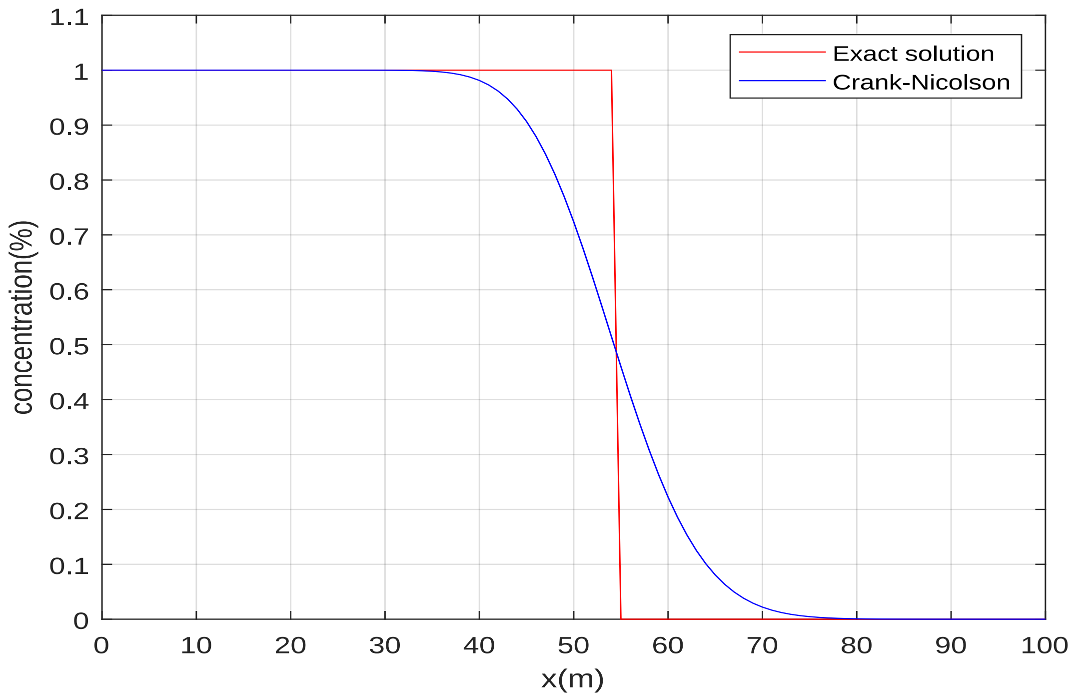

Figure 3.2: Crank-Nicolson Linear Limited 1D advection problem solution versus exact solution.

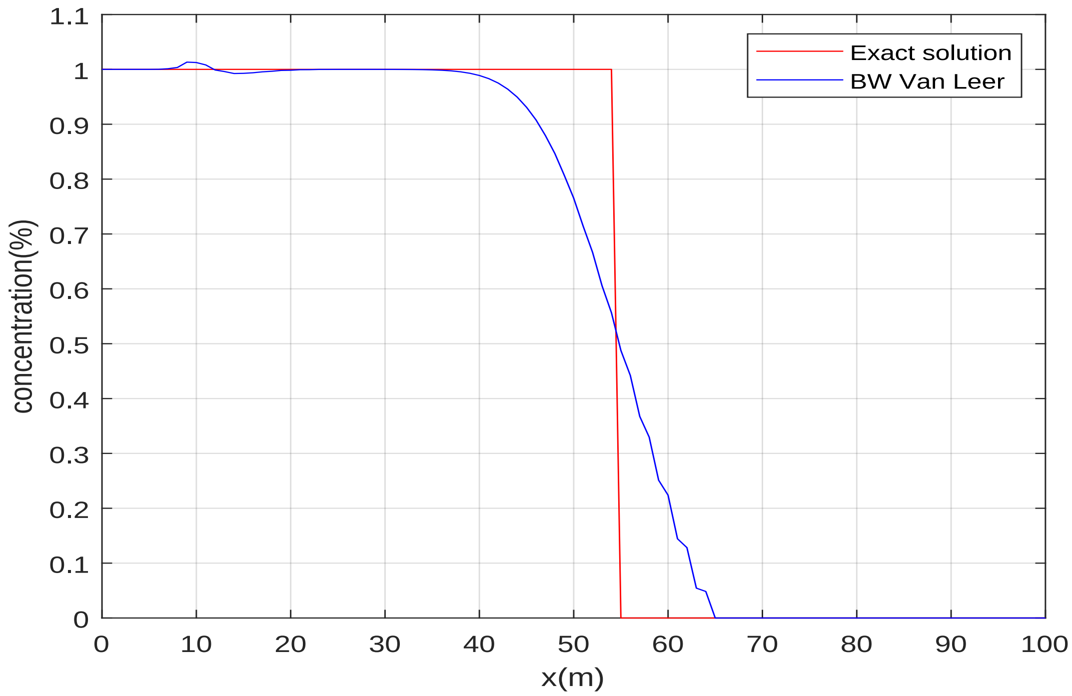

Figure 3.3: Backward Van Leer 1D advection problem solution versus exact solution.

Chapter 4

Description of LES simulations

4.1 Flow domain and flow conditions

In this dissertation, by making use of the OpenFOAM toolbox, the turbulent open-channel flow, at the laboratory flume at UGent, was modeled through the use of the Large Eddy Simulation technique, using a standard Smagorinsky SGS model, with a Smagorinsky constant, C_s, of 0.158 (Rodi et al. (2013)) and the governing Navier-Stokes, continuity and scalar transport equations were discretized using the Finite Volume Method and coupled using the PISO algorithm.

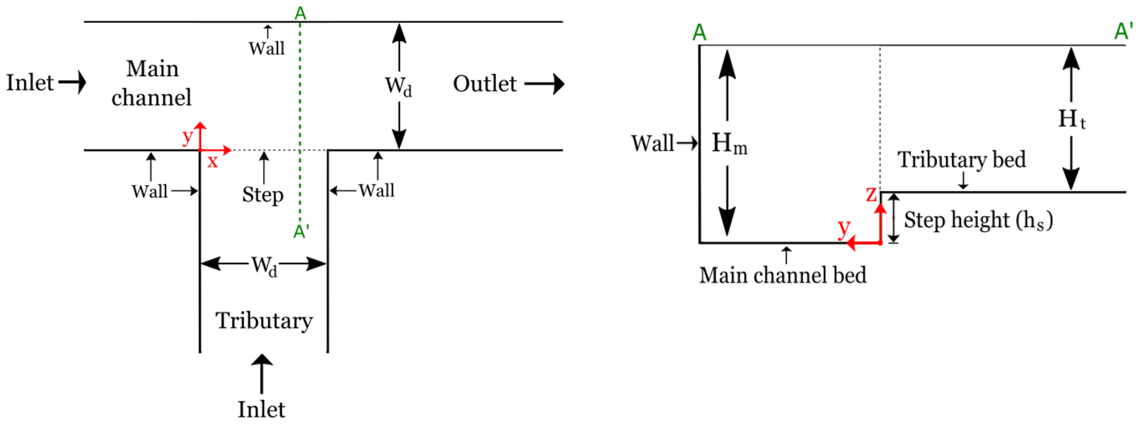

Figure 4.1: Schematic representation of the laboratory flume at UGent.

A schematic representation of the flume can be observed in Figure 4.1. Through observation of the scheme, is possible to understand the chosen coordinate system. The positive x-axis was oriented in the downstream direction of the main channel, the positive y-axis oriented in the downstream direction of the tributary, pointing to the main channel wall opposite to the step and the positive z-axis is oriented upwards in the vertical direction. The origin of the coordinate system was situated at the bed level of the main channel at the upstream corner of the channel junction.

The open-channel confluence had rectangular channels with equal width (W_d) and with discordant and horizontal beds. The bed discordance ratio is defined as:

$$\sigma = \frac{h_s}{h_d} \tag{4.1}$$

Where h_s is the height of the step and h_d the downstream water depth. It is important to also refer the discharge ratio, q, which is an important parameter influencing how the three-dimensional flow behaves (Schindfessel (2017)):

$$q = \frac{Q_{main}}{Q_{tot}} = \frac{Q_{main}}{Q_{main} + Q_{trib}} \tag{4.2}$$

Where Q_{main} is the entering discharge of the main channel, Q_{trib} the tributary one and Q_{tot} is the downstream discharge. Not only the discharge ratio is important, but also the downstream Froude number, Fr, is to be accounted for since it affects the flow patterns and water level (Ramos et al. (2019b)):

$$Fr = \frac{u_d}{\sqrt{g h_d}} \tag{4.3}$$

Where u_d is the averaged downstream velocity and g the gravitational acceleration. The lab conditions at UGent were a Froude scaled version of Weber et al. (2001), with a downstream Froude number Fr$\approx$ 0.36 and a flow ratio q$\approx$ 0.583. This selected flow situation is linked to a downstream Reynolds number, Re of around 73721, which ensures a turbulent flow.

Table 4.1: Flow conditions used in the simulations.

h_d [m]	q [-]	σ [-]	h_s [m]	u_d [m/s]	Q_{tot} [m^3/s]	Q_{main} [m^3/s]	Q_{trib} [m^3/s]	Re [-]	Fr [-]
0.148	0.583	0.25	0.037	0.435	0.0257	0.015	0.0107	73721	0.361

4.2 Numerical domain and mesh

The numerical domain of the studied flume was discretized through structured meshes and it is presented in Figure 4.2. All distances were normalized by the channel width, $W_d = 0.40$ m, which makes data simpler to be visualized and analyzed. As such the x, y and z vectors are transformed into dimensionless vectors named x/W_d, y/W_d and z/W_d, respectively. Both tributary and the upstream main channel had a length of 5 W_d (2 m) and the downstream main channel a length of 10 W_d (4 m). The height of the domain, from the channel bed, was 0.375 W_d (0.15 m), which means that the main channel height would be the same as the domain height, and the height of the tributary would be 0.2825 W_d (0.113 m), because of the step height, h_s. However since an approximation to a free-surface was considered instead of a rigid lid (explained in Sub-section 4.3), the channels heights varied throughout the channels, instead of having the fixed values mentioned before. As such, in Table 4.2, $\sim W_d$ means a variable water surface height.

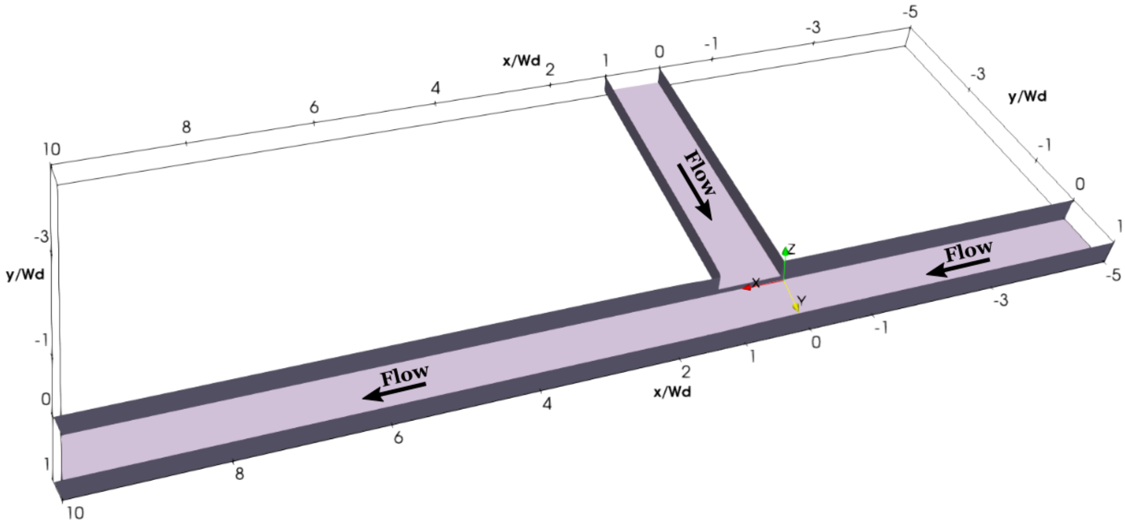

Figure 4.2: 3D simulation domain of the studied numerical flume.

The meshes were generated using the OpenFOAM utility, *blockMesh*. *BlockMesh* reads from a dictionary file named *blockMeshDict*, where the user provides different parameters such as the size and geometry of each hexahedral block, which then are aggregated and the mesh is generated (Greenshields (2018)). The number of cells and their expansion ratio, which allows the mesh to be refined or graded, can be specified, providing the user with more control over the mesh. The amount of cells used for the main and tributary channels are presented in Table 4.2.

Table 4.2: Number of mesh cells in the domain.

	Upstream channels				**Downstream main channel**		
Spatial dimension	Longitudinal	Lateral	Vertical$_{main}$	Vertical$_{trib}$	Longitudinal	Lateral	Vertical
Lenght Scale	$5W_d$	W_d	$\sim W_d$	$\sim W_d$	$10W_d$	W_d	$\sim W_d$
Number of Cells	1050	80	45	33	1350	80	45

The upstream main channel and the upstream tributary channel both have the same length and width, but their height differs, because of the bed discordance between the main and tributary channel beds. As such the upstream tributary channel has less amount of cells in comparison with the amount of cells in the upstream main channel.

The cells in the confluence zone, where both channels meet, were graded and refined to ensure that the numerical model was able to resolve accurately the high turbulence scales of this particularly complex zone of the flow. Since LES only resolves the turbulence scales that are bigger than the mesh size, the size of the cells at x/W_d=0 were made smaller and the following cells were progressively stretched in the x direction until x/W_d=1, where the cells were the same size as the cells outside of this zone (Figure 4.3). As such, by decreasing the size of the cells in this specific

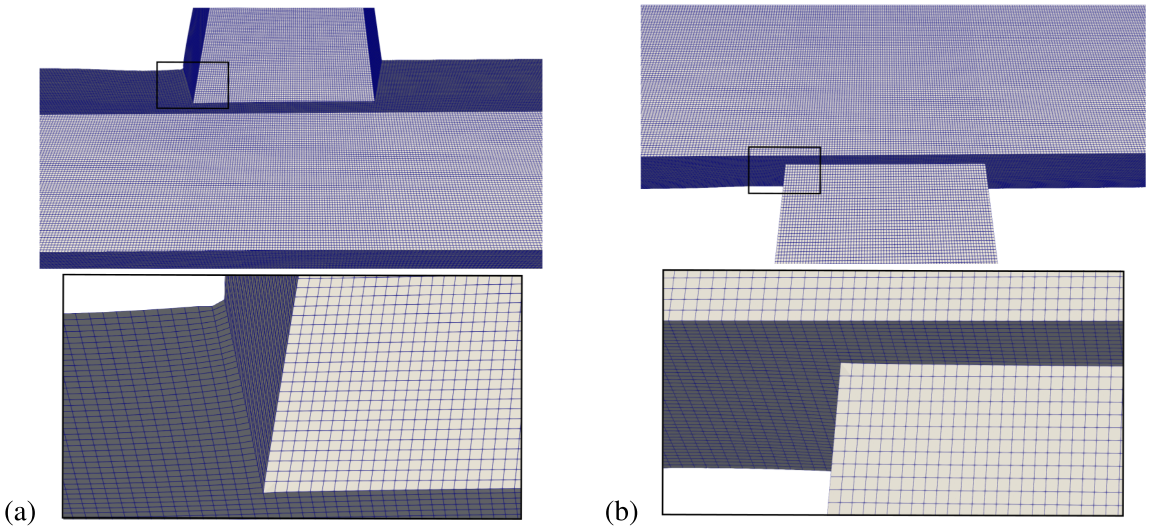

Figure 4.3: Confluence mesh: (a) top view of the downstream junction corner; (b) bottom view of the downstream junction corner.

zone and not the entirety of the mesh (with zones of no significant importance for this study), is possible to assure better results with less computational power, which increases with the decrease in size of each cell in the mesh.

4.3 Boundary conditions

The LES simulations are performed in finite-size computational domains chosen by the user, using the OpenFOAM capabilities. As such, in order to solve the governing differential equations it is required to set appropriate boundary conditions for the considered variables, at all boundaries (Schindfessel (2017)). The domain boundaries were as illustrated in Figure 4.4 and the considered variables were the pressure, the subgrid-scale viscosity, the velocity vector and the passive scalar transport concentration.

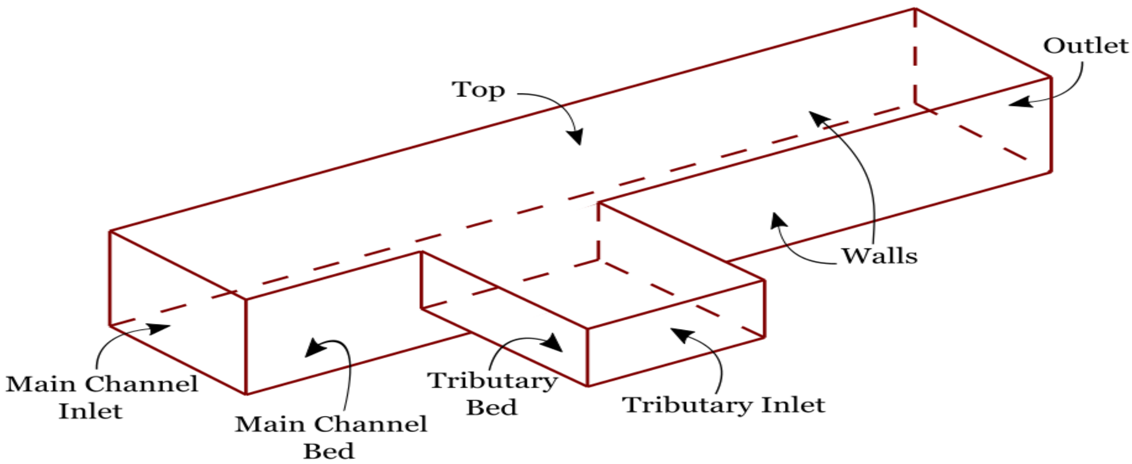

Figure 4.4: Scheme of the considered boundaries in the simulation.

As described by Tabor and Baba-Ahmadi (2010), turbulence at the inlet contributes to the turbulence within the domain, for the exception of some cases, and the boundary should vary stochastically and enable turbulent properties to be easily specified. The inlet velocity should then be turbulent, providing a more realistic boundary condition. This was done by mapping a specified flow field in the inlet for each tributary and main channel, like in the work of Schindfessel (2017).

A zero gradient boundary condition was implemented on the velocity at the outlet, meaning that the velocity is developed in space and its gradient is equal to zero, perpendicular to the boundary (OpenCFD Ltd (-d)). At the walls and at the beds of the channels the boundary condition sets the velocity to zero. For the top boundary a curved rigid-lid is considered, in order to have a better approximation to a free-surface. Therefore a slip condition is used for the velocity, meaning that the top has no effect on the fluid velocity in the planes parallel and close to the boundary. As described by Ramos et al. (2019b) the curved rigid-lid is defined as the surface elevation that evolves from the time-averaged pressure field in the flat rigid-lid simulation. The height of the surface elevation can be deduced through Equation 4.4.

$$h_{CRL} = h_{FRL} + \frac{pMean}{\rho g} \tag{4.4}$$

Where h_{CRL} is the curved rigid lid height from the channel bed, h_{FRL} is the flat rigid lid height from the channel bed, pMean is the averaged pressure on the flat lid, ρ and g are the density of the fluid and the gravitational acceleration, respectively.

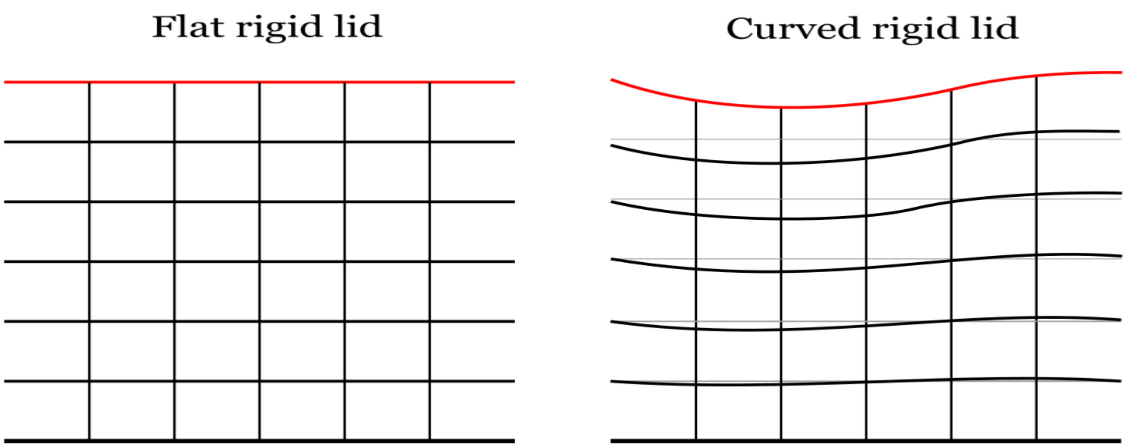

Figure 4.5: Schematic view of a Rigid Lid versus a Curved Rigid Lid (adapted from Ramos et al. (2019b)).

In relation to the subgrid-scale viscosity a zero gradient condition was set for the tributary and main channel inlets, at the outlet and at the top. For the walls and bed, a condition is set where the wall roughness is considered. This was done through the use of a wall model available in OpenFOAM, *nutURoughWallFunctionFvPatchScalarField* (OpenCFD Ltd (-c)).

For the pressure a zero gradient condition was set for both inlets, walls, top and at the outlet the boundary condition setting its value to zero.

The boundary conditions applied for the passive scalar concentration, s, was a zero gradient to all boundaries, for the exception of the main inlet, which was fixed to zero, and the tributary inlet, fixed to one.

4.3.1 Mixing of the passive scalar

The dimensionless parameter E, used by Dalmon et al. (2015), is adopted to quantify the non-uniformity of mixing, downstream of the confluence:

$$E = \frac{1}{s_{us}} \left(\sum_{n=1}^{n} \frac{A_i (sMean_i - s_{avg})^2}{A_{cs}} \right)^{1/2} \tag{4.5}$$

Where, s_{us} is the imposed upstream concentration (i.e the concentration, in this case, at the tributary inlet), n is the number of mesh cells in a cross-section with total area A_{cs}, $sMean_i$ is the time-averaged concentration in a mesh cell in the cross-section, with area A_i (i.e $\sum_{n=1}^{n} A_i = A_{cs}$), and s_{avg} is the total averaged concentration at the cross section. When the dimensionless parameter E assumes a zero value, it is considered that the flow achieved complete mixing.

Chapter 5

Results and Discussion

5.1 Surface water levels

Since it was used a curved rigid lid to approximate the surface water levels to a free-surface in all simulations it can be said that the surface water heights were not accurately calculated, but instead deduced from the time-averaged pressure on the rigid-lid simulation, as given by Equation 4.4. As such, Figure 5.1 gives the longitudinal surface water levels along the main channel, for three lateral positions. It is important to note that the values shown in Figure 5.1 are the same between all considered simulations, since the considered boundaries do not change from simulation to simulation and the pressure was solved the same way for all of them (see Subchapter 4.3).

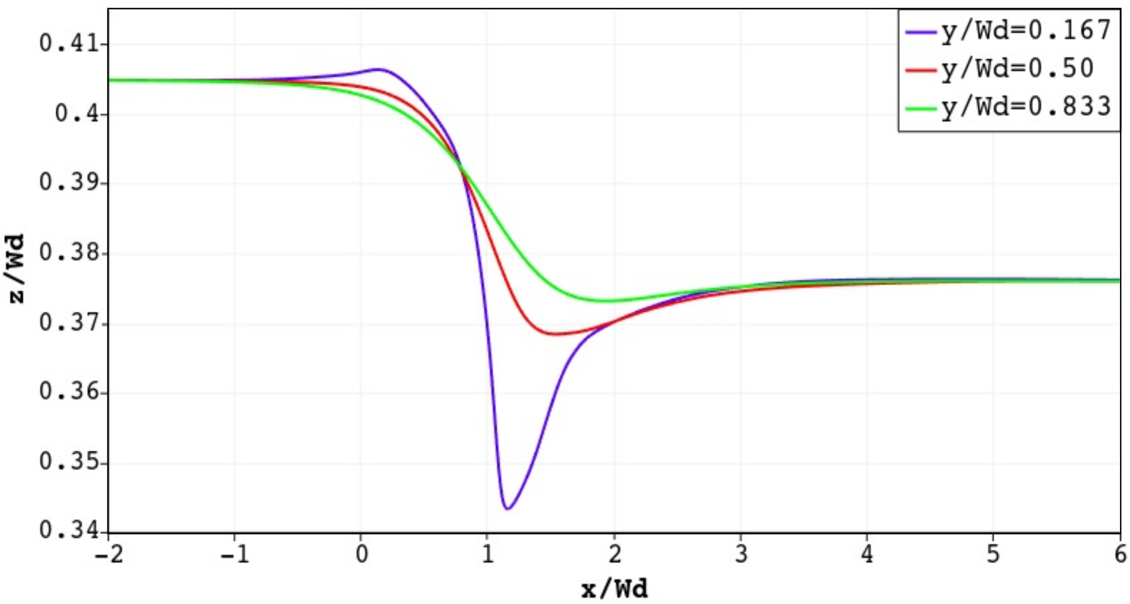

Figure 5.1: Surface water profile along the main channel.

Although it was not possible to validate the model through experimental work, the work of Ramos et al. (2019a) can be used as reference since a similar 90^{o} open-channel confluence with a bed discordance ratio of 0.25 was studied. Therefore by comparing the profile of the surface water levels in Figure 5.1 with the profile of the surface water levels in the work cited (see red dashed line in Figure C.1, Appendix C) is possible to see an approximate similarity between the two. As such, is possible to assume that the simulations in the present work might be valid, or close to it. Considering that the present flow conditions are a Froude-scaled version of the cited work, this might be one of the reasons for the distinguishable differences between the two. Notice that the considered confluence on the cited work has a channel width more than twice the size, compared to the one considered in the present work. It has been previously observed that the confluence channel size can affect the hydrodynamics in the CHZ (e.g. Ashmore and Parker (1983); Best and Reid (1984)), which can also be a reason for the differences in profiles. Note that the aforementioned comparison does not validate the passive scalar transport results but might validate the hydrodynamic results, which are resolved with the passive scalar transport in order to obtain the LES results.

5.2 Time-averaged concentrations

As a mean to analyze and compare the performance of the studied schemes on the simulation of a passive scalar concentration, a post-processing of the data was performed by using the open-source software ParaView version 5.8.1. As such 10 horizontal (i.e. through the z/W_d plane) and 8 vertical (i.e. through the x/W_d plane) cuts were made (See Appendix A). Note that, since there is very few literature relatively to the passive scalar concentration in confluences (Pouchoulin et al. (2018)), and since it was not possible to do experimental work for this dissertation due to the global pandemic caused by the virus Covid 19, the following results could not be validated. As such, is not possible to ascertain which of the schemes shows the most accurate results, but instead is possible to show the differences between each other providing information of what to expect when using one of these schemes to study the passive scalar concentrations in future works.

A plan view cut on $z/W_d = 0.25$ (Figure 5.2) and a cross sectional cut on $x/W_d = 2$ (Figure 5.3) of the time-averaged passive scalar concentration, for each scheme studied are presented. As mentioned before a pristine flow, coming from the upstream main channel, and a passive scalar with maximum concentration of 1, coming from the upstream tributary channel, was considered. Through observation alone of both figures, it could be said that the Backward Linear Limited TVD scheme seems to have the highest numerical diffusion from the three schemes, since it tends to smear out the strong gradients of the exact solution in the numerical solution, thus producing a fade effect (see Figure 5.2, between $x/wd = 5$ and $x/wd = 6.5$ and between $y/wd = 0.7$ and $y/wd = 1$). Likewise, the Backward Van Leer Limited TVD seems to have the least numerical diffusion, thus being the best to capture the high gradients. Numerical diffusion leads to less accurate results, specially since strong gradients will not appear where they are supposed to. Notice that, since there is no way to know the exact solution, is not possible to say with certainty that the Backward Linear Limited TVD scheme is in fact the one with the highest numerical diffusion and the Backwards Van Leer Limited TVD scheme the least, but the results from the 1D problem seem in accordance with the aforementioned assumption. Furthermore, this might be an explanation for the significant, although minimal, visible differences between the results of the schemes, which can be seen throughout all the downstream main channel flow (See Appendix A).

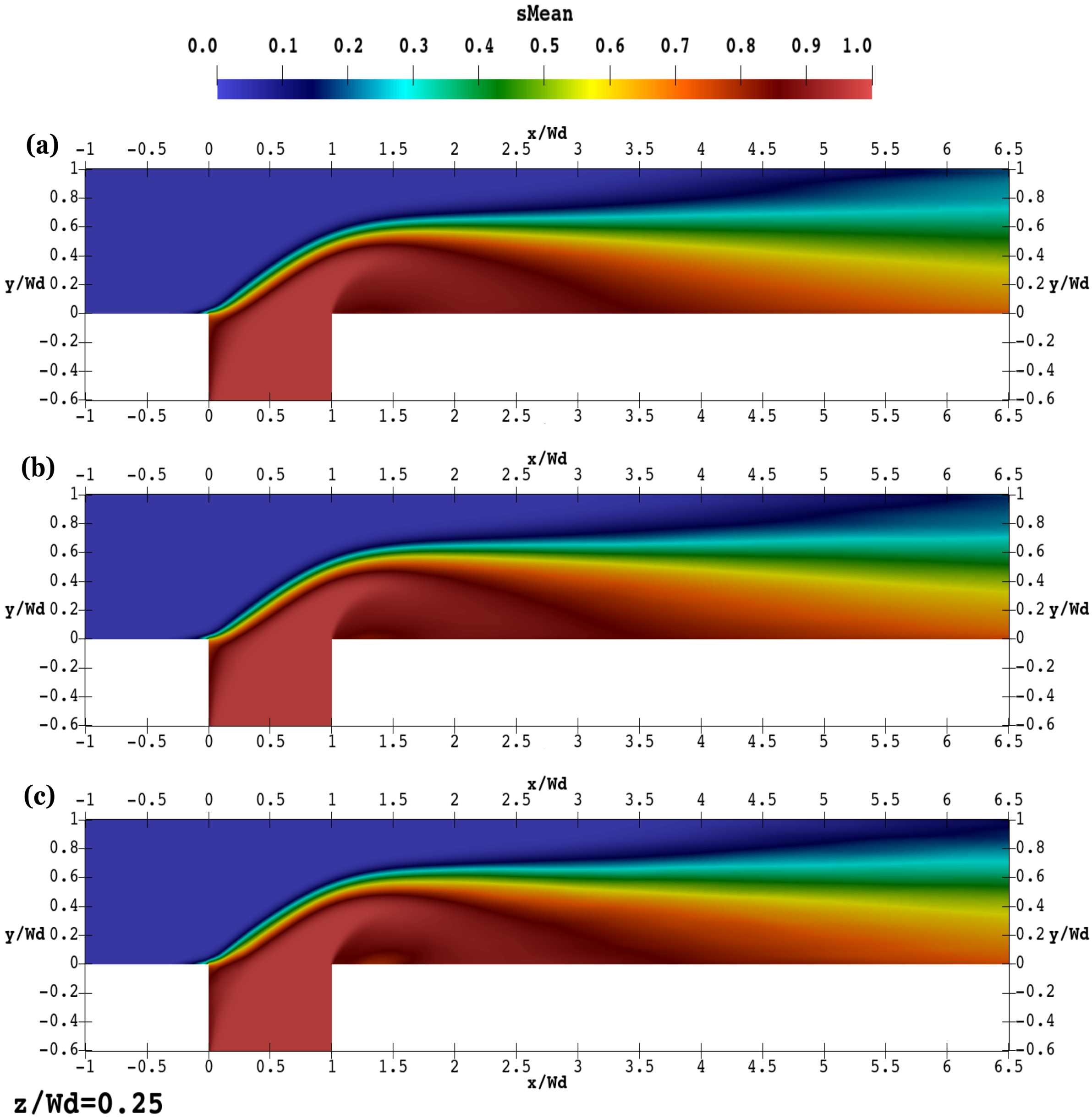

Figure 5.2: Time-averaged concentration, sMean, in the plan view $z/W_d = 0.25$ for the studied schemes: (a) Backward Linear Limited TVD scheme; (b) Crank-Nicolson Linear Limited TVD scheme; (c) Backward Van Leer Limited TVD scheme.

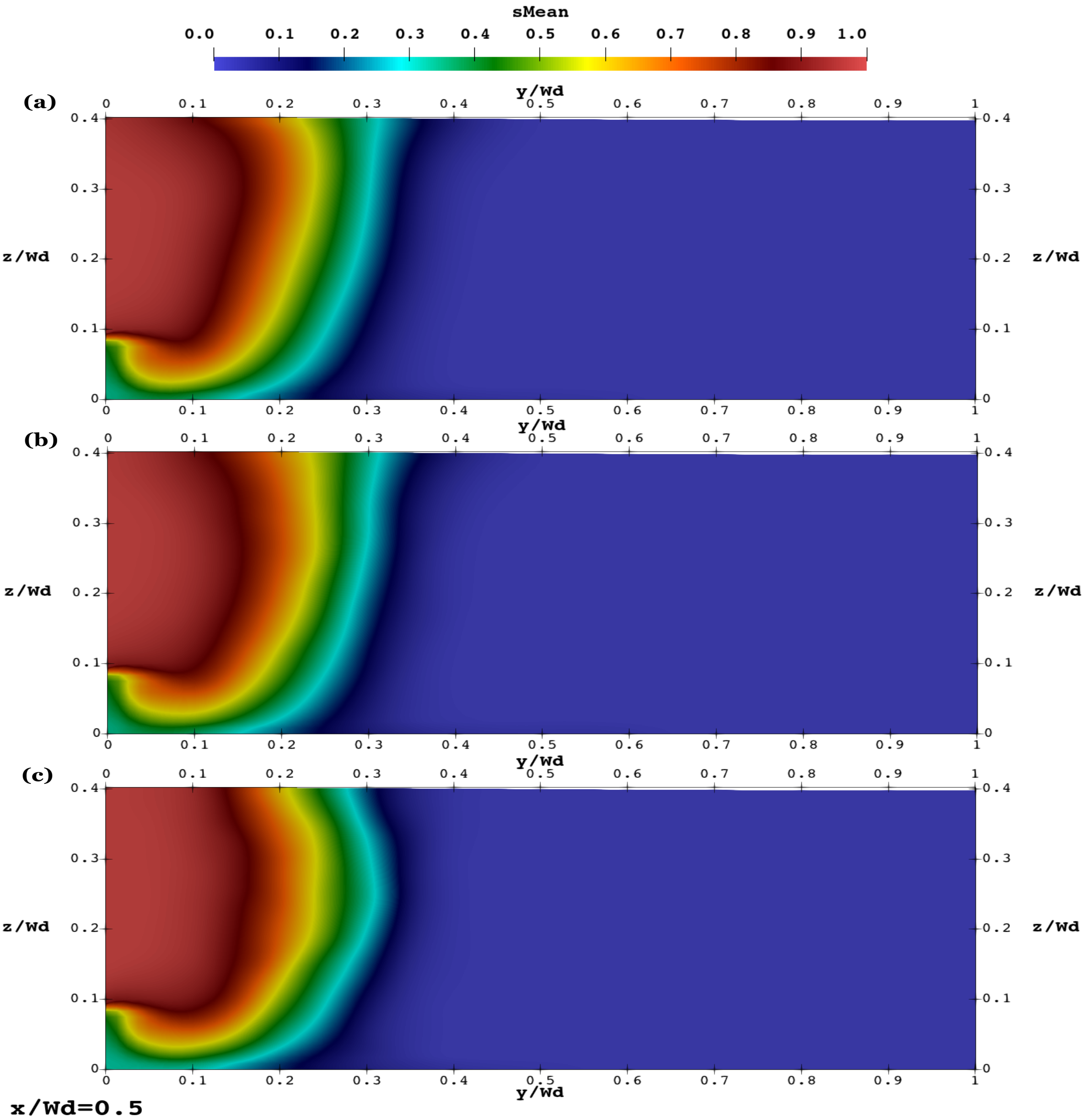

Figure 5.3: Time-averaged concentration, sMean, in the cross section $x/W_d = 0.5$ for the studied schemes: (a) Backward Linear Limited TVD scheme; (b) Crank-Nicolson Linear Limited TVD scheme; (c) Backward Van Leer Limited TVD scheme.

Moreover, through observation of all the results for the time-averaged concentrations (see Appendix A), and based on the proposed model of Best (1987) (Figure 2.1), is possible to distinguish some hydrodynamic structures, such as the mixing layer and the contraction zone. Notice that in the case of the Backward Van Leer Limited TVD scheme is possible to observe what it seems to be the recirculation zone, in the downstream junction corner (between $x/wd = 1$ and $x/wd = 1$), which is less visible in the Crank-Nicolson Linear Limited TVD scheme and Backward Linear Limited TVD scheme. Through the results of this dissertation alone is not possible to substantiate that what is represented is in fact the recirculation zone, since no study on the velocity field was carried out. However, a large portion of the literature substantiates the existence of this structure in this type of confluence, at the downstream junction corner (e.g. Schindfessel (2017); Ramos et al. (2019a)). As such, the Backward Van Leer Limited TVD scheme might be a good choice to study the distribution of contaminants in the recirculation zone, in comparison to the other two numerical schemes.

5.3 Mixing coefficient

The studied time-averaged concentrations, mentioned above, were predicted through the simulated passive scalar concentration in the flow and with it, by means of Equation 4.5, was possible to quantify the non-uniformity of mixing in the downstream main channel. As such, in the following figure the dimensionless parameter E, for each scheme was quantified.

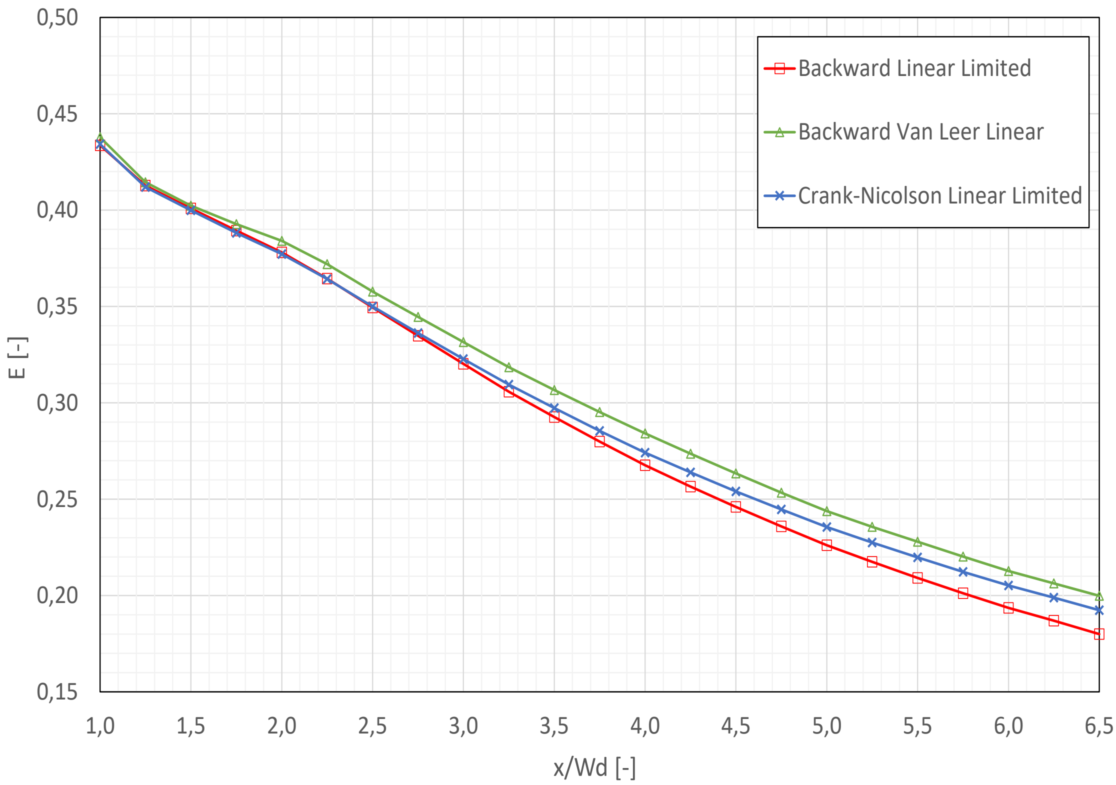

Figure 5.4: Evolution of the mixing parameter E throughout the downstream main channel.

Through observation of the figure, the Backward Linear Limited scheme showed a higher degree of mixing, compared to the other two schemes. Although, the difference between the amount of non-uniformity mixing, for each scheme, was small. Through a carefully analysis of Equation 4.5, the reason for the difference between schemes can only be explained due to differences in the $(sMean_i - s_{avg})$ term of the equation. All other variables are the same between all the studied schemes. The imposed upstream concentration, s_{us}, is fixed to 1 at the tributary and A_i and A_{cs} do not change between schemes, since the mesh is the same for each simulation.

So a smaller $(sMean_i - s_{avg})$ shows a decreasing time-averaged concentration from cell to cell. Therefore, is possible to assume that due to higher numerical diffusion the values of the passive scalar in the solution of the Backward Linear Limited scheme was lower compared to the other schemes, thus complementing the aforementioned assumption that the Backward Linear Limited scheme had the highest numerical diffusivity, followed by the Crank-Nicolson Linear Limited TVD scheme and the Backward Van Leer limited TVD scheme, which the latter showed to had the least numerical diffusivity.

In literature (e.g. Boyer et al. (2006); Lane et al. (2008); Launay et al. (2015); Zhang et al. (2020)), confluences with discordant beds tend to be associated with fast mixing, since bed discordance increases mixing efficiency and in the majority of cases causes the contaminants to be quickly distributed in the flow and complete mixing is achieved very close to the confluence. As such, observing Figure 5.4, the values seem to be in accordance with the literature, since the evolution of the mixing parameter E is accentuated and it is approaching zero very close to the confluence. Notice that, as mentioned before, when $E = 0$ it is considered that the flow achieved complete mixing.

5.4 Monotonicity

As mentioned before, numerical schemes might suffer from spurious oscillations. These oscillations might produce nonphysical values. For example, for the case studied in this dissertation, a nonphysical value will be when a solution gives a value of scalar concentration over 1 or under 0, which the first is not possible because there is no addition of passive scalar in the flow, other than the initial amount, and the second because in the physical world it is impossible for a contaminant to assume negative values. Therefore there is only a maximum of $s = 1$ and a minimum of $s = 0$. If there is an overshoot or an undershoot of these values the numerical scheme does not fulfill monotonicity. As such, in order to analyse the monotonicity of the studied schemes, the instant scalar concentration was studied for different probes at different locations of the flow (probe positions are illustrated in Figure C.2, Appendix C and the instant scalar concentration for each probe, for every numerical scheme are illustrated in Appendix B)

Observing Figure 5.5, Figure 5.6 and Figure 5.7, every numerical scheme showed nonphysical values. From the three, the Backwards Van Leer Limited TVD seems to give more bounded results, since the values that went over 1 and under 0, are smaller than in the other two numerical schemes. Although the Backward Van Leer Limited TVD scheme was better than the others in terms of boundedness (i.e. values between 0 and 1), for the transport of a passive scalar all three schemes failed to maintain boundedness which is not good, since the results will not be a representation of reality. According to the literature about these schemes and the results from the 1D problem, this schemes should provide monotone and diffusive results. However, since the results were diffusive, but were not monotone, one can suppose that the combination of the time stepping scheme with the divergence scheme for each considered scheme might not be the best one for this case. Another possibility is that the grid size and, or, the time step were not small enough, thus producing errors and therefore nonphysical values.

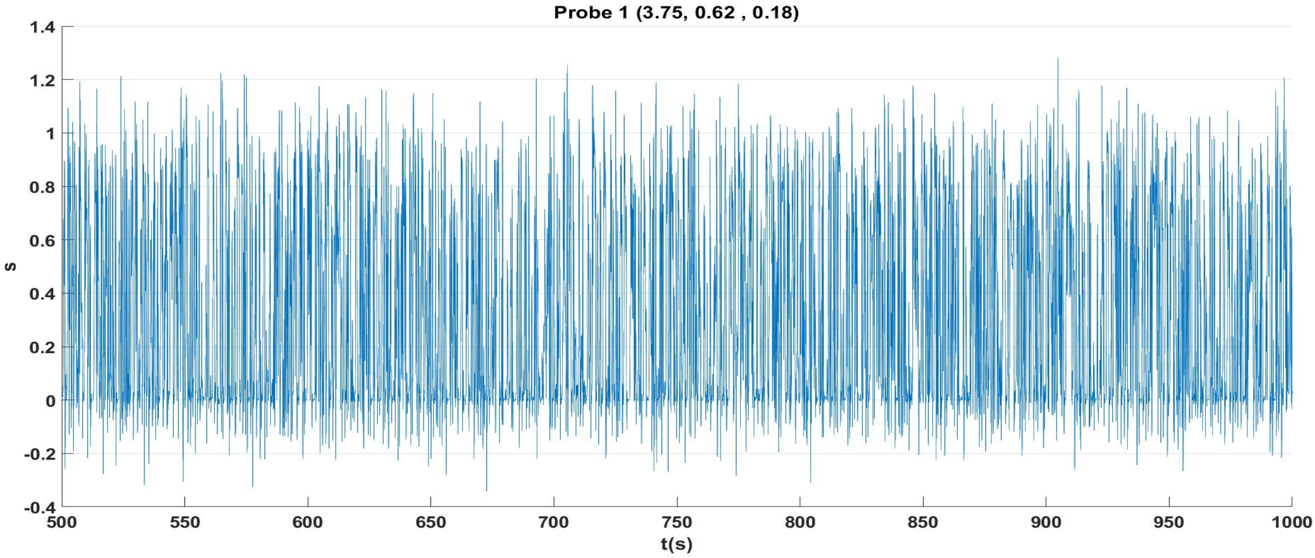

Figure 5.5: Backward Linear Limited TVD scheme probe 1 boundedness.

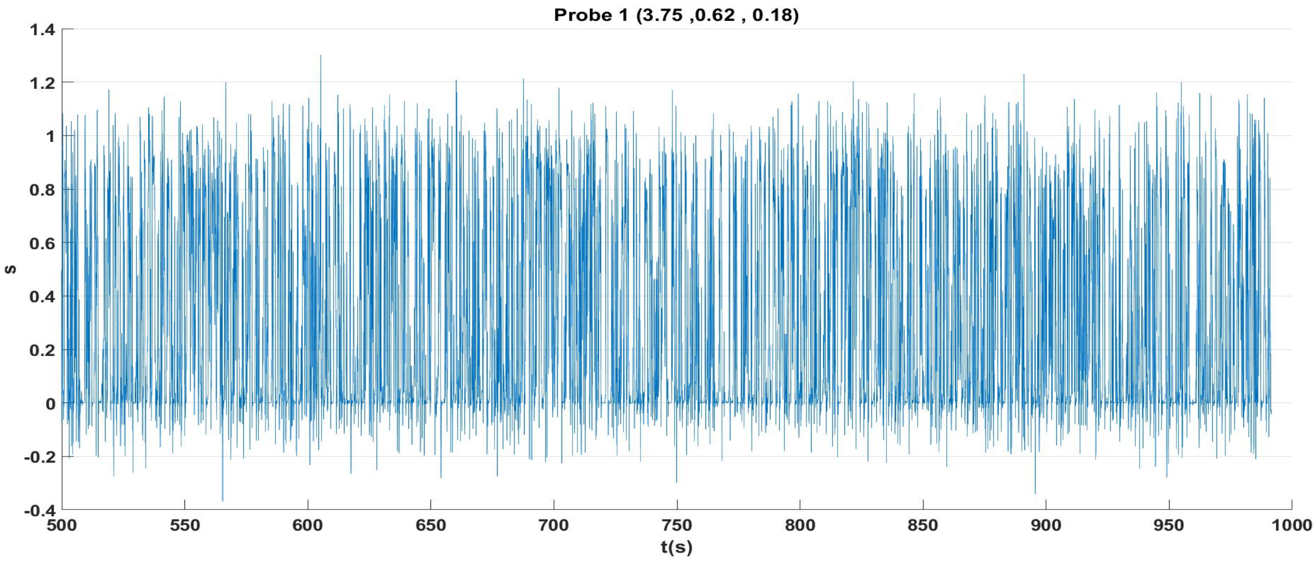

Figure 5.6: Crank-Nicolson Linear Limited TVD scheme probe 1 boundedness.

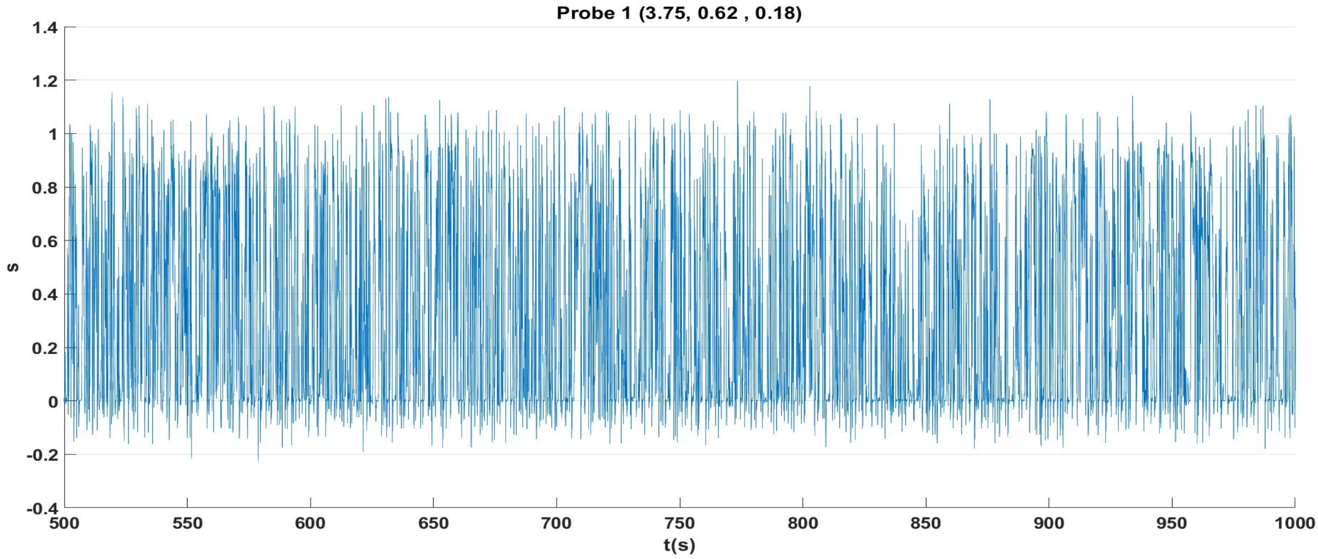

Figure 5.7: Van Leer Limited TVD scheme probe 1 boundedness.

5.5 Moving Averages

The moving average, in this dissertation, gives local probe time-averaged concentrations. Using a Matlab script, each average was calculated over a sliding window of time, across neighboring instant scalar concentrations. The considered windows of time were 4 seconds, 40 seconds and 400 seconds. Since all of the window sizes have an even time, it can be said that the window is centered about the current and previous concentration, for each probe. Furthermore the same 4 probes were studied for each scheme (probe positions are illustrated in Figure C.2, Appendix C).

Observing Figure 5.8, Figure 5.9 and Figure 5.10, it is possible to observe that, as the window of time is increased, each probe in all the numerical schemes converge into a single value. Considering the position of each probe and by having an idea of the values of the time-averaged concentrations at those locations, which can be observed or deducted from the results of the LES time-averaged concentration presented (A), it is possible to compare between the numerical schemes how easily they are able to converge to those specific values. Considering that the probes are in the zone of the mixing layer, for the exception of probe 4, it can be said that the Backward Linear Limited TVD scheme has an easier time to give results for the mixing layer. As such might be the best to study this zone of the flow. The other two schemes were very similar in terms of convergence, thus there is no way to say which one, from the two, was the best for this particular case. Notice that by increasing the window of time is normal that the values will converge around $s = 0.5$. As the chosen probes are located in the zone of the mixing layer, it means that the flow with maximum scalar concentration is mixing with the flow with minimum scalar concentration. Knowing that the main channel discharge is 0.015 m^3/s and the tributary discharge is 0.0107 m^3/s (see Chapter 4) the concentration at these probe locations will decrease and will fluctuate around

$s = 0.5$, since the amount of pollutant will be the same while the volume increases to more than double. Furthermore, since the position of probe 4 is in the tributary and by knowing that in this location the scalar concentration will not change and will always be one, this is a good way of showing that the schemes are fairly stable. The reason why the other probes show so much oscillation is because at the mixing layer the instant values throughout the time is not constant and will be constantly oscillation, due to the mixing of the flow with scalar concentration with the pristine flow.

Notice that careful attention should be paid to the position of probe 1, by looking at Figure C.2, Figure A.16, Figure A.17 and by knowing that the probe is located at $z/Wd = 0.18$ and $y/Wd = 0.62$, since by only looking at Figure C.2, incorrect assumptions about the converging value might be taken. Considering its position the values from the matlab script are concordant with the LES simulations. It is also important to note that this convergence is not a numerical convergence. There are two ways to study numerical convergence. With physical values, which then are used as a reference solution for the convergence test (i.e. experimental results are required in order to do the test), or as an alternative, by using a numerical solution with very refined space and time steps, as the reference solution (Jeong et al. (2019)). From this analysis one can only assume which of the schemes would, with more ease and in less time, produce results for a certain structure of the flow. As mentioned before, the Backward Linear Limited TVD scheme might be a good choice to study the mixing layer.

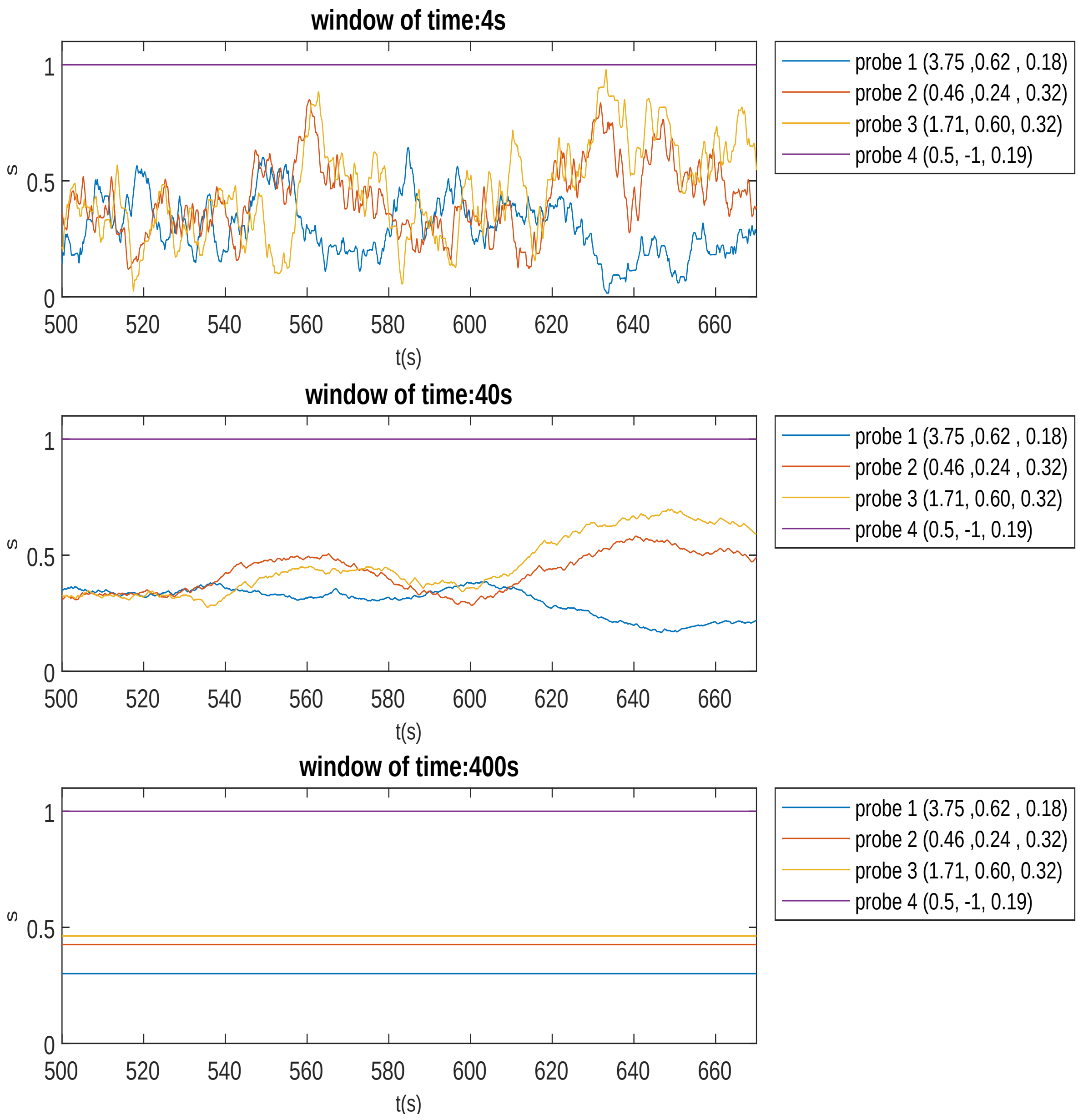

Figure 5.8: Moving averages of the Backward Linear Limited TVD scheme.

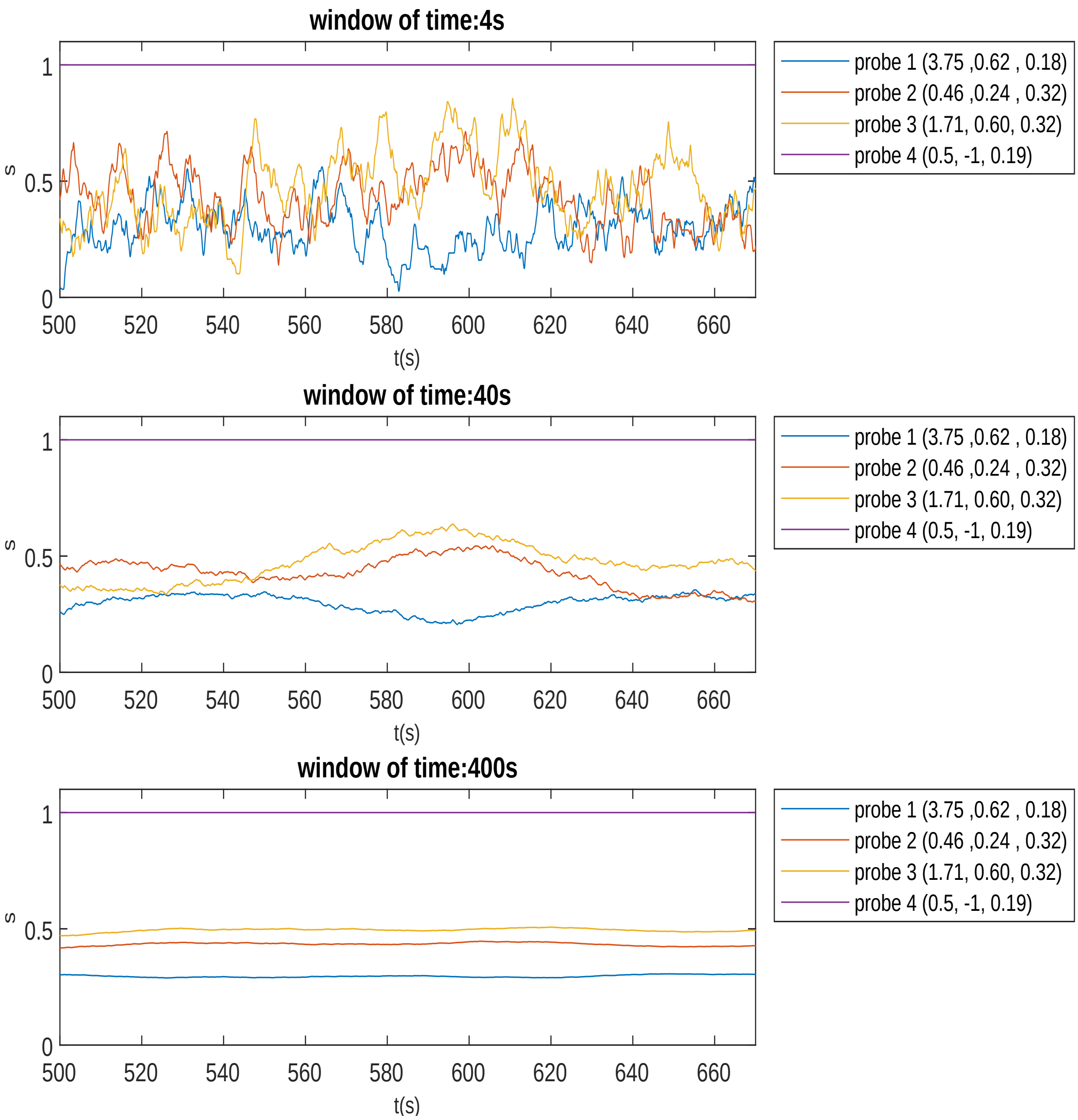

Figure 5.9: Moving averages of the Crank-Nicolson Linear Limited TVD scheme.

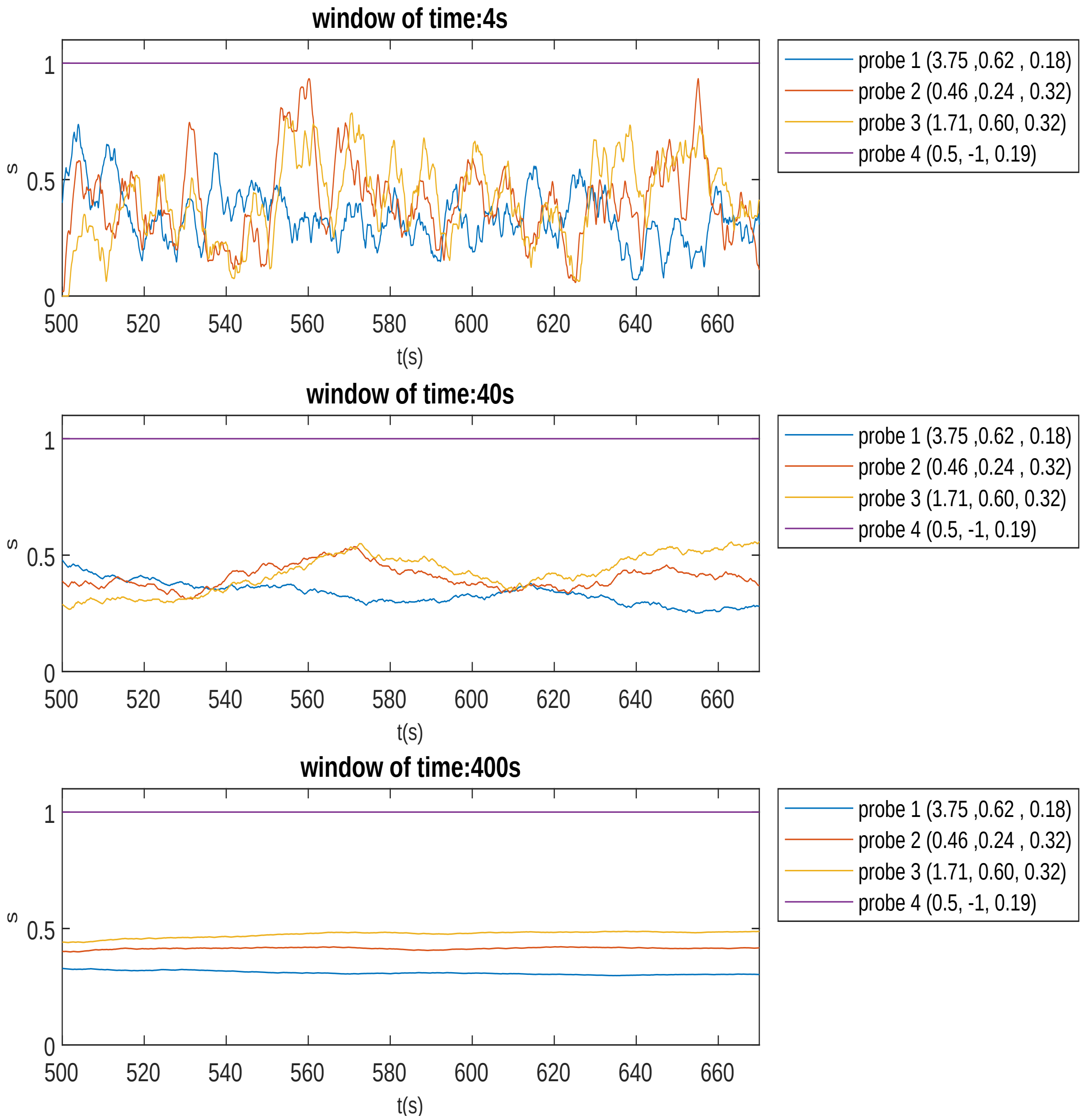

Figure 5.10: Moving averages of the Backward Van Leer Limited TVD scheme.

Chapter 6

Conclusions and recommendations

6.1 Conclusion

The main objective of this dissertation was initially to study the influence of the mixing layer in a 90^o T-shaped confluence with discordant beds, since its an important zone that influences the transport of pollutants and nutrients in the flow. However some of the foreseen work was not possible to conclude due to limitations imposed by the Covid-19 lockdown of 2020. As such to accommodate these setbacks, the objective was changed to critically compare the performance of alternative discretization methods in OpenFOAM for predicting the time-averaged concentration field in the 90^o T-shaped confluence with discordant beds.

Unfortunately, because of the lack of literature on the passive scalar transport in 90^o T-shaped confluences with a bed discordance ratio of 0.25 and the lack of experimental studies, made it impossible to validate the simulations and, as such, conclude which is the best scheme for predicting the mean concentration field. However since all conditions were used equally, throughout all the simulations, and by only changing the schemes to solve the passive scalar transport in the flow, was possible to critically compare their performance.

With the results obtained, from the simulations and from the simple 1D problem studied in this dissertation, is possible to assume that the Backward Van Leer Limited TVD scheme showed to be the best to capture the sharp gradients, showing less numerical diffusivity comparatively with the other two methods. In regards to monotonicity the results from the 1D problem were not in agreement with the results from the LES. According to the literature the results from TVD schemes are monotone and diffusive, as the results of the 1D problem showed. As such, it is possible to assume that the chosen numerical schemes were not appropriate to study the transport of a passive scalar, or that the choice of time step and grid size was not small enough, thus favoring oscillations in the solution, which produced nonphysical values.

6.2 Suggestions for Future Work

In view of the work carried out throughout this dissertation, the following topics are suggested:

- A more in-depth study of the considered numerical schemes, in order to understand if the combinations of the chosen time stepping schemes with the correspondent divergence schemes is appropriate. This way is possible to analyse with certainty if the schemes are appropriate, or not, for the study of the passive scalar transport, which would permit to rule out any doubts in regards to the chosen grid size and time step.

- Do a experimental study of the transport of a passive scalar concentration in a 90^{o} degree T-shaped confluence with a bed discordance ratio of 0.25, to validate and compare the results in this dissertation, in order to understand which of the schemes gives the most accurate results. By knowing which scheme behaves the best for these types of simulations, future works will have the possibility to use CFD more efficiently, while giving more focus on how pollutants behave in the confluence.

- An in-depth study of the mixing layer, providing a better understanding on how this zone of the flow influences pollutants and nutrients in the flow.

References

Adak, M. (2020). *Comparison of Explicit and Implicit Finite Difference Schemes on Diffusion Equation*, pages 227–238. ISBN 978-981-15-3614-4. doi: 10.1007/978-981-15-3615-1_15. Cited on page 22.

Ames, W. F. (1992). 1 - fundamentals. In AMES, W. F., editor, *Numerical Methods for Partial Differential Equations (Third Edition)*, Computer Science and Scientific Computing, pages 1 – 49. Academic Press, San Diego, third edition edition. ISBN 978-0-08-057130-0. doi: https://doi.org/10.1016/B978-0-08-057130-0.50008-7. URL http://www.sciencedirect.com/science/article/pii/B9780080571300500087. Cited on pages 11 and 13.

Ascher, U. M. (2008). *Numerical Methods for Evolutionary Differential Equations*. CAMBRIDGE. ISBN 0898716527. URL https://www.ebook.de/de/product/8259200/uri_m_ascher_numerical_methods_for_evolutionary_differential_equations.html. Cited on page 18.

Ashmore, P. and Parker, G. (1983). Confluence scour in coarse braided streams. *Water Resources Research*, 19(2): 392–402. doi: 10.1029/wr019i002p00392. Cited on pages 7 and 36.

Bathe, K.-J. and Baig, M. M. I. (2005). On a composite implicit time integration procedure for nonlinear dynamics. *Computers & Structures*, 83(31-32): 2513–2524. doi: 10.1016/j.compstruc.2005.08.001. Cited on page 14.

Bathe, K.-J. and Noh, G. (2012). Insight into an implicit time integration scheme for structural dynamics. *Computers & Structures*, 98-99: 1–6. doi: 10.1016/j.compstruc.2012.01.009. Cited on page 14.

Bertoluzza, S., Falletta, S., Russo, G., and Shu, C.-W. (2009). *Numerical Solutions of Partial Differential Equations*. Springer Basel AG. ISBN 9783764389406. URL https://www.ebook.de/de/product/22841546/silvia_bertoluzza_silvia_falletta_giovanni_russo_chi_wang_shu_numerical_solutions_of_partial_differential_equations.html. Cited on page 19.

Best, J. L. (1987). FLOW DYNAMICS AT RIVER CHANNEL CONFLUENCES: IMPLICATIONS FOR SEDIMENT TRANSPORT AND BED MORPHOLOGY. In *Recent Developments in Fluvial Sedimentology*, pages 27–35. SEPM (Society for Sedimentary Geology). doi: 10.2110/pec.87.39.0027. Cited on pages 7, 8, and 38.

Best, J. L. and Reid, I. (1984). Separation zone at open-channel junctions. *Journal of Hydraulic Engineering*, 110(11): 1588–1594. doi: 10.1061/(asce)0733-9429(1984)110:11(1588). Cited on pages 7 and 36.

Best, J. L. and Roy, A. G. (1991). Mixing-layer distortion at the confluence of channels of different depth. *Nature*, 350(6317): 411–413. doi: 10.1038/350411a0. Cited on pages 7 and 8.

Bilal, A., Xie, Q., and Zhai, Y. (2020). Flow, sediment, and morpho-dynamics of river confluence in tidal and non-tidal environments. *Journal of Marine Science and Engineering*, 8(8): 591. doi: 10.3390/jmse8080591. Cited on page 7.

Biron, P., Roy, A. G., and Best, J. L. (1996a). Turbulent flow structure at concordant and discordant open-channel confluences. *Experiments in Fluids*, 21(6): 437–446. doi: 10.1007/bf00189046. Cited on page 8.

Biron, P., Best, J. L., and Roy, A. G. (1996b). Effects of bed discordance on flow dynamics at open channel confluences. *Journal of Hydraulic Engineering*, 122(12): 676–682. doi: 10.1061/(asce)0733-9429(1996)122:12(676). Cited on page 8.

Biron, P. M., Ramamurthy, A. S., and Han, S. (2004). Three-dimensional numerical modeling of mixing at river confluences. *Journal of Hydraulic Engineering*, 130(3): 243–253. doi: 10.1061/(asce)0733-9429(2004)130:3(243). Cited on page 9.

Bombar, G. and Cardoso, A. (2020). Effect of the sediment discharge on the equilibrium bed morphology of movable bed open-channel confluences. *Geomorphology*, 367: 107329. doi: 10.1016/j.geomorph.2020.107329. Cited on page 7.

Bouchez, J., Lajeunesse, E., Gaillardet, J., France-Lanord, C., Dutra-Maia, P., and Maurice, L. (2010). Turbulent mixing in the amazon river: The isotopic memory of confluences. *Earth and Planetary Science Letters*, 290(1-2): 37–43. doi: 10.1016/j.epsl.2009.11.054. Cited on page 8.

Boyer, C., Roy, A. G., and Best, J. L. (2006). Dynamics of a river channel confluence with discordant beds: Flow turbulence, bed load sediment transport, and bed morphology. *Journal of Geophysical Research*, 111(F4). doi: 10.1029/2005jf000458. Cited on pages 8 and 40.

Bradbrook, K. F., Biron, P. M., Lane, S. N., Richards, K. S., and Roy, A. G. (1998). Investigation of controls on secondary circulation in a simple confluence geometry using a three-dimensional numerical model. *Hydrological Processes*, 12(8): 1371–1396. doi: https://doi.org/10.1002/(SICI)1099-1085(19980630)12:8<1371::AID-HYP620>3.0.CO;2-C. URL https://onlinelibrary.wiley.com/doi/abs/10.1002/%28SICI%291099-1085%2819980630%2912%3A8%3C1371%3A%3AAID-HYP620%3E3.0.CO%3B2-C. Cited on page 9.

Bradbrook, K. F., Lane, S. N., and Richards, K. S. (2000a). Numerical simulation of three-dimensional, time-averaged flow structure at river channel confluences. *Water Resources Research*, 36(9): 2731–2746. doi: 10.1029/2000wr900011. Cited on page 9.

Bradbrook, K. F., Lane, S. N., Richards, K. S., Biron, P. M., and Roy, A. G. (2001). Role of bed discordance at asymmetrical river confluences. *Journal of Hydraulic Engineering*, 127(5): 351–368. doi: 10.1061/(asce)0733-9429(2001)127:5(351). Cited on page 9.

Bradbrook, K., Lane, S., Richards, K., Biron, P., and Roy, A. (2000b). Large eddy simulation of periodic flow characteristics at river channel confluences. *Journal of Hydraulic Research*, 38 (3): 207–215. doi: 10.1080/00221680009498338. Cited on page 9.

Brio, M. (2010). *Numerical time-dependent partial differential equations for scientists and engineers*. Elsevier, Amsterdam Boston. ISBN 9780121339814. Cited on page 15.

Bryan, R. B. and Kuhn, N. J. (2002). Hydraulic conditions in experimental rill confluences and scour in erodible soils. *Water Resources Research*, 38(5): 21–1–21–13. doi: 10.1029/2000wr000140. Cited on page 8.

Causon, P. and Mingham, P. (2010). *Introductory Finite Difference Methods for PDEs*. Bookboon. ISBN 9788776816421. URL https://books.google.pt/books?id=9wrZ4XL6gGMC. Cited on pages 13 and 14.

Chandrashekar, P. (2013). Linear hyperbolic conservation laws. Available in http://math.tifrbng.res.in/~praveen/notes/acfd2013/linear.pdf, accessed for the last time in 20th January 2021. Cited on page 18.

Coleman, G. and Sandberg, R. (2010). A primer on direct numerical simulation of turbulence – methods, procedures and guidelines. Cited on page 11.

Constantinescu, G. (2013). LE of shallow mixing interfaces: A review. *Environmental Fluid Mechanics*, 14(5): 971–996. doi: 10.1007/s10652-013-9303-6. Cited on page 10.

Constantinescu, G., Miyawaki, S., Rhoads, B., Sukhodolov, A., and Kirkil, G. (2011). Structure of turbulent flow at a river confluence with momentum and velocity ratios close to 1: Insight provided by an eddy-resolving numerical simulation. *Water Resources Research*, 47(5). doi: 10.1029/2010wr010018. Cited on page 9.

Courant, R., Friedrichs, K. O., and Lewy, H. (1967). On the partial difference equations of mathematical physics. *IBM Journal, 11*, pages 215–234. Cited on page 15.

Dalmon, A., Mignot, E., Riviere, N., Kouyi, G. L., Momplot, A., Gonzalez, C., and Escauriaza, C. (2015). Mélange à l'aval d'une confluence d'écoulements à surface libre. In 22ème Congrès Français de Mécanique. AFM, Association Française de Mécanique. [Document in French]. Cited on page 34.

European Commission. (-). Additional tools the eu water framework directive - integrated river basin management for europe. Available in https://ec.europa.eu/environment/water/water-framework/index_en.html, accessed for the last time in 13th February 2021. Cited on page 2.

European Parliament and Council directive 2000/60/EC. (2000). establishing a framework for community action in the field of water policy. Official Journal L327, p. 1. Cited on page 2.

Gaudet, J. M. and Roy, A. G. (1995). Effect of bed morphology on flow mixing length at river confluences. *Nature*, 373(6510): 138–139. doi: 10.1038/373138a0. Cited on pages 8 and 9.

Greenshields, C. (2018). Openfoam v6 user guide: 5.3 mesh generation with blockmesh. Available in https://cfd.direct/openfoam/user-guide/v6-blockmesh/, accessed for the last time in 22th August 2020. Cited on page 31.

Gualtieri, C., Angeloudis, A., Bombardelli, F., Jha, S., and Stoesser, T. (2017). On the values for the turbulent schmidt number in environmental flows. *Fluids*, 2(2): 17. doi: 10.3390/fluids2020017. Cited on page 11.

Hellevik, L. R. (2020). Numerical methods for engineers. Available in http://folk.ntnu.no/leifh/teaching/tkt4140/._main074.html#mjx-eqn-8.60, accessed for the last time in 13th September 2020. Cited on page 19.

Horák, J. and Hejcman, M. (2016). Contamination characteristics of the confluence of polluted and unpolluted rivers – range and spatial distribution of contaminants of a significant mining centre (kutná hora, czech republic) . *Soil and Water Research*, 11(No. 4): 235–243. doi: 10.17221/118/2015-swr. Cited on page 9.

Jeong, D., Li, Y., Lee, C., Yang, J., Choi, Y., and Kim, J. (2019). Verification of convergence rates of numerical solutions for parabolic equations. *Mathematical Problems in Engineering*, 2019: 1–10. doi: 10.1155/2019/8152136. Cited on page 43.

Jin, T., Cunha Ramos, P., Schindfessel, L., and De Mulder, T. (2020). Numerical study of the flow and passive scalar transport in an open-channel confluence with a flat and a degraded fixed bed. In Uijttewaal, W., Franca, D. V., Chavarrias, V., and Arbos, C. Y., editors, *River Flow 2020*, pages 1324–1332, Delft, The Netherlands. CRC Press, Taylor and Francis Group. ISBN 9780367627737. Cited on page 9.

Kennedy, B. A. (1984). On playfair's law of accordant junctions. *Earth Surface Processes and Landforms*, 9(2): 153–173. doi: 10.1002/esp.3290090207. Cited on page 7.

Kenworthy, S. T. and Rhoads, B. L. (1995). Hydrologic control of spatial patterns of suspended sediment concentration at a stream confluence. *Journal of Hydrology*, 168(1-4): 251–263. doi: 10.1016/0022-1694(94)02644-q. Cited on pages 7 and 9.

Kundu, P. (2012). *Fluid mechanics*. Academic Press, Waltham, MA. ISBN 9780123821003. Cited on pages 13 and 15.

Kärrholm, F. P. and Tao, F. (2008). On performance of advection schemes in the prediction of diesel spray and fuel vapour distributions. Cited on pages 21 and 22.

Lane, S. N., Parsons, D. R., Best, J. L., Orfeo, O., Kostaschuk, R. A., and Hardy, R. J. (2008). Causes of rapid mixing at a junction of two large rivers: Río paraná and río paraguay, argentina. *Journal of Geophysical Research*, 113(F2). doi: 10.1029/2006jf000745. Cited on pages 8 and 40.

Lane, S., Bradbrook, K., Richards, K., Biron, P., and Roy, A. (1999). The application of computational fluid dynamics to natural river channels: three-dimensional versus two-dimensional approaches. *Geomorphology*, 29(1-2): 1–20. doi: 10.1016/s0169-555x(99)00003-3. Cited on page 9.

Laney, C. (1998). *Computational gasdynamics*. Cambridge University Press, Cambridge New York, NY. ISBN 9780511605604. Cited on page 19.

Launay, M., Coz, J. L., Camenen, B., Walter, C., Angot, H., Dramais, G., Faure, J.-B., and Coquery, M. (2015). Calibrating pollutant dispersion in 1-d hydraulic models of river networks. *Journal of Hydro-environment Research*, 9(1): 120–132. doi: 10.1016/j.jher.2014.07.005. Cited on pages 9 and 40.

Leer, B. V. (1974). Towards the ultimate conservative difference scheme. II. monotonicity and conservation combined in a second-order scheme. *Journal of Computational Physics*, 14(4): 361–370. doi: 10.1016/0021-9991(74)90019-9. Cited on page 22.

Lewis, Q. W. and Rhoads, B. L. (2015). Rates and patterns of thermal mixing at a small stream confluence under variable incoming flow conditions. *Hydrological Processes*, 29(20): 4442–4456. doi: 10.1002/hyp.10496. Cited on pages 8 and 9.

Luo, H., Fytanidis, D. K., Schmidt, A. R., and García, M. H. (2018). Comparative 1d and 3d numerical investigation of open-channel junction flows and energy losses. *Advances in Water Resources*, 117: 120–139. doi: 10.1016/j.advwatres.2018.05.012. Cited on page 9.

Mosley, M. P. (1976). An experimental study of channel confluences. *The Journal of Geology*, 84 (5): 535–562. ISSN 00221376, 15375269. doi: 10.1086/628230. URL http://www.jstor.org/stable/30066212. Cited on page 7.

Mulder, T. D. (2020). Hydraulica, Part V: Introduction to Numerical Hydraulics - Finite Difference Methods for 1D Flow and Transport Problems, course notes. Ghent University. Cited on pages 14, 15, 16, 17, 18, and 22.

NASA. (2020). How much water is on earth? Available in https://spaceplace.nasa.gov/water/en/, accessed for the last time in 12th October 2020. Cited on page 1.

Olaiju, O. A., Hoe, Y. S., Ogunbode, E. B., Fabi, J. K., and Egba, E. I. (2018). Achieving a sustainable environment using numerical method for the solution of advection equation in fluid dynamics. *Chemical Engineering Transactions*, (63): 631–636. doi: https://doi.org/10.3303/CET1863106. Cited on page 11.

OpenCFD Ltd. (-a). Openfoam: User guide v2006; backward time scheme. Available in https://www.openfoam.com/documentation/guides/latest/doc/guide-schemes-time-backward.html, accessed for the last time in 20th January 2021. Cited on page 21.

OpenCFD Ltd. (-b). Openfoam: User guide v2006; crank-nicolson time scheme. Available in https://www.openfoam.com/documentation/guides/latest/doc/guide-schemes-time-crank-nicolson.html, accessed for the last time in 24th January 2021. Cited on page 23.

OpenCFD Ltd. (-c). Openfoam: User guide v2006; nuturoughwallfunction. Available in https://www.openfoam.com/documentation/guides/latest/doc/guide-bcs-wall-turbulence-nutURoughWallFunction.html, accessed for the last time in 31th August 2020. Cited on page 33.

OpenCFD Ltd. (-d). Openfoam: User guide v2006; zero gradient. Available in https://www.openfoam.com/documentation/guides/latest/doc/guide-bcs-general-zero-gradient.html#sec-bcs-general-zero-gradient-properties, accessed for the last time in 31th August 2020. Cited on page 33.

Pouchoulin, S., Mignot, E., Rivière, N., and Coz, J. L. (2018). Numerical simulations on mixing of passive scalars in river confluences. *E3S Web of Conferences*, 40: 05019. doi: 10.1051/e3sconf/20184005019. Cited on pages 9 and 36.

Rafei, M. E., Könözsy, L., and Rana, Z. (2017). Investigation of numerical dissipation in classical and implicit large eddy simulations. *Aerospace*, 4(4): 59. doi: 10.3390/aerospace4040059. Cited on page 14.

Ramos, P. X., Schindfessel, L., Pêgo, J. P., and Mulder, T. D. (2019a). Influence of bed elevation discordance on flow patterns and head losses in an open-channel confluence. *Water Science and Engineering*, 12(3): 235–243. doi: 10.1016/j.wse.2019.09.005. Cited on pages 35, 39, and 83.

Ramos, P. X., Schindfessel, L., Pêgo, J. P., and Mulder, T. D. (2019b). Flat vs. curved rigid-lid LES computations of an open-channel confluence. *Journal of Hydroinformatics*, 21(2): 318–334. doi: 10.2166/hydro.2019.109. Cited on pages 9, 30, and 33.

Rhoads, B. L. and Sukhodolov, A. N. (2001). Field investigation of three-dimensional flow structure at stream confluences: 1. thermal mixing and time-averaged velocities. *Water Resources Research*, 37(9): 2393–2410. doi: 10.1029/2001wr000316. Cited on page 9.

Richtmyer, R. (1967). *Difference methods for initial-value problems*. Interscience Publishers, New York. ISBN 9780470720400. Cited on page 15.

Riddaway, R. W. (2002). Numerical methods revised march 2001. Meteorological Training Course Lecture Series © ECMWF, 2002. URL http://archipelago.uma.pt/pdf_library/Riddaway_2002_ECMWF.pdf. Cited on pages 11, 12, and 16.

Rodi, W. (2017). Turbulence modeling and simulation in hydraulics: A historical review. *Journal of Hydraulic Engineering*, 143(5): 03117001. doi: 10.1061/(asce)hy.1943-7900.0001288. Cited on page 11.

Rodi, W., Constantinescu, G., and Stoesser, T. (2013). *Large-Eddy Simulation in Hydraulics*. Taylor & Francis Ltd. ISBN 9780203797570. URL https://www.ebook.de/de/product/21128887/wolfgang_rodi_george_constantinescu_thorsten_stoesser_large_eddy_simulation_in_hydraulics.html. Cited on pages 10, 11, and 29.

Schemel, L. E., Kimball, B. A., Runkel, R. L., and Cox, M. H. (2007). Formation of mixed al–fe colloidal sorbent and dissolved-colloidal partitioning of cu and zn in the cement creek – animas river confluence, silverton, colorado. *Applied Geochemistry*, 22(7): 1467–1484. doi: 10.1016/j.apgeochem.2007.02.010. Cited on page 9.

Schindfessel, L. (2017). Numerical and experimental modeling of the hydrodynamics of open channel confluences with dominant tributary inflow (doctoral dissertation, ghent university). URL http://hdl.handle.net/1854/LU-8529669. Available in http://hdl.handle.net/1854/LU-8529669. Cited on pages 30, 32, 33, and 39.

Schindfessel, L., Creëlle, S., and Mulder, T. D. (2015). Flow patterns in an open channel confluence with increasingly dominant tributary inflow. *Water*, 7(12): 4724–4751. doi: 10.3390/w7094724. Cited on page 9.

Serres, B. D., Roy, A. G., Biron, P. M., and Best, J. L. (1999). Three-dimensional structure of flow at a confluence of river channels with discordant beds. *Geomorphology*, 26(4): 313–335. doi: 10.1016/s0169-555x(98)00064-6. Cited on page 8.

Shakibainia, A., Tabatabai, M. R. M., and Zarrati, A. R. (2010). Three-dimensional numerical study of flow structure in channel confluences. *Canadian Journal of Civil Engineering*, 37(5): 772–781. doi: 10.1139/l10-016. Cited on page 9.

Sharifipour, M., Bonakdari, H., Zaji, A. H., and Shamshirband, S. (2015). Numerical investigation of flow field and flowmeter accuracy in open-channel junctions. *Engineering Applications of Computational Fluid Mechanics*, 9(1): 280–290. doi: 10.1080/19942060.2015.1008963. Cited on pages 9 and 10.

Shu, C.-W. (1988). Total-variation-diminishing time discretizations. *SIAM Journal on Scientific and Statistical Computing*, 9(6): 1073–1084. doi: 10.1137/0909073. Cited on page 18.

Simoes, F. J. and Wang, S. S.-Y. (1997). Numerical prediction of three-dimensional mixing in a compound open channel. *Journal of Hydraulic Research*, 35(5): 619–642. doi: 10.1080/00221689709498398. Cited on page 11.

Sukhodolov, A. N., Krick, J., Sukhodolova, T. A., Cheng, Z., Rhoads, B. L., and Constantinescu, G. S. (2017). Turbulent flow structure at a discordant river confluence: Asymmetric jet dynamics with implications for channel morphology. *Journal of Geophysical Research: Earth Surface*, 122(6): 1278–1293. doi: 10.1002/2016jf004126. Cited on page 8.

Sweby, P. K. (1984). High resolution schemes using flux limiters for hyperbolic conservation laws. *SIAM Journal on Numerical Analysis*, 21(5): 995–1011. ISSN 00361429. URL http://www.jstor.org/stable/2156939. Cited on page 21.

Tabor, G. and Baba-Ahmadi, M. (2010). Inlet conditions for large eddy simulation: A review. *Computers & Fluids*, 39(4): 553–567. doi: 10.1016/j.compfluid.2009.10.007. Cited on page 33.

Ullrich, P. (2010). AOSS 605: The Art of Climate Modeling - Lectures on Numerical Methods. Available in http://www-personal.umich.edu/~paullric/AOSS605-NumericalMethodsLectures.pdf, accessed for the last time in 5th September 2020. Cited on page 17.

Vreugdenhil, C. (1989). *Computational Hydraulics : an Introduction*. Springer Berlin Heidelberg, Berlin, Heidelberg. ISBN 9783642955785. Cited on page 13.

Weber, L. J., Schumate, E. D., and Mawer, N. (2001). Experiments on flow at a 90° open-channel junction. *Journal of Hydraulic Engineering*, 127(5): 340–350. doi: 10.1061/(asce)0733-9429(2001)127:5(340). Cited on page 30.

WHO. (2019). Drinking-water. Available in https://www.who.int/news-room/fact-sheets/detail/drinking-water, accessed for the last time in 10th February 2021. Cited on page 3.

World Resources Institute. (2015). Aqueduct projected water stress country rankings. Available in https://www.wri.org/resources/data-sets/aqueduct-projected-water-stress-country-rankings, accessed for the last time in 12th October 2020. Cited on page 2.

Xue, M. (2001). Chapter 3. Finite Difference Methods for Hyperbolic Equations. Available in http://twister.ou.edu/CFD2001/Chapter3_123.pdf, accessed for the last time in 10th September 2020. Cited on page 14.

Yuan, S., Tang, H., Xiao, Y., Chen, X., Xia, Y., and Jiang, Z. (2018). Spatial variability of phosphorus adsorption in surface sediment at channel confluences: Field and laboratory experimental evidence. *Journal of Hydro-environment Research*, 18: 25–36. doi: 10.1016/j.jher.2017.10.001. Cited on page 9.

Zhang, D., Jiang, C., Liang, D., and Cheng, L. (2015). A review on TVD schemes and a refined flux-limiter for steady-state calculations. *Journal of Computational Physics*, 302: 114–154. doi: 10.1016/j.jcp.2015.08.042. Cited on pages 18 and 26.

Zhang, T., Feng, M., Chen, K., and Cai, Y. (2020). Spatiotemporal distributions and mixing dynamics of characteristic contaminants at a large asymmetric confluence in northern china. *Journal of Hydrology*, 591: 125583. doi: 10.1016/j.jhydrol.2020.125583. Cited on pages 9 and 40.

Zijlema, M. (2015). Computational modelling of flow and transport. TU Delft, Department Hydraulic Engineering. Available in http://resolver.tudelft.nl/uuid:5e7dac47-0159-4af3-b1d8-32d37d2a8406, accessed for the last time in 10th December 2020. Cited on pages 16 and 17.

Appendix A

Passive Scalar Transport Simulation Results

A.1 Plan view cuts on the main channel for the time-averaged concentrations

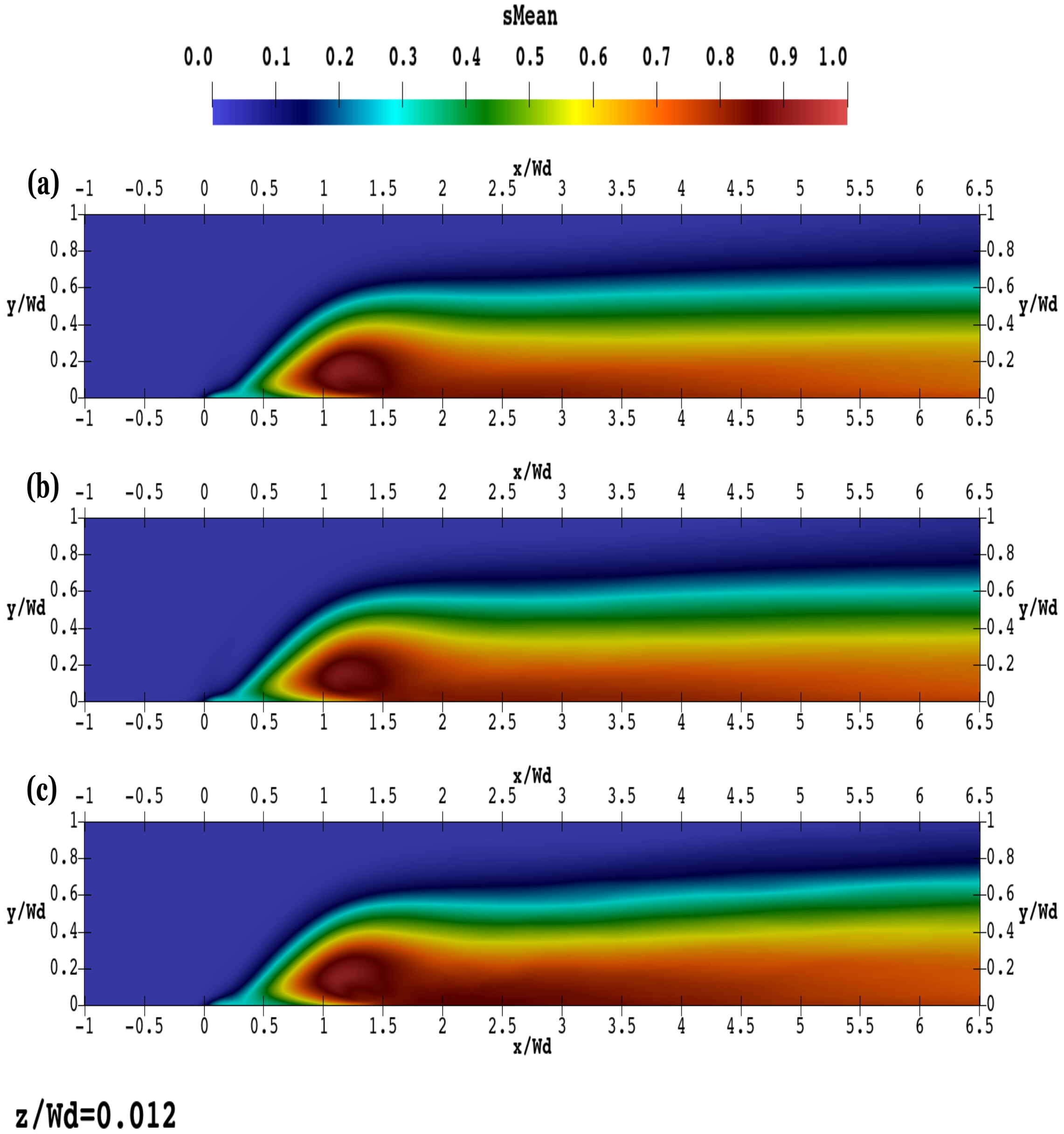

Figure A.1: Time-averaged concentration, sMean, in the plan view $z/W_d = 0.012$ for the studied schemes: (a) Backward LinearLimited TVD scheme; (b) Crank-Nicolson LinearLimited TVD scheme; (c) Backward Van Leer Limited TVD scheme.

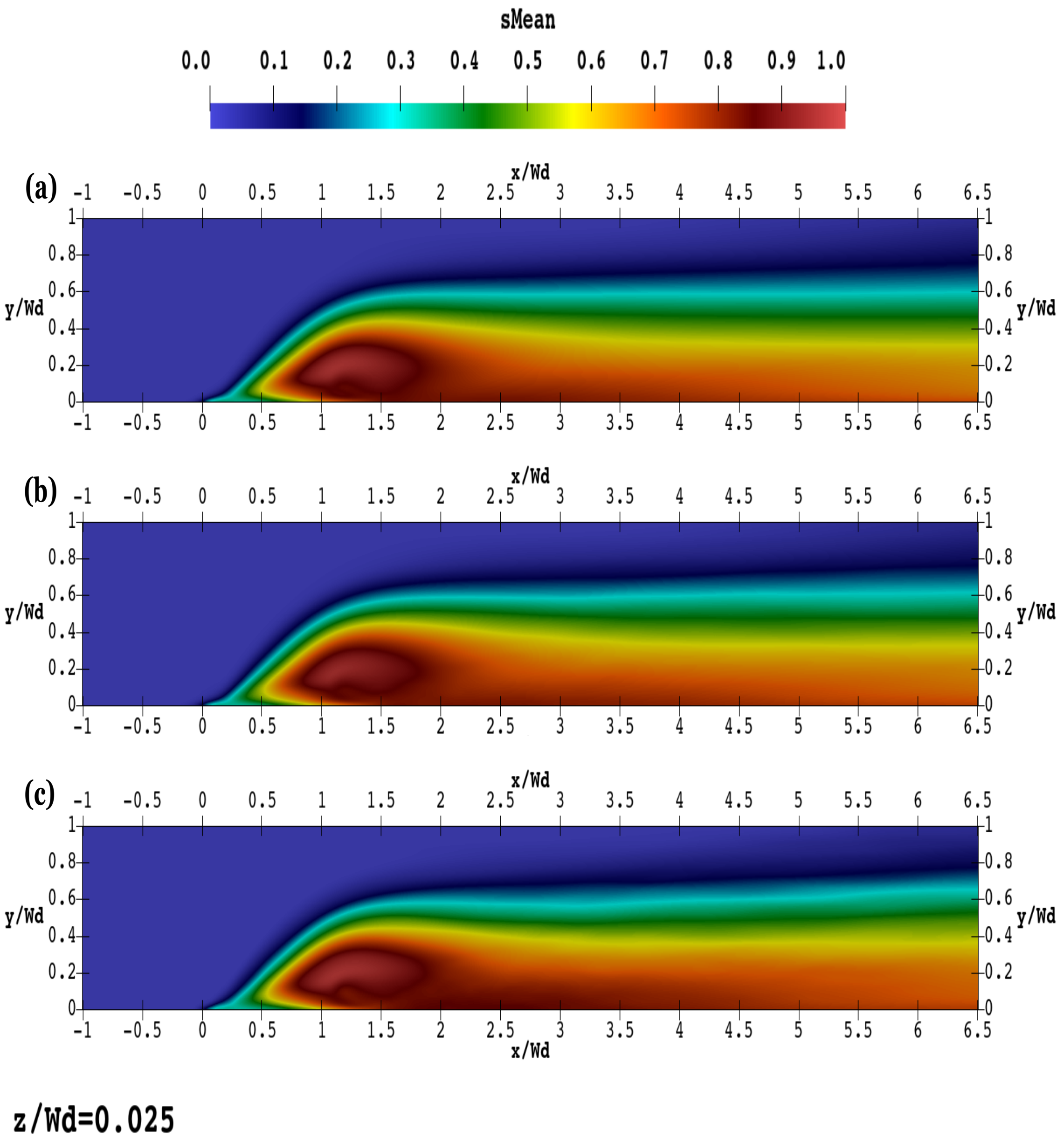

Figure A.2: Time-averaged concentration, sMean, in the plan view $z/W_d = 0.025$ for the studied schemes: (a) Backward LinearLimited TVD scheme; (b) Crank-Nicolson LinearLimited TVD scheme; (c) Backward Van Leer Limited TVD scheme.

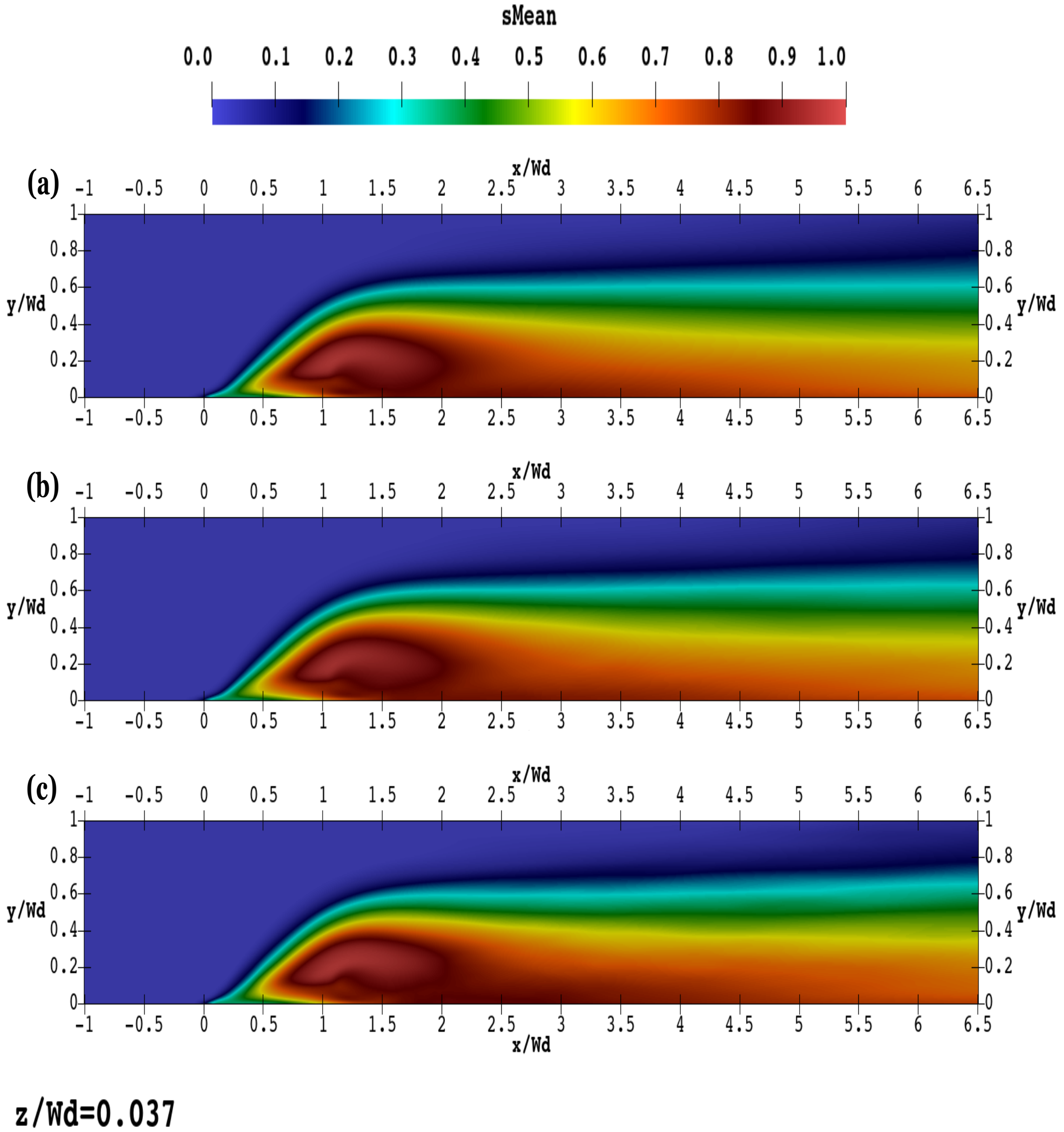

Figure A.3: Time-averaged concentration, sMean, in the plan view $z/W_d = 0.037$ for the studied schemes: (a) Backward LinearLimited TVD scheme; (b) Crank-Nicolson LinearLimited TVD scheme; (c) Backward Van Leer Limited TVD scheme.

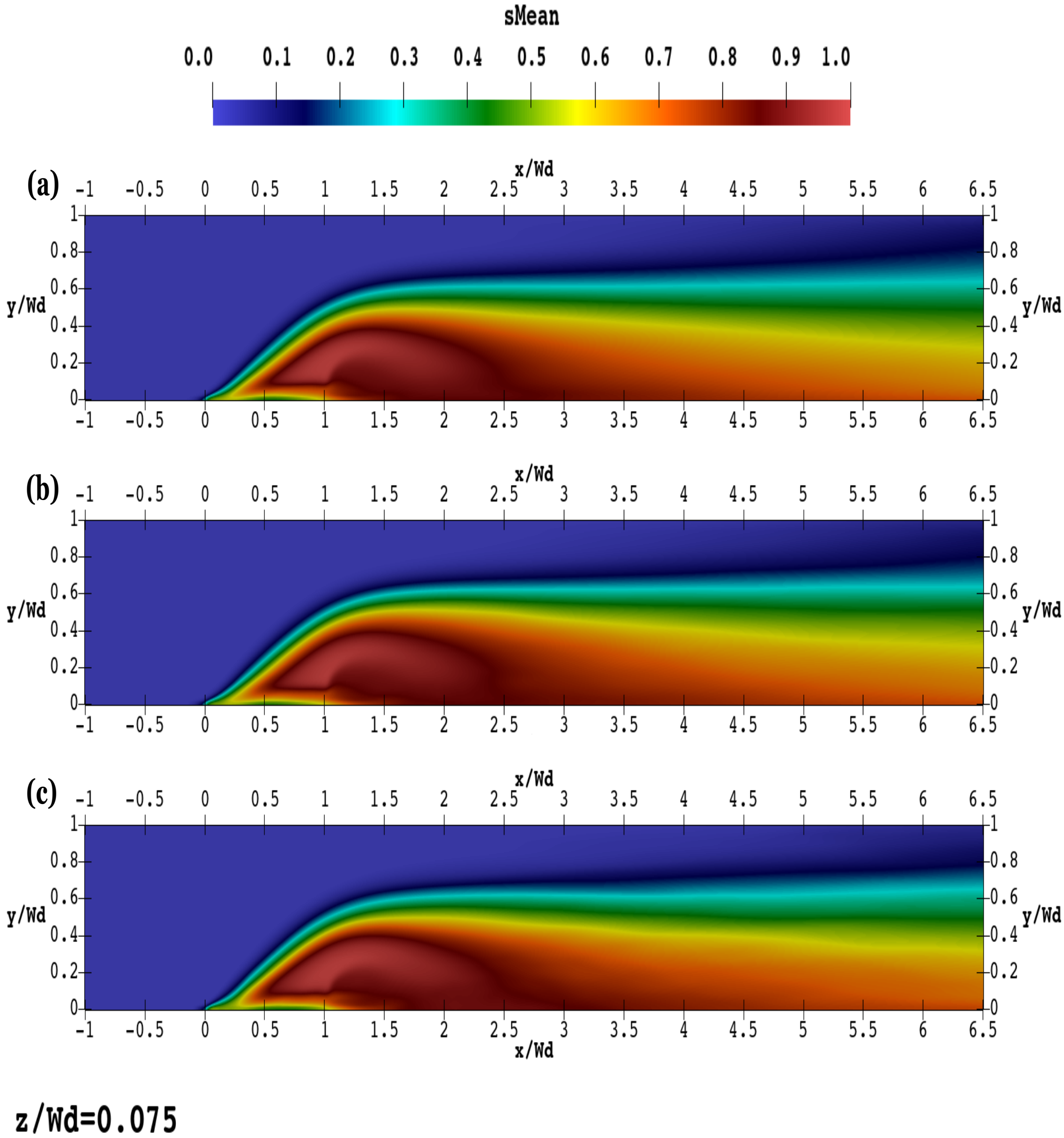

Figure A.4: Time-averaged concentration, sMean, in the plan view $z/W_d = 0.075$ for the studied schemes: (a) Backward LinearLimited TVD scheme; (b) Crank-Nicolson LinearLimited TVD scheme; (c) Backward Van Leer Limited TVD scheme.

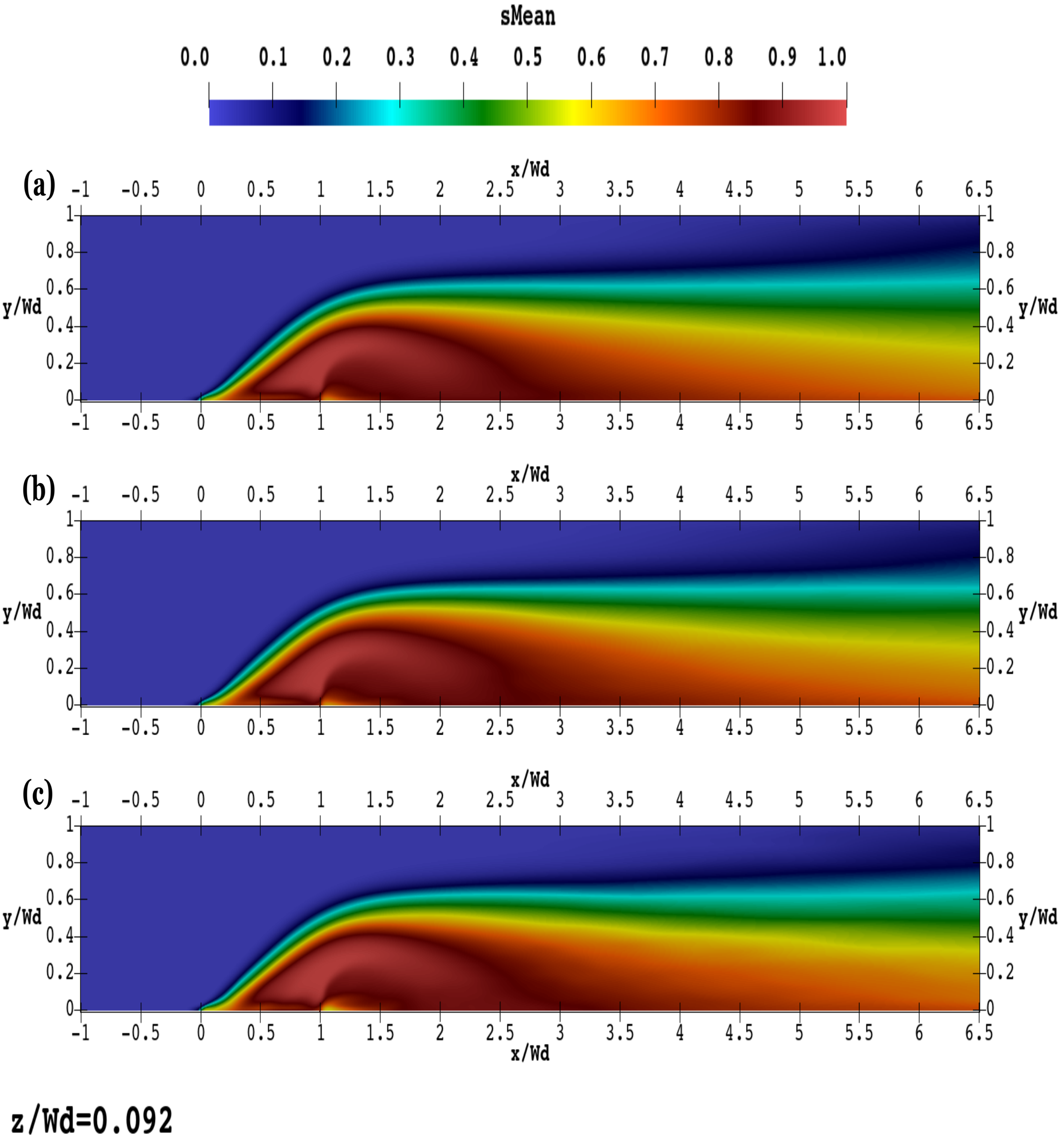

Figure A.5: Time-averaged concentration, sMean, in the plan view $z/W_d = 0.092$ for the studied schemes: (a) Backward LinearLimited TVD scheme; (b) Crank-Nicolson LinearLimited TVD scheme; (c) Backward Van Leer Limited TVD scheme.

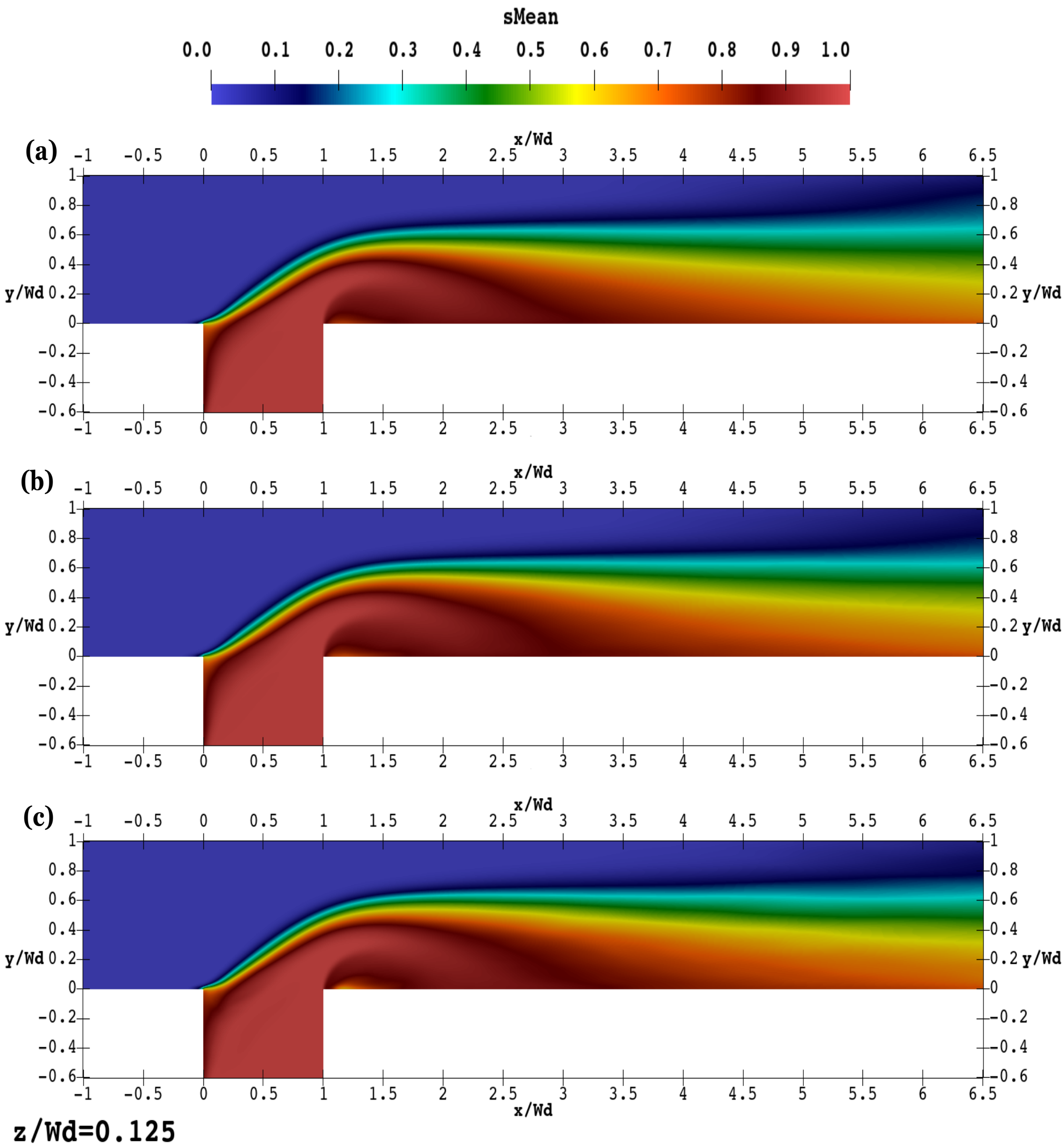

Figure A.6: Time-averaged concentration, sMean, in the plan view $z/W_d = 0.125$ for the studied schemes: (a) Backward LinearLimited TVD scheme; (b) Crank-Nicolson LinearLimited TVD scheme; (c) Backward Van Leer Limited TVD scheme.

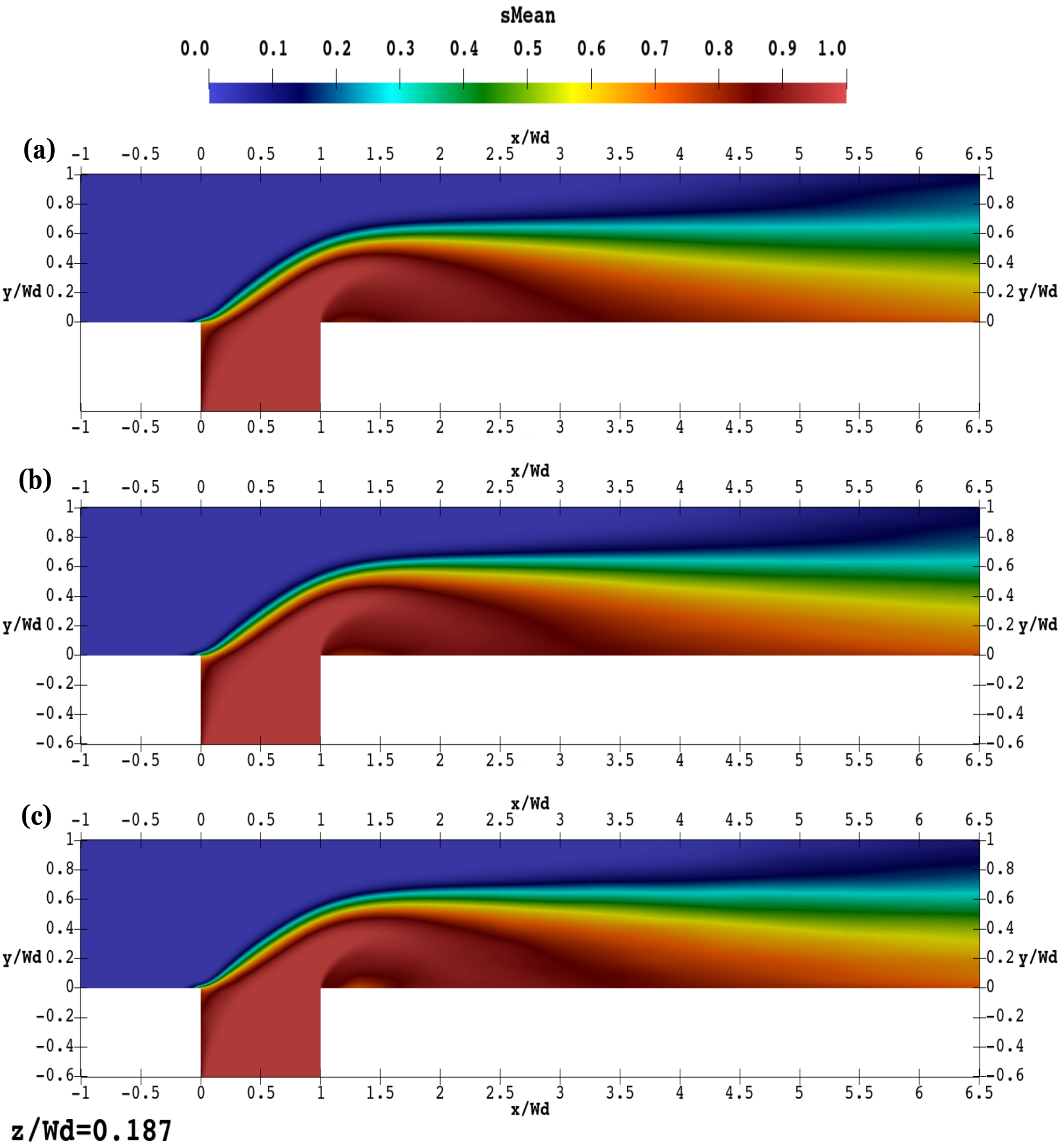

Figure A.7: Time-averaged concentration, sMean, in the plan view $z/W_d = 0.187$ for the studied schemes: (a) Backward LinearLimited TVD scheme; (b) Crank-Nicolson LinearLimited TVD scheme; (c) Backward Van Leer Limited TVD scheme.

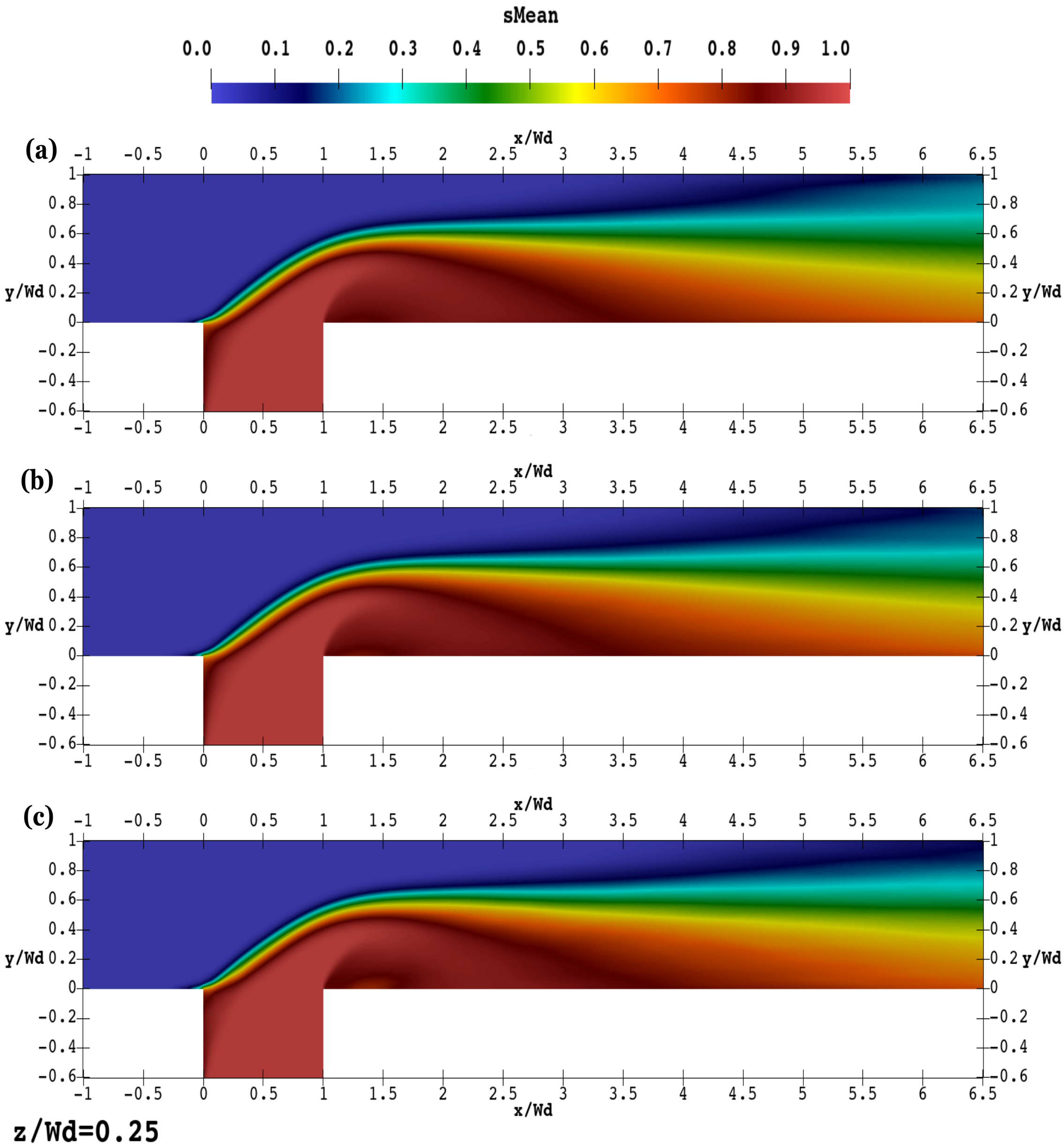

Figure A.8: Time-averaged concentration, sMean, in the plan view $z/W_d = 0.25$ for the studied schemes: (a) Backward LinearLimited TVD scheme; (b) Crank-Nicolson LinearLimited TVD scheme; (c) Backward Van Leer Limited TVD scheme.

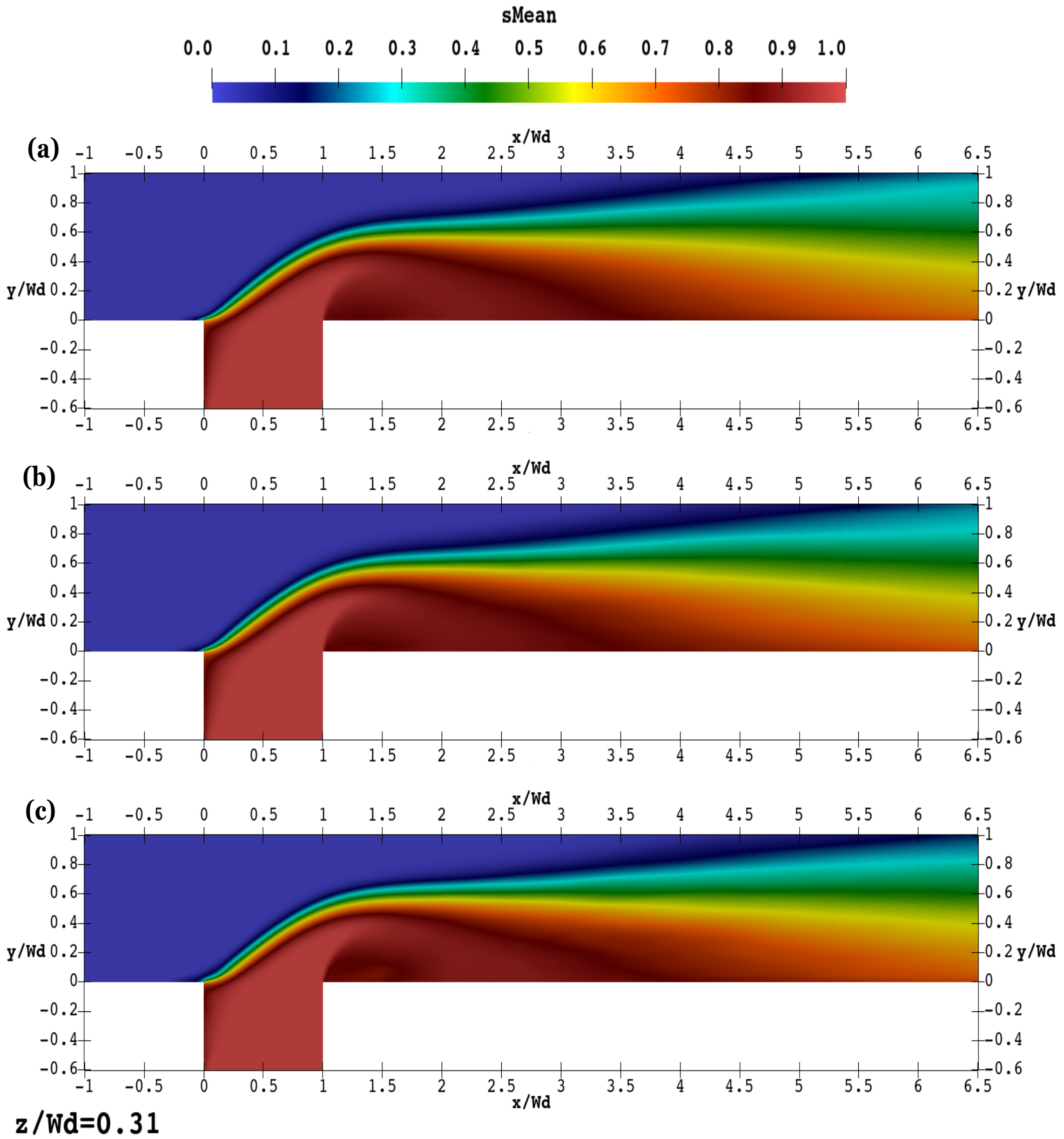

Figure A.9: Time-averaged concentration, sMean, in the plan view $z/W_d = 0.31$ for the studied schemes: (a) Backward LinearLimited TVD scheme; (b) Crank-Nicolson LinearLimited TVD scheme; (c) Backward Van Leer Limited TVD scheme.

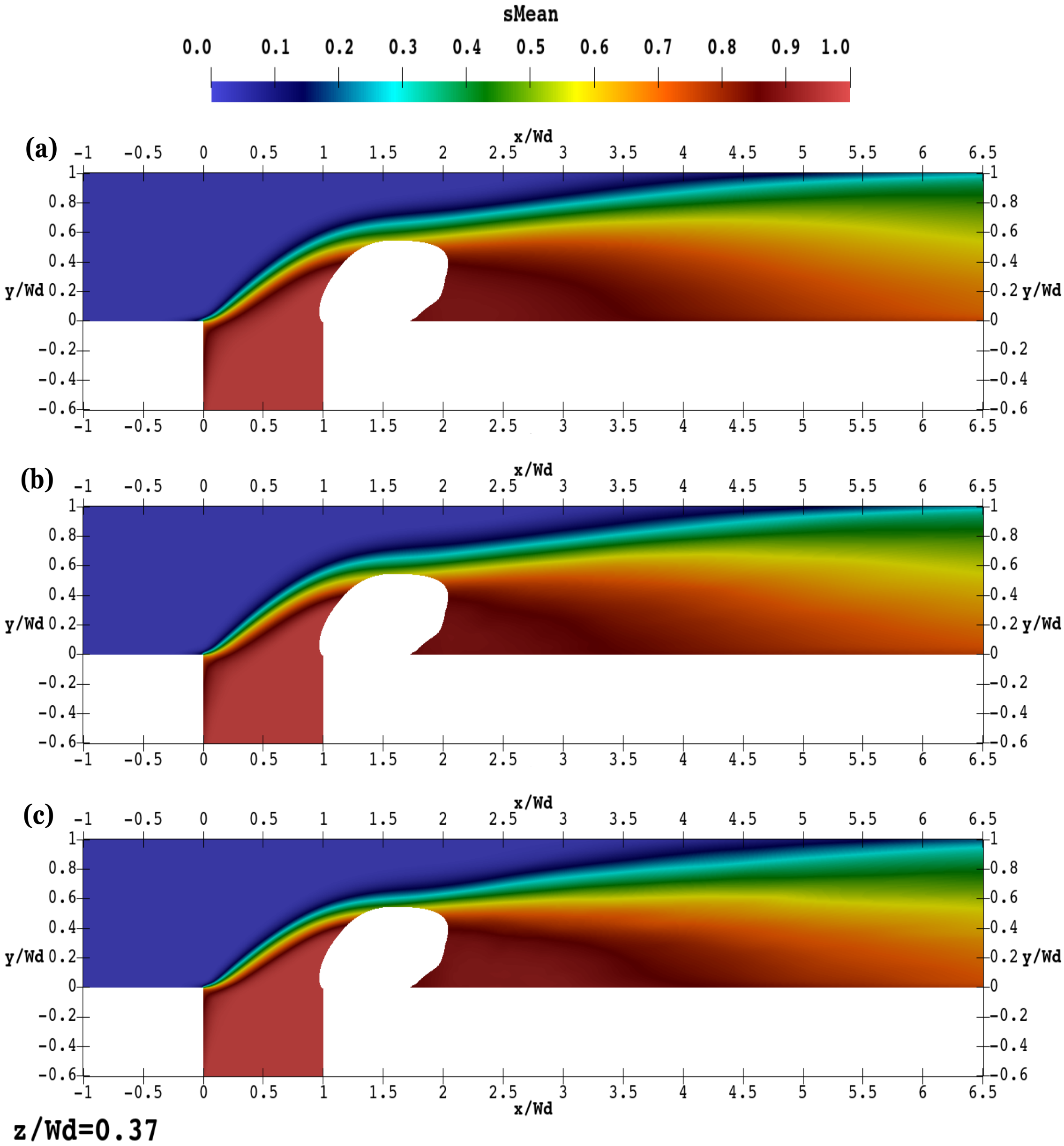

Figure A.10: Time-averaged concentration, sMean, in the plan view $z/W_d = 0.37$ for the studied schemes: (a) Backward LinearLimited TVD scheme; (b) Crank-Nicolson LinearLimited TVD scheme; (c) Backward Van Leer Limited TVD scheme.[1]

[1]Notice that the white zone without data means that the cut was above the data in that specific area (i.e. the flow surface height in that specific area was lower than $z/Wd = 0.37$).

A.2 Cross Section cuts on the main channel for the time-averaged concentrations

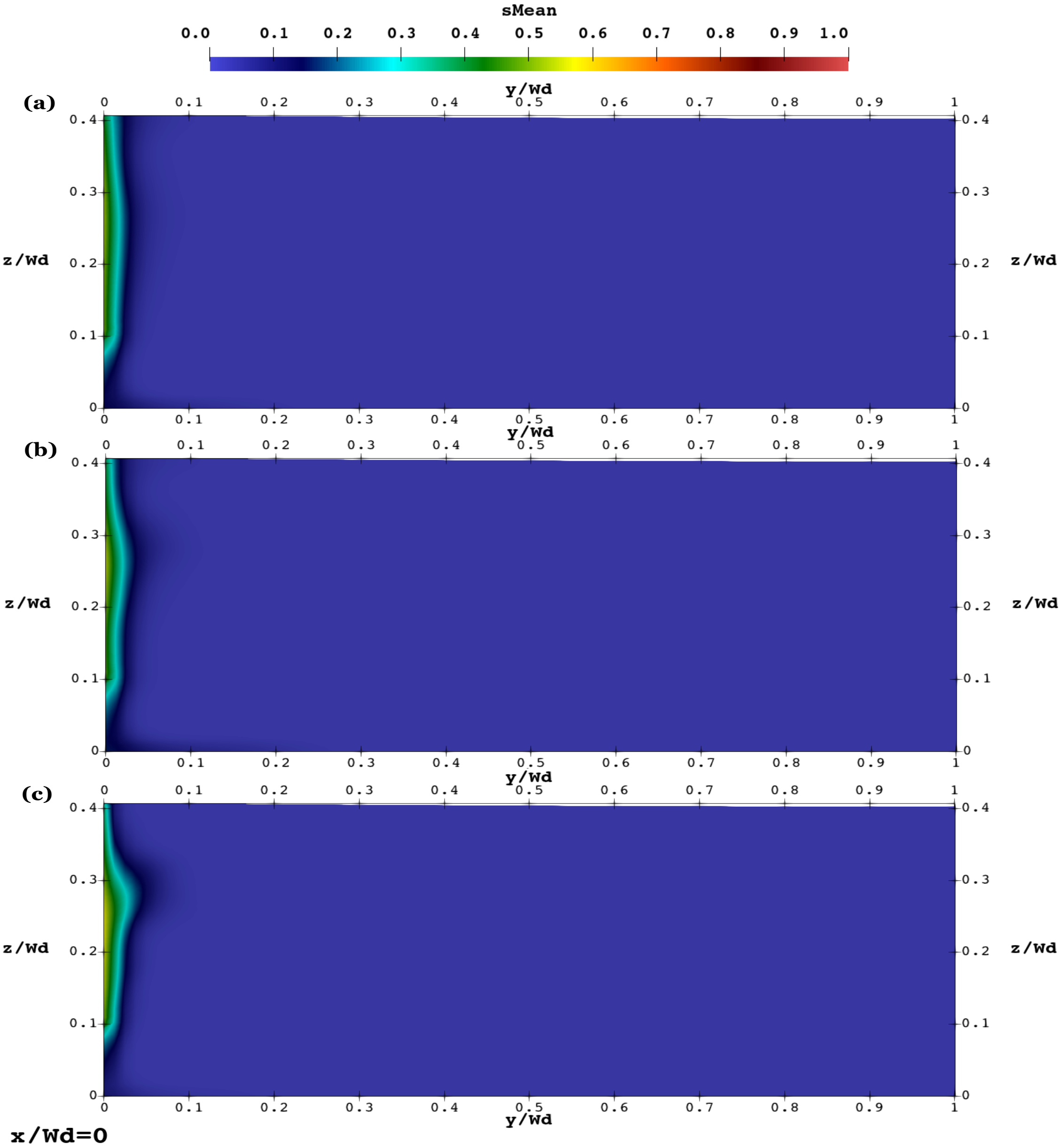

Figure A.11: Time-averaged concentration, sMean, in the cross section $x/W_d = 0$ for the studied schemes: (a) Backward LinearLimited TVD scheme; (b) Crank-Nicolson LinearLimited TVD scheme; (c) Backward Van Leer Limited TVD scheme.

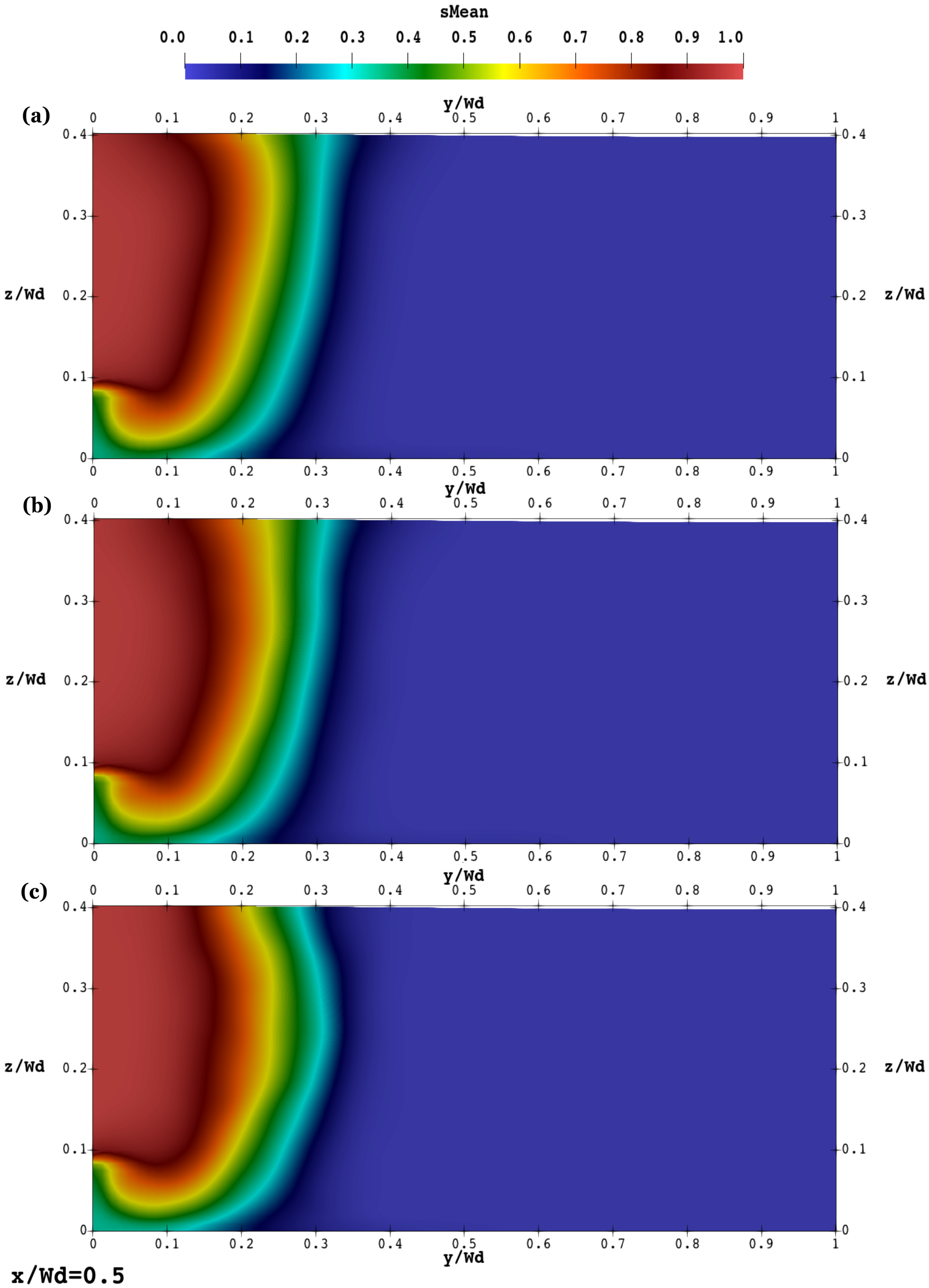

Figure A.12: Time-averaged concentration, sMean, in the cross section $x/W_d = 0.5$ for the studied schemes: (a) Backward LinearLimited TVD scheme; (b) Crank-Nicolson LinearLimited TVD scheme; (c) Backward Van Leer Limited TVD scheme.

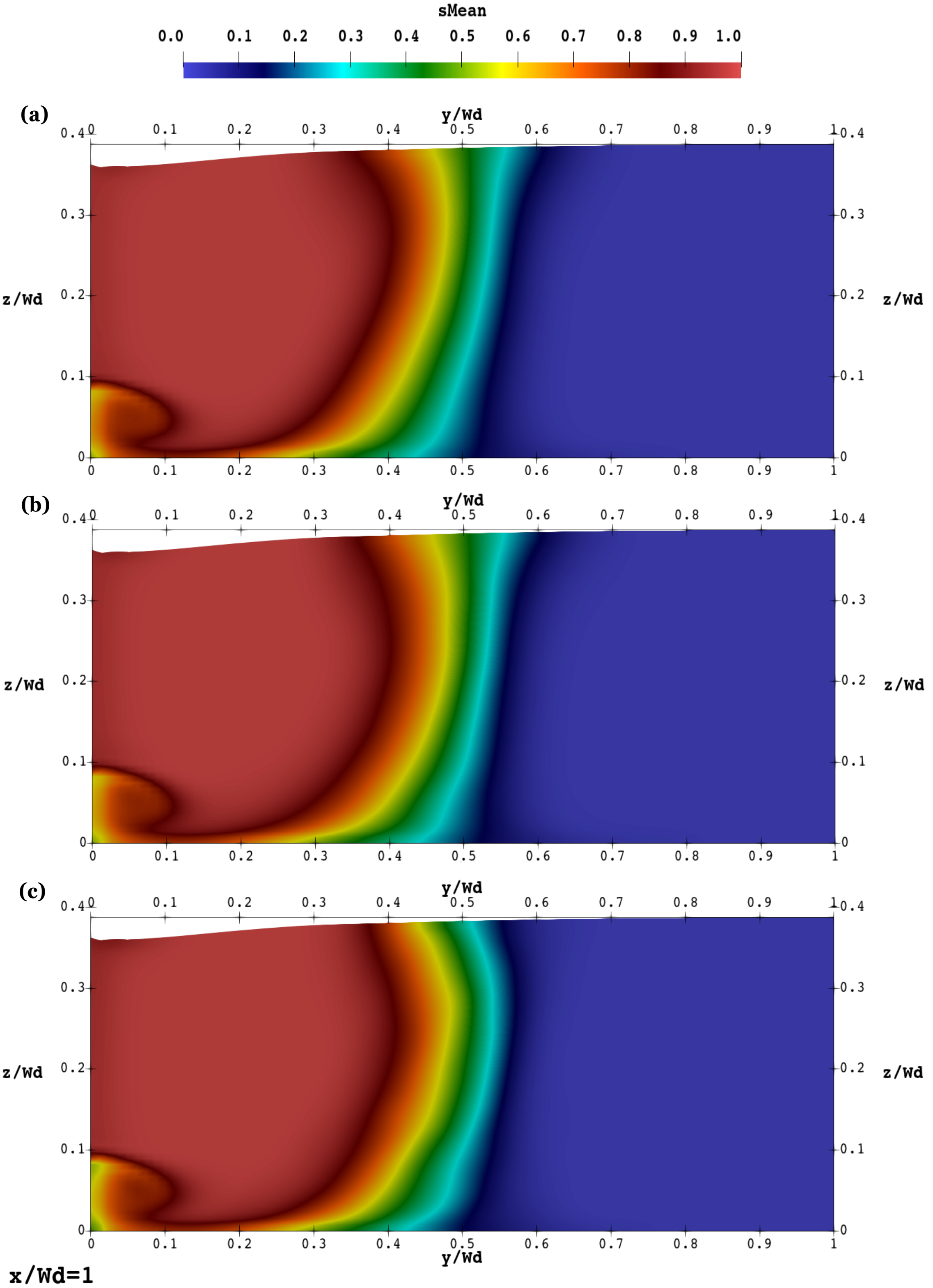

Figure A.13: Time-averaged concentration, sMean, in the cross section $x/W_d = 1$ for the studied schemes: (a) Backward LinearLimited TVD scheme; (b) Crank-Nicolson LinearLimited TVD scheme; (c) Backward Van Leer Limited TVD scheme.

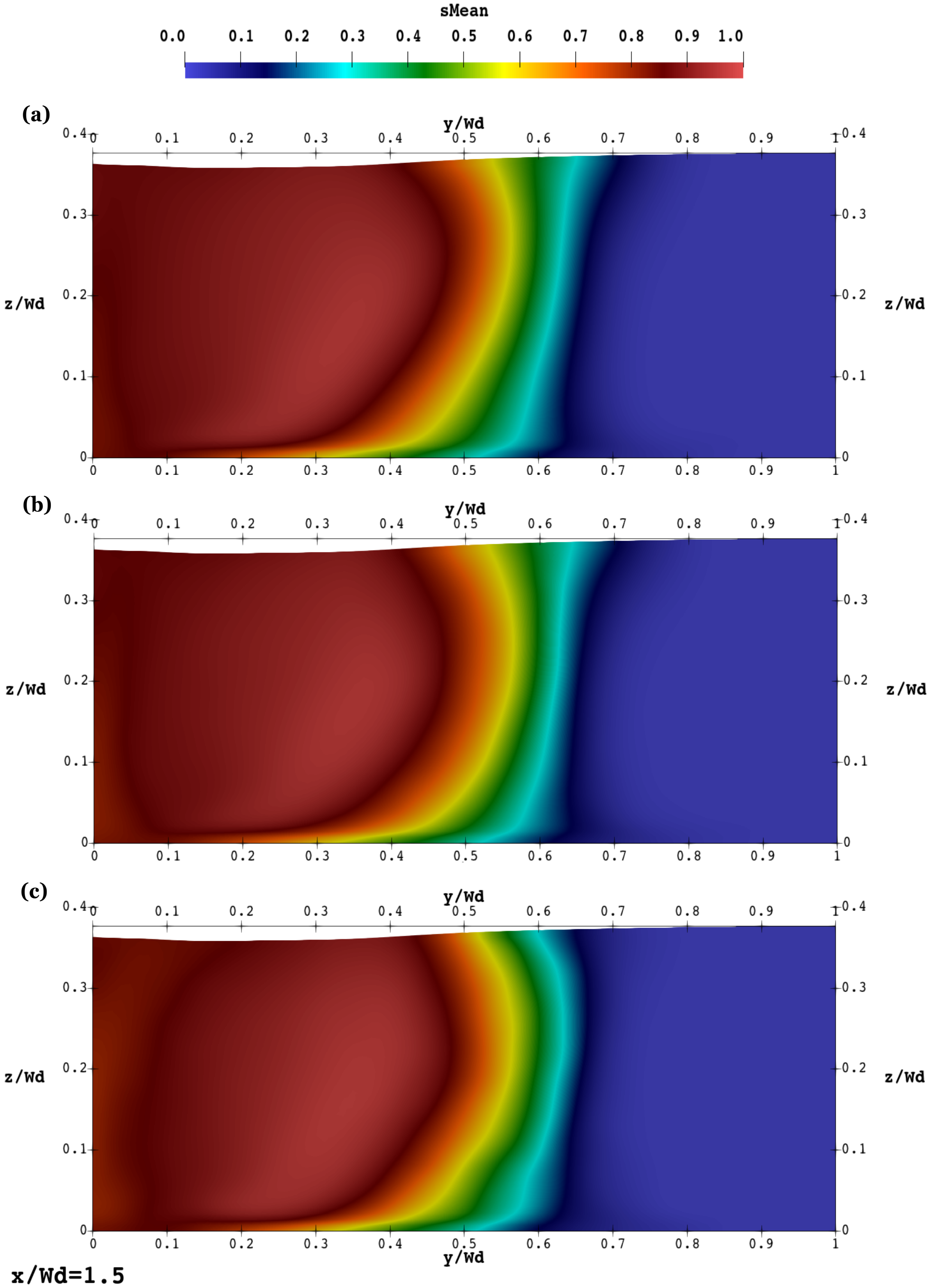

Figure A.14: Time-averaged concentration, sMean, in the cross section $x/W_d = 1.5$ for the studied schemes: (a) Backward LinearLimited TVD scheme; (b) Crank-Nicolson LinearLimited TVD scheme; (c) Backward Van Leer Limited TVD scheme.

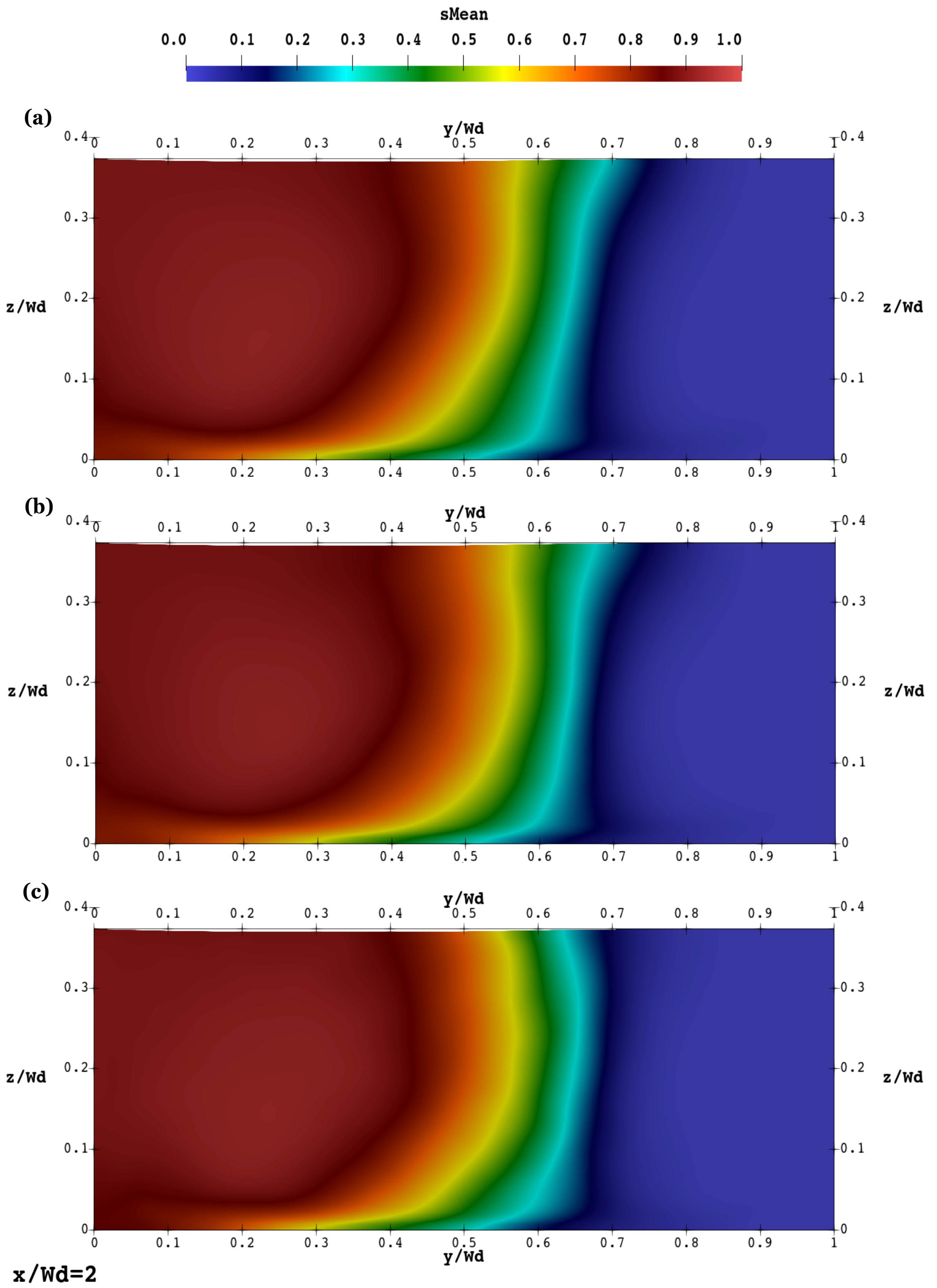

Figure A.15: Time-averaged concentration, sMean, in the cross section $x/W_d = 2$ for the studied schemes: (a) Backward LinearLimited TVD scheme; (b) Crank-Nicolson LinearLimited TVD scheme; (c) Backward Van Leer Limited TVD scheme.

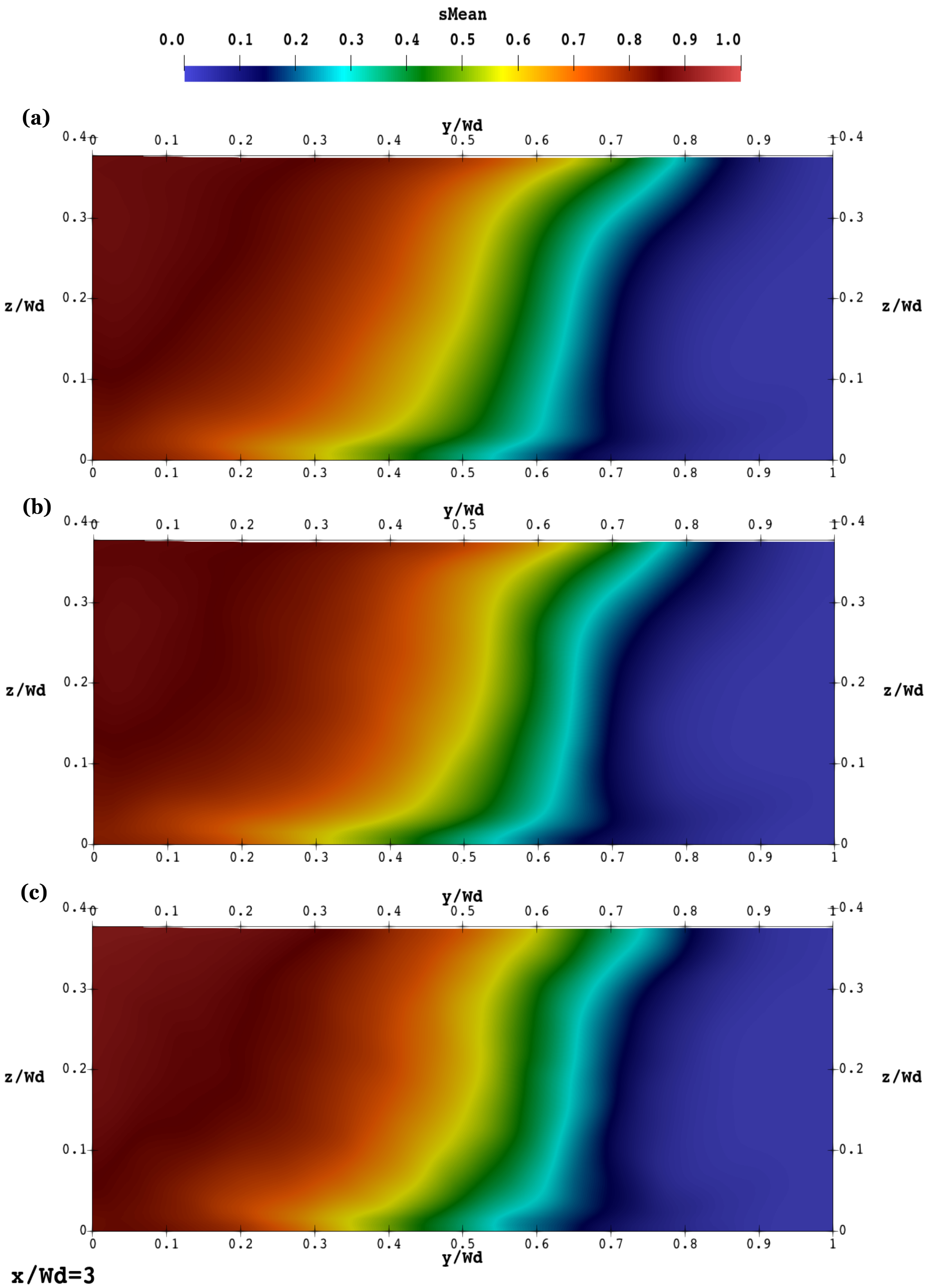

Figure A.16: Time-averaged concentration, sMean, in the cross section $x/W_d = 3$ for the studied schemes: (a) Backward LinearLimited TVD scheme; (b) Crank-Nicolson LinearLimited TVD scheme; (c) Backward Van Leer Limited TVD scheme.

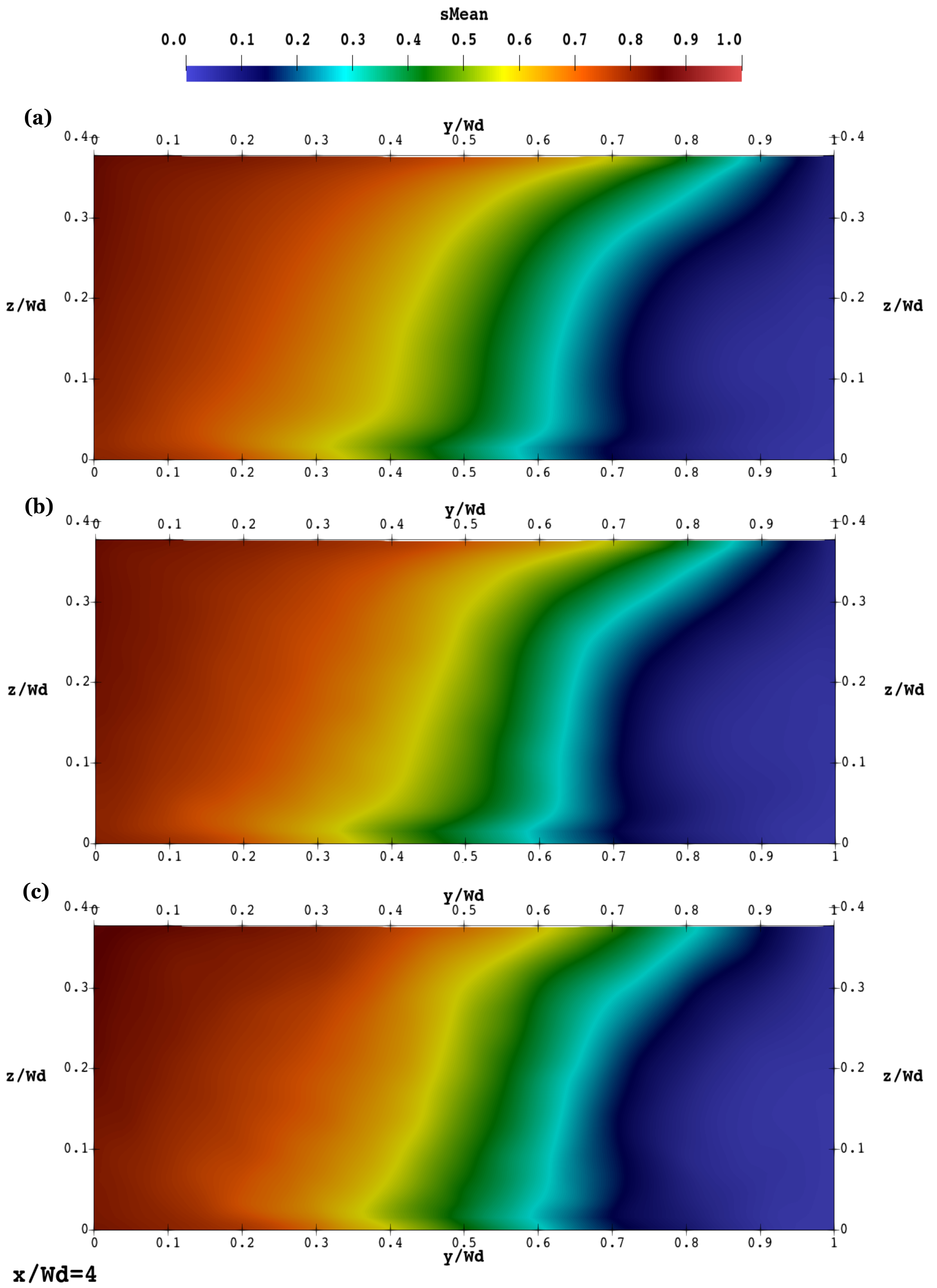

Figure A.17: Time-averaged concentration, sMean, in the cross section $x/W_d = 4$ for the studied schemes: (a) Backward LinearLimited TVD scheme; (b) Crank-Nicolson LinearLimited TVD scheme; (c) Backward Van Leer Limited TVD scheme.

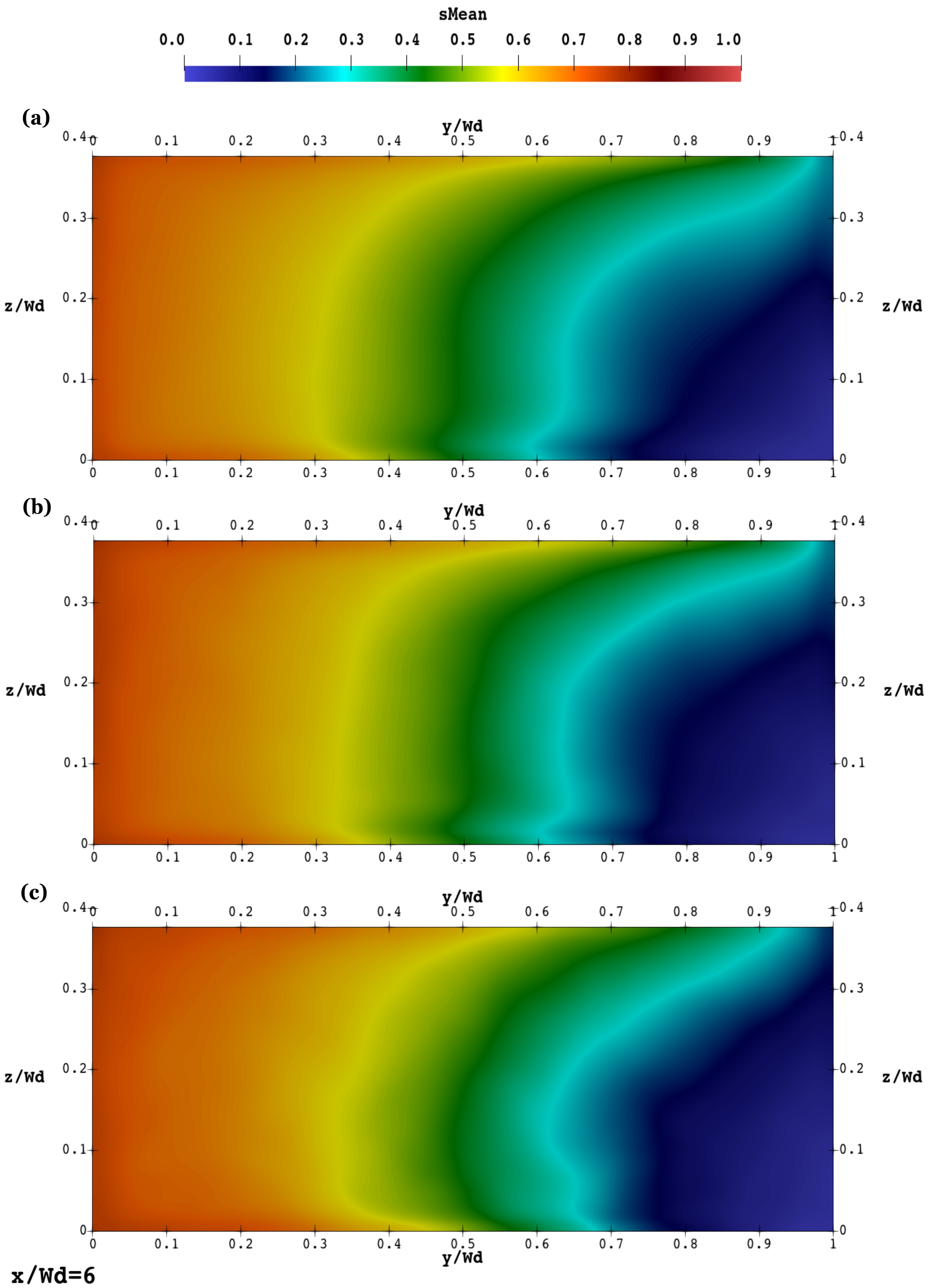

Figure A.18: Time-averaged concentration, sMean, in the cross section $x/W_d = 6$ for the studied schemes: (a) Backward LinearLimited TVD scheme; (b) Crank-Nicolson LinearLimited TVD scheme; (c) Backward Van Leer Limited TVD scheme.

Appendix B

Numerical schemes Monotonicity

B.1 Probe 1 boundedness

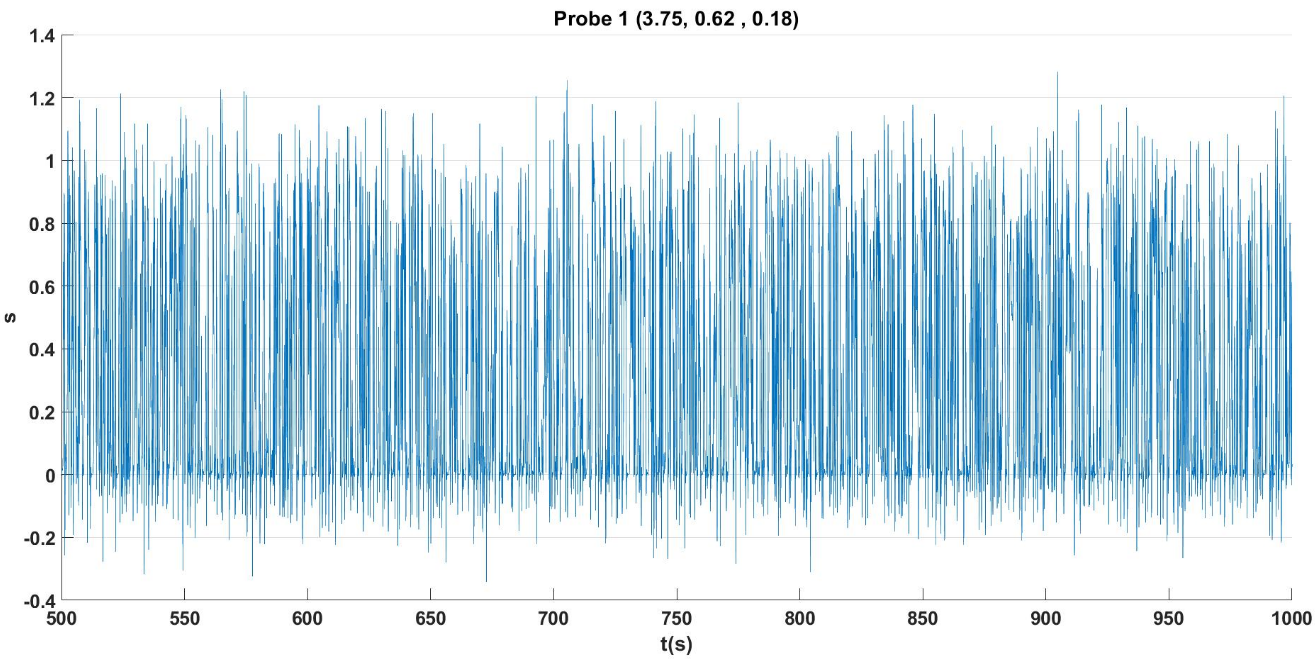

Figure B.1: Backward Linear Limited TVD scheme Probe 1 boundedness.

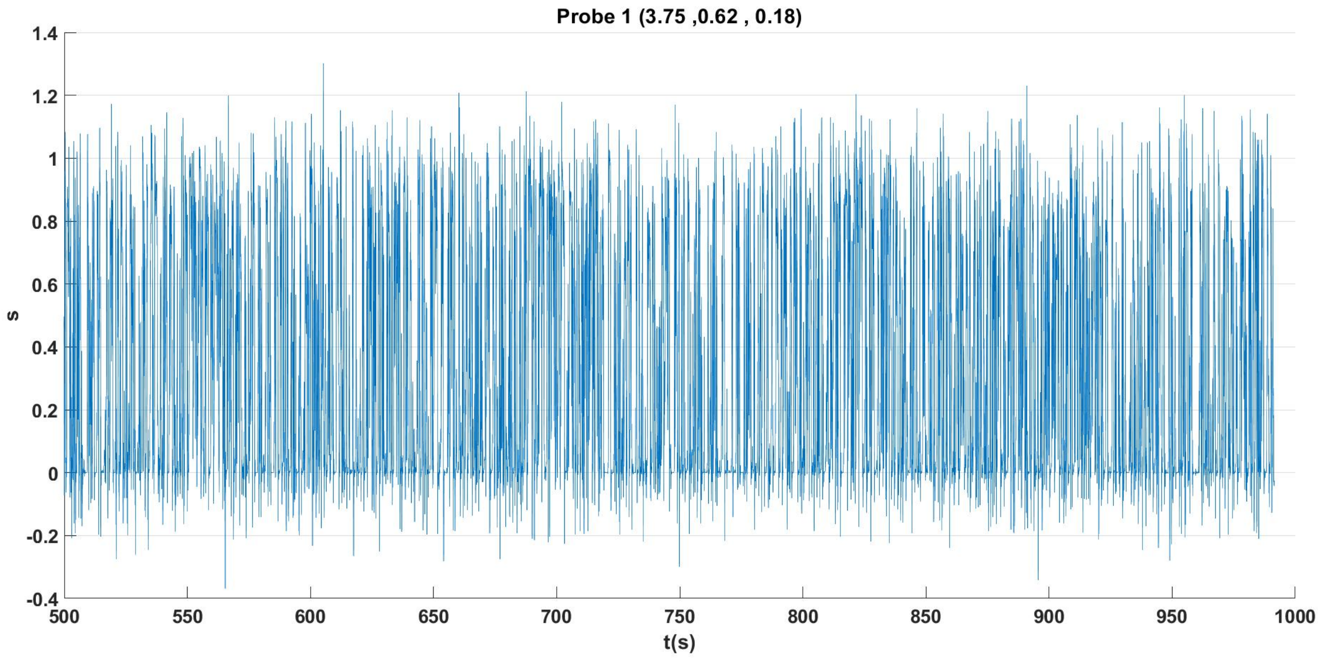

Figure B.2: Crank-Nicolson Linear Limited TVD scheme Probe 1 boundedness.

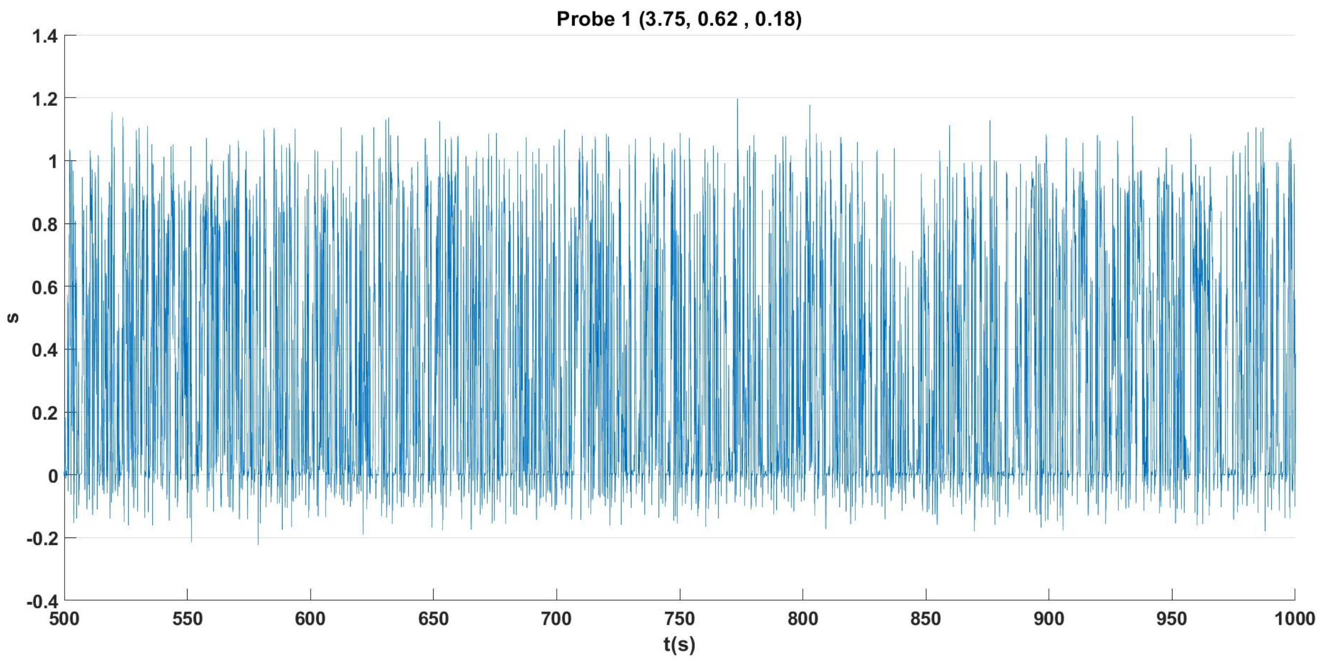

Figure B.3: Backward Van Leer Limited TVD Scheme Probe 1 boundedness.

B.2 Probe 2 boundedness

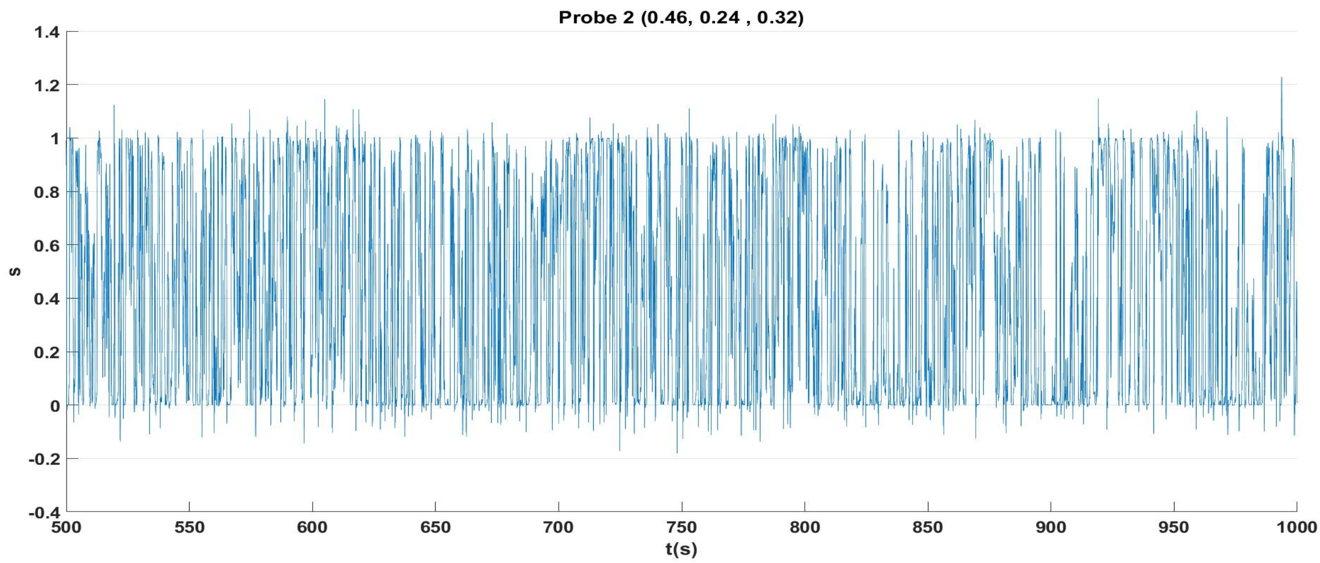

Figure B.4: Backward Linear Limited TVD scheme Probe 2 boundedness.

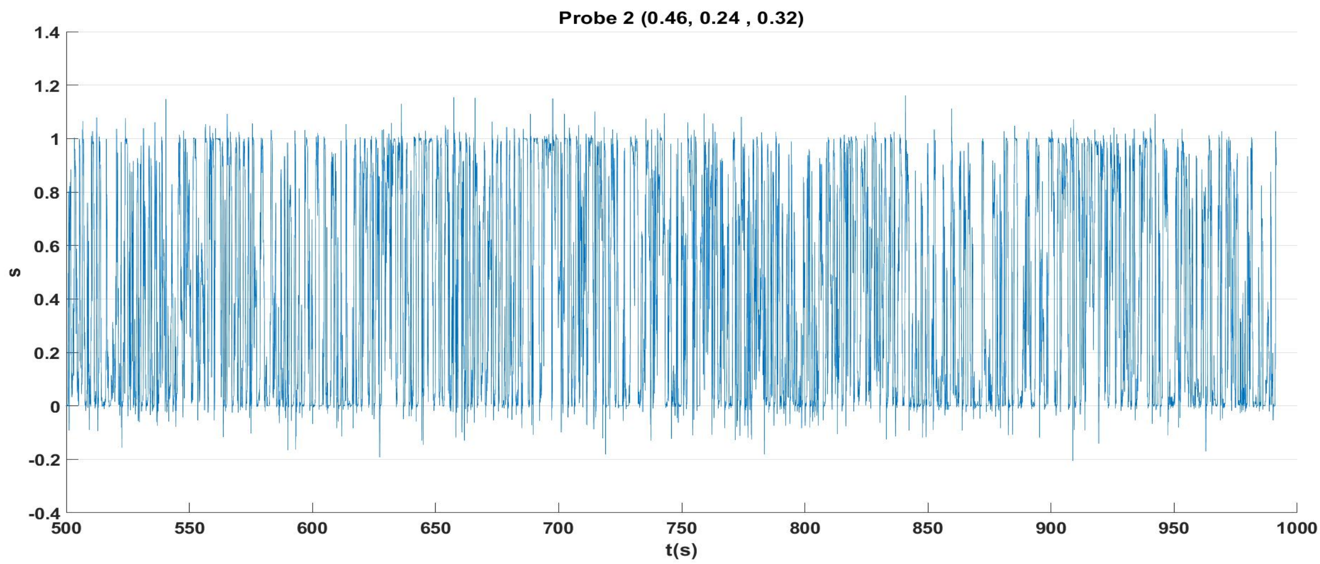

Figure B.5: Crank-Nicolson Linear Limited TVD scheme Probe 2 boundedness.

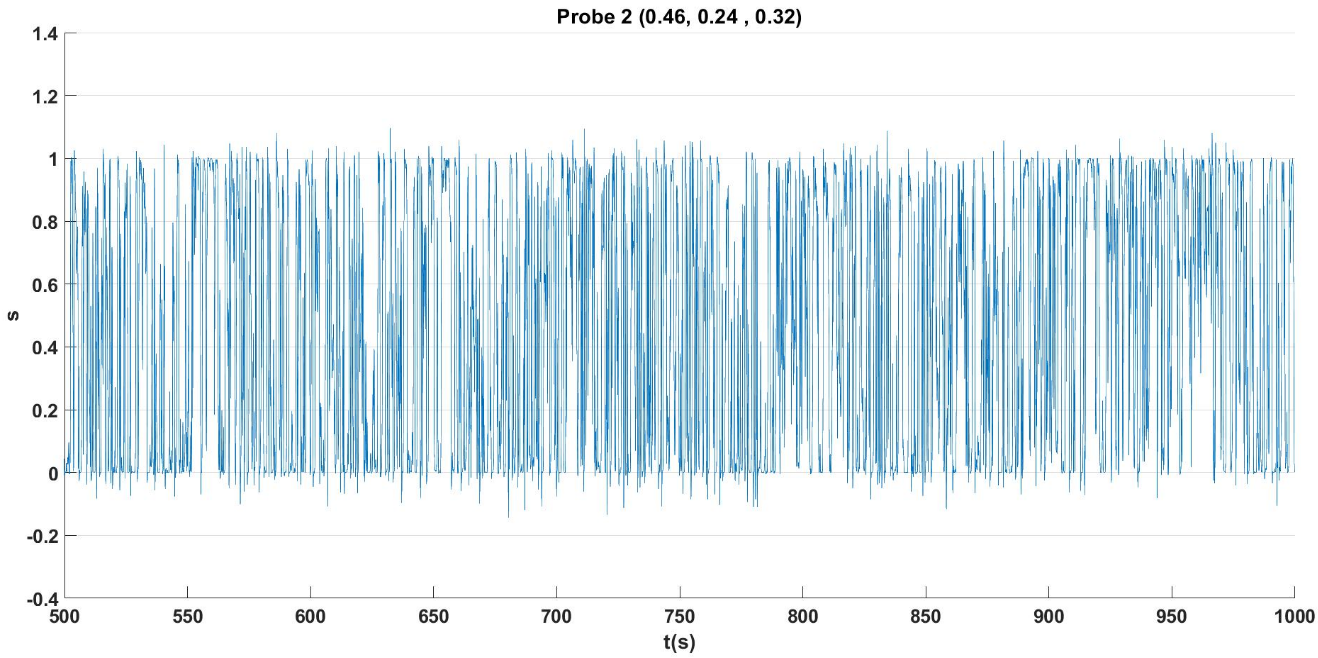

Figure B.6: Backward Van Leer Limited TVD Scheme Probe 2 boundedness.

B.3 Probe 3 Boundedness

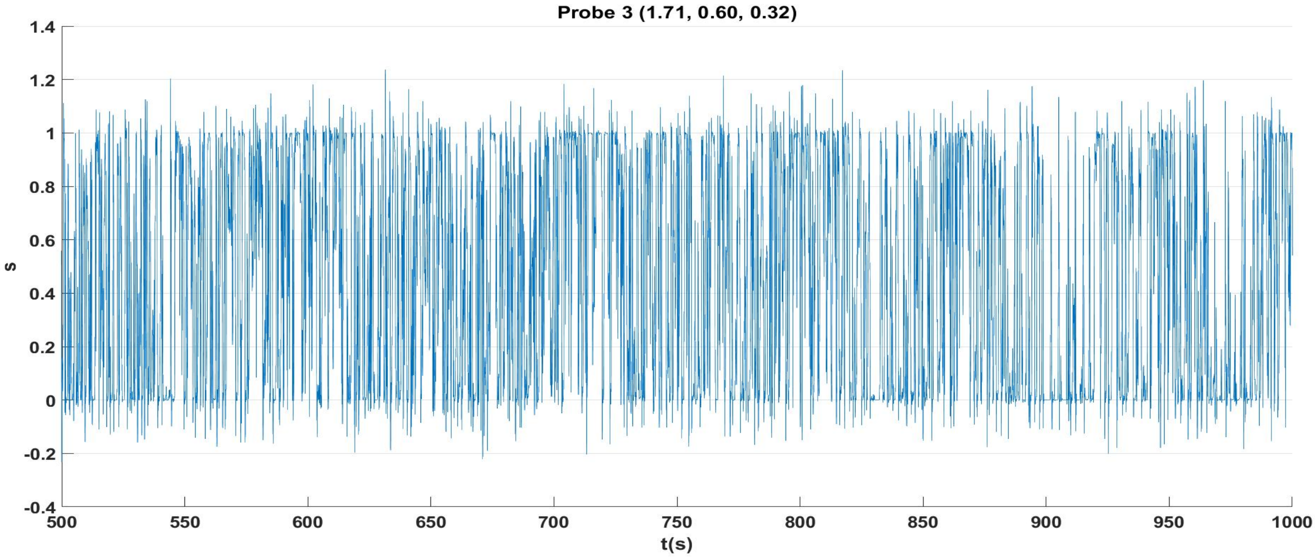

Figure B.7: Backward Linear Limited TVD scheme Probe 3 boundedness.

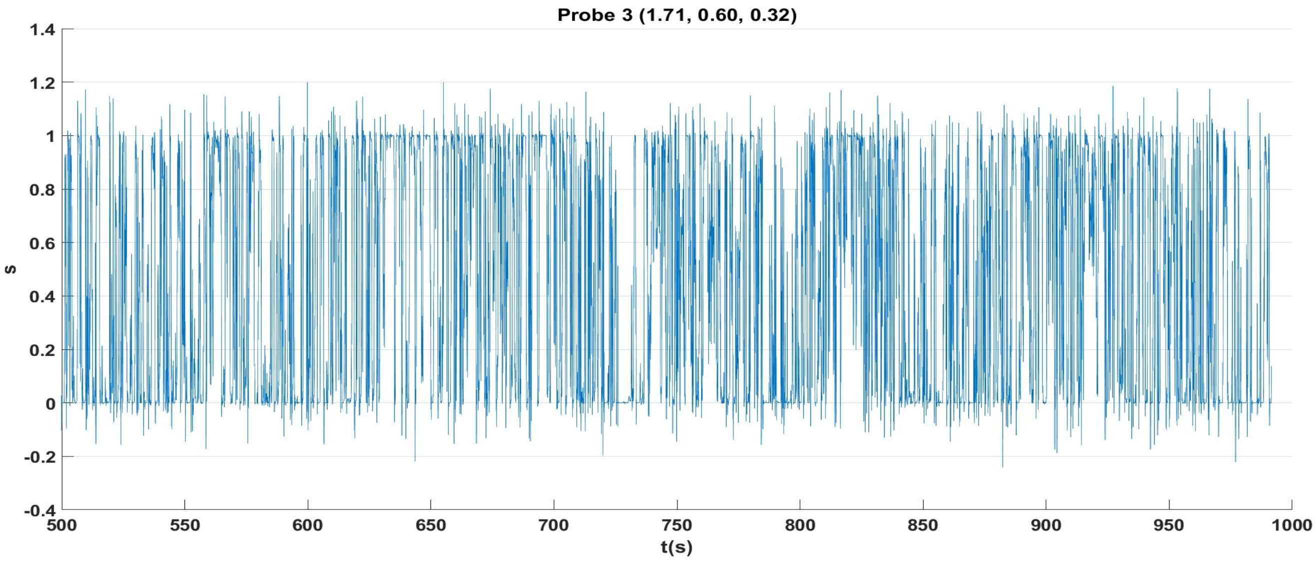

Figure B.8: Crank-Nicolson Linear Limited TVD scheme Probe 3 boundedness.

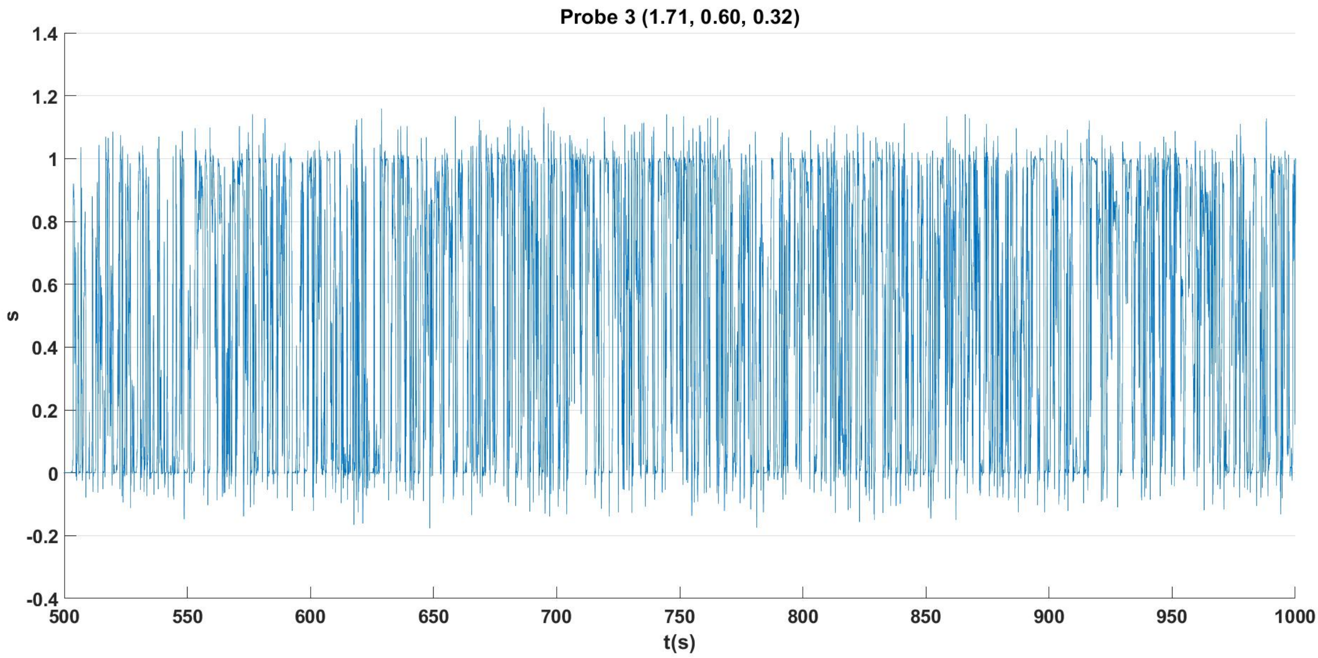

Figure B.9: Backward Van Leer Limited TVD Scheme Probe 3 boundedness.

Appendix C

Complementary Data

C.1 Surface Water Levels

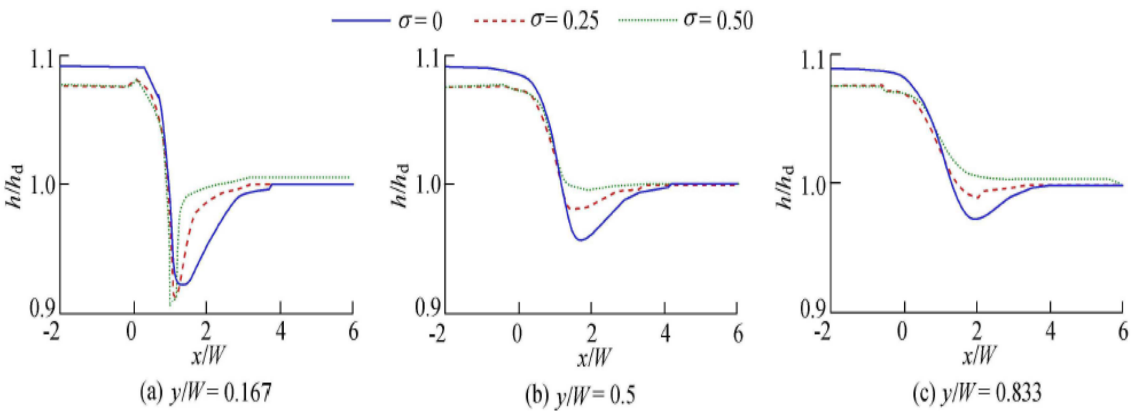

Figure C.1: "Water depths along three longitudinal transects calculated with pressures on rigid lid for simulations in different cases" (Retrieved from Ramos et al. (2019a)).

C.2 Considered Probe Locations

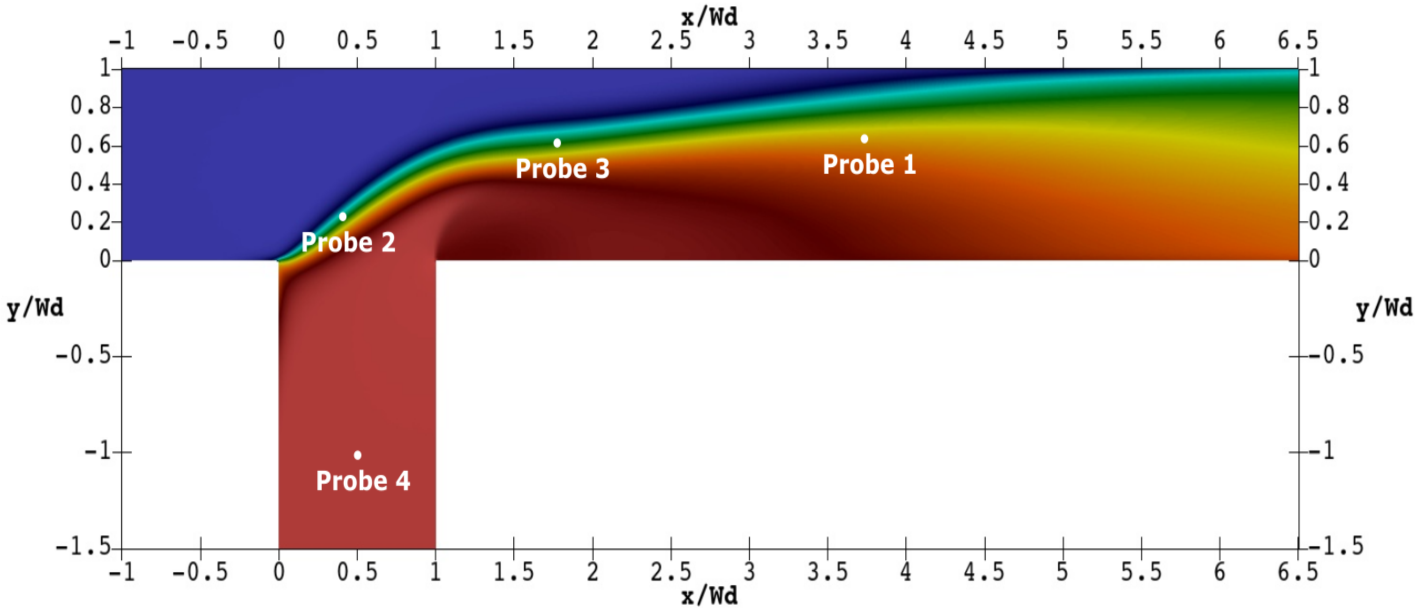

Figure C.2: Location of the considered probes, using the data from the Backward Limited Linear TVD scheme simulation as an example.